# Investigating the Effects of Salicylic Acid on Intercellular Trafficking via Plasmodesmata

**A Dissertation Presented for the**
**Doctor of Philosophy**
**Degree**
**The University of Tennessee, Knoxville**

**Amie Fornah Sankoh**
**May 2023**

# DEDICATION

I dedicate this dissertation to my hero, my father, Daniel Santigie Fornah. Thank you for your unconditional love, support, and most importantly for being the most influential person in my life. This educational achievement would never have been possible if it wasn't for your involvement. Despite being Deaf at a very young age, you did everything to support my education. Thank you, daddy, for being the first person to support my education journey. I look forward to making education more accessible to everyone, especially the Deaf and Hard of hearing community.

# ACKNOWLEDGEMENTS

I owe a great deal of gratitude to my advisors, Dr. Tessa Burch-Smith and Dr. Daniel Roberts, for their assistance, advocacy, and support over the last few years. Thank you for teaching and training me how to become a more independent scientist and for showing me how to become more confident in myself as a researcher. I especially want to thank Dr. Tessa Burch-Smith, who made this work possible. Her guidance and invaluable advice carried me throughout all the stages of writing my project. Thank you for your ongoing mentorship and support throughout the entire thesis process. Because of your huge contribution, I am about to obtain a degree I had never dreamed possible, and I have produced results that will change our perspective on the role of plasmodesmata and hormones for communication in plant development and defense.

I would like to heartily thank my committee members, Dr. Todd Pagano, Dr. Brad Binder, and Dr. Andreas Nebenführ for their contributions and taking their time to advise me. My educational and committee experiences have been beneficial. Thank you for the positive experience and especially for your helpful comments and suggestions. I also would like to thank Dr. Sarah Lebeis who took part in my primary committee meeting and candidacy qualification exam. I would like to especially thank Dr. Todd Pagano for being the first influential person in my scientific research journey. It feels like yesterday; I remembered visiting your office in my last year as an undergraduate with zero confidence in pursuing a higher education. I never imagined myself writing a

dissertation but here I am! Thank you for your open-mindedness, compassion, and guidance at each step of my journey.

I would like to thank all the amazing friends I made in the doctoral program. Thank you, Dr. Craig Conner, Dr. Sterling Field, Mohammed Azim, and Sam Nuzzi for keeping me sane, celebrating all my milestones and some disappointments, and most importantly, for supporting me throughout the entire PhD journey. I would like to thank all past members and current members of Dr. Burch-Smith and Dr. Roberts' Lab for their insights, instrumentals, and experimental training.

I am grateful to the University of Tennessee for giving me this opportunity to pursue science at the highest level, and grateful to the office of Student Disability Services (SDS) and my designated interpreter, Kristi Pearson, whose American Sign Language (ASL) interpretation services were critical in giving me access during my courses and meetings. Thank you to the University of Tennessee and Danforth Center's facilities, for making this project and dissertation possible, and a special thank you to the Program for Excellence & Equity in Research (PEER), National Science Foundation (NSF) and National Institutes of Health (NIH) for the funds and supports.

To my best friend, sister and many more, Dr. Gloshanda Lawyer, thank you for all the support since day one and for your willingness to give a presentation to my lab members on Deaf in Stem and addressing the challenges faced by graduate students and Deaf students. Because of you, my lab became a better and improving place. Thank you especially for keeping me sane and making sure I don't lose my mind in this challenging program. Thank you for always encouraging me to take care of myself.

I would like to thank my family and friends from all over the world. From Africa, especially Sierra Leone, to the USA. Thank you for your continuous support and understanding when undertaking my research and writing my dissertation. Thank you for all the prayers because they are what sustained me this far.

I would explicitly like to thank the Deaf community for their belief in me, and especially for helping me overcome imposter syndrome. To all the deaf students, it was a privilege to mentor, teach, and tutor you. Thank you for your inspiration to be the best version of myself.

I want to thank me for trusting me. I want to thank me for doing and going through all this hard work. I want to thank me for never quitting and continue to be unstoppable. I want to thank me for always being a giver and trying to give more than I receive. I want to thank me for trying to do more rights than wrong. I want to thank me for just being always me.

Ultimately, I would like to thank God for not only keeping me alive but protecting me through all the difficulties I faced in my life. Thank you for guiding me day by day to overcome every challenge that comes my way.

# ABSTRACT

Plasmodesmata (PD) are plasma membrane-lined pores in plant cell walls that allow trafficking of small molecules and macromolecules, including metabolites, signaling molecules, and some hormones, from one plant cell to another. Interestingly, the plant hormone salicylic acid (SA) does not traffic via PD, but instead moves through the apoplast, but it can function to influence PD trafficking. Indeed, SA is a critical hormonal signal that regulates this cell-to-cell permeability in response to pathogen infection. Previous studies have shown SA to regulate plasmodesmata through regulation of callose, which can occlude PD and limit transport. This study focuses on investigating the cellular mechanisms of how SA could directly or indirectly regulate intercellular trafficking by adjusting PD permeability. Here, we present approaches to investigate how SA is connected to PD transport in epidermal leaf tissues of *N. benthamiana*. We seek to understand how SA regulates PD through callose accumulation or decumulation at PD in a time and concentration dependent manner. We addressed what callose dynamics are associated with SA-mediated changes to intercellular trafficking by investigating the correlation between callose deposition and PD movement using callose staining with aniline blue and an intercellular GFP transport assay. We also measured PD distribution in SA-treated tissue using a fluorescent PD marker. SA regulates intercellular trafficking via PD by adjusting callose at PD. Short treatment (1hr SA treatment) with SA show reduces cell-to-cell movement. Long treatment with SA reduces intercellular trafficking and, unexpectedly, we observed an increase in cell-to-cell trafficking at 4 hours of SA treatment. Method 1, which required

fixed tissues was used to accurately quantify callose dynamics that are associated with SA-mediated changes to intercellular trafficking. We observed strong correlations between PD relative permeability and callose deposition. We also found that SA does not regulate PD formation at the times tested. The results that SA exerts complex regulatory control over PD-mediated intercellular trafficking through callose dynamics.

# TABLE OF CONTENTS

# LIST OF FIGURES

# CHAPTER 1

# INTRODUCTION TO INTERCELLULAR COUMMICATION AND HORMONES

https://doi.org/10.1002/ajb2.1733

Sankoh, Amie F., and Tessa M. Burch-Smith. "**Approaches for investigating plasmodesmata and effective communication.**" *Current opinion in plant biology* 64 (2021): 102143.

## I. OVERVIEW OF PLASMODESMATA

Plants require trafficking of metabolites and signaling molecules between cells and systemically to coordinate plant development and mount coordinated responses to abiotic and biotic stresses. With a few exceptions, almost all the plant cells are connected to their neighbors by plasmodesmata (PD), and the plant can therefore be thought to have a symplast. PD are structurally complex nanopores that provide continuity of the plasma membranes and cytosols of connected cells. In many cases, the endoplasmic reticulum is also continuous between cells as a specialized structure, the desmotubule, which resides in the center of the pore. The major conduit for cell-to-cell trafficking is likely the cytoplasmic sleeve, the space between the desmotubule and the plasma membrane[1] (Figure 1). A major function of PD is the delivery of fixed carbon from photosynthesis to the phloem for further distribution to importing tissues in the plant. In addition to sugars, PD also traffic water, ions, small solutes, and macromolecules including proteins and RNAs. Recent work has further highlighted PD in systemic signaling, particularly the distribution of reactive oxygen species in response to local high-

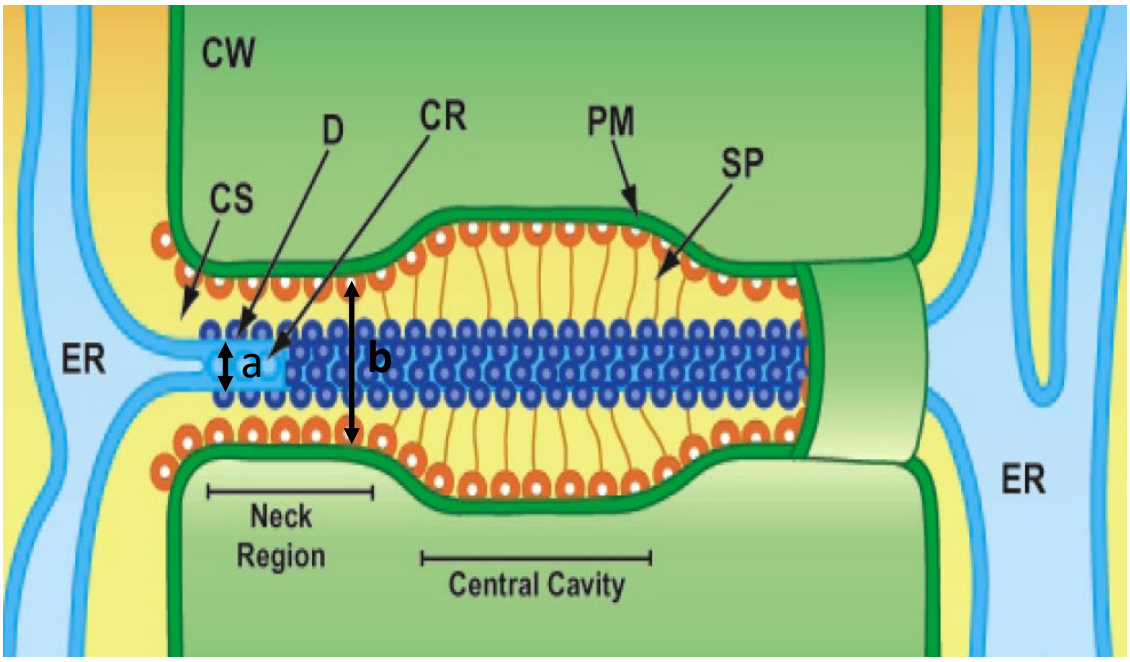


**Figure 1: Details of plasmodesmatal structure:**

Diagram of Plasmodesma (PD) highlighting cell wall (CW), cytoplasmic sleeve (CS), central rod (CR), plasma membrane (PM), and spoke-like tethers (SP). PD consists of membranes and spaces directly connecting the cytoplasm of neighboring plant cells allowing molecule trafficking, which is essential for cellular communication. PD are lined with the plasma membrane containing a narrow tube structure called the desmotubule (D) which is derived from the smooth endoplasmic reticulum (ER) of the connected cells. The diameter indicated for the desmotubule (D) (a) is between 10 and 15 nm. The diameter of the neck region (b) is between 30 and 50 nm.

light stress and demonstrated the role of PD-localized proteins in regulating this process[2]. Viruses have evolved to take advantage of PD for their spread throughout the plant[3]. Understanding how PD regulates the movement of signaling molecules is crucial to unraveling plant responses to stress and the environment.

PD are diverse and can be roughly grouped into three different morphological forms: simple, twinned, and branched, also referred to as complex[4]. Transmission electron microscopy (TEM) studies of PD in *Nicotiana* sp and other plants have shown that PD are usually 30-50 nm in diameter. Simple PD consists of a single pore, and they likely form during cytokinesis following mitosis when strands of ER become trapped in the new cell wall that forms between daughter cells, thereby representing primary PD[4,5]. Secondary PD are added to cell walls independent of mitosis and cytokinesis and they often form near existing PD giving rise to more complex structures referred to as twinned[6] and branched PD[7]. Simple PD can be modified into complex PD as during the sink to source transition in leaves[8] or during the maturation of phloem cells[9]. Other classes of PD have recently been described, suggesting that PD are even more structurally diverse. Type I (apparently lacking a cytoplasmic sleeve) and Type II (having a cytoplasmic sleeve) PD were identified in Arabidopsis roots by TEM tomography[10]. There are also funnel-shaped PD that function in phloem loading[11] .

A current challenge in plasmodesmal cell biology is correlating PD structure with function. For example, complex PD have been reported to traffic less than simple PD[8] , but mutants with increased trafficking have more complex PD than do their wild-type counterparts[12]. In order to decipher PD structure-function relationships, attempts have

been made to measure PD permeability (trafficking capacity) and structure while causing minimal perturbations to tissues under examination.

## II. PLASMODESMATA AND PLANT DEVELOPMENT: HORMONES

"…[The] plant has means to control the symplastic continuity of its parts and to regulate the degree of isolation of its constituent cells. This form of regulation is a counterpart to that which results from the release and action of hormones. One is led to speculate whether hormones themselves might act in part by opening or closing symplastic pathways." (Carr, 1976, p. 287)

Plant development depends on local positional cues and on mobile non-cell-autonomous signals that can act at short or long distances. Plant hormones are growth factors that mediate local cell events as well as coordinate long-distance processes that affect the entire plant[13]. While hormones often act beyond the confines of single cells, the mechanisms by which this is accomplished are longstanding unknowns, as exemplified by the quote above (Carr, 1976). The cytoplasmic connections between cells formed by PD essentially render groups of cells as symplasts whose boundaries depend on the permeability of PD at any given cell interface. Symplastic fields change with developmental progression, and links to hormone action can be easily identified[4], although data examining causation is not readily available in the literature. Thus, how hormones influence PD remains poorly understood, but there has recently been increasing attention to the role of PD in mediating hormonal flux and signaling (Figure 2).

PD directly connect neighboring cells allowing the intercellular trafficking of small molecules like metabolites and hormones as well as macromolecules like small RNAs and protein transcription factors that act as signaling molecules during development and defense, making PD crucial for communication between plant cells. The desmotubule at the center of the PD consists of compressed endoplasmic reticulum (ER) and thus allows ER continuity between cells. The major conduit for cell-to-cell trafficking is likely the cytoplasmic sleeve, the fluid-filled space between the desmotubule and the delimiting plasma membranes of the connected cells (Figure 1). PD trafficking is often regulated by the controlled accumulation of callose, a β−1,3-glucan, in the cell wall surrounding a plasmodesma[14,15] (Figure 2). Callose deposition reduces intercellular trafficking, while the converse occurs when callose is removed. A hallmark of plant development is the restriction of PD-mediated intercellular flux into groups of cells undergoing a specific developmental program distinct from their neighbors', a state termed symplastic isolation. Symplastic isolation is often marked by callose accumulation at PD of cells at the boundary of this group of cells, but it can also involve structural modification of PD. The importance of PD regulation in development is exemplified by studies of callose deposition during lateral root formation, where induction of callose deposition restricted the cell-to-cell trafficking of the SHORT-ROOT transcription factor and microRNA165 and disrupted protoxylem formation in developing roots[16]. While the callose-mediated isolation can be reversed after the developmental transition, structural modifications to PD are usually permanent[4]. Although symplastic

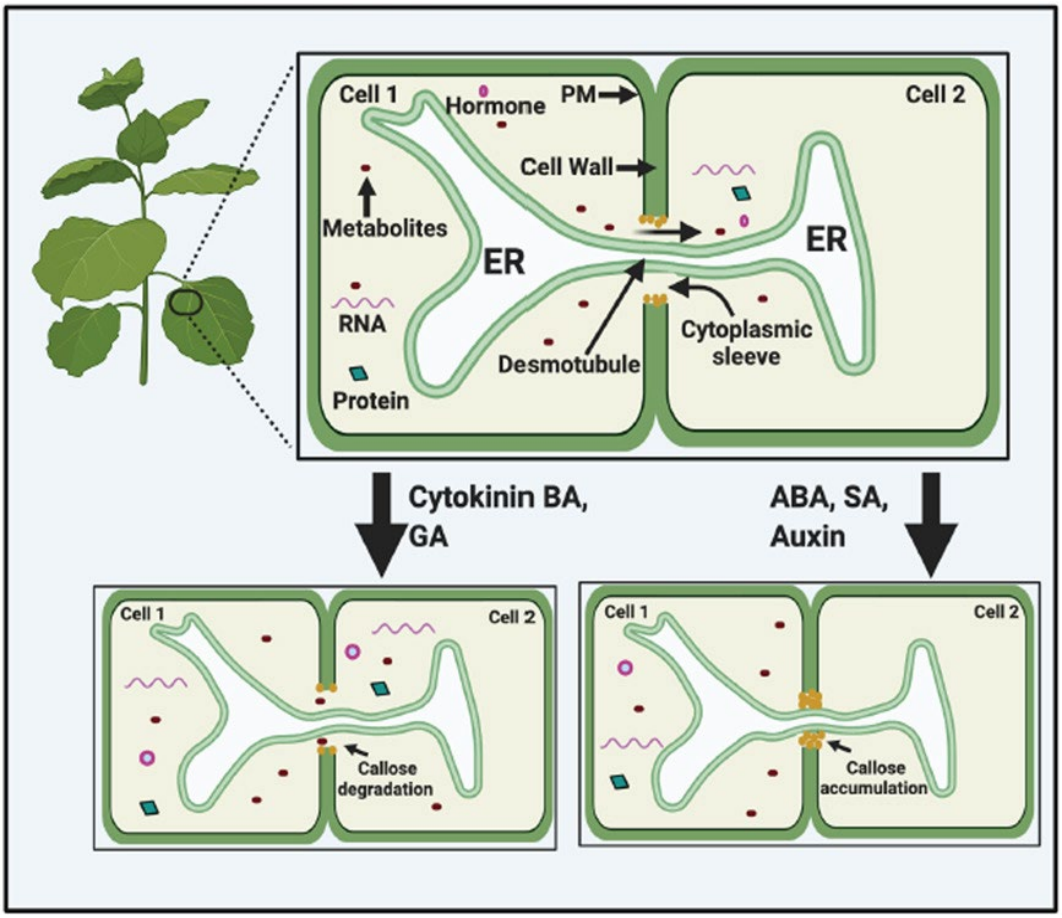


**Figure 2: The effect of hormones on plasmodesmata-mediated trafficking**.

Schematic of two plant cells connected to each other by PD and the movement of metabolites and signaling molecules between the two cells. The hormones ABA, SA, and auxin can restrict intercellular trafficking through the deposition of callose in the cell wall at the PD. ABA may also decrease pore size through an alternative mechanism. The hormones cytokinin and GA cause the removal of callose at PD and increase intercellular trafficking. Cytokinins can also increase the formation of secondary PD. Created with BioRender.com

isolation has been assumed to be important for controlling hormonal and signaling fluxes, experimental evidence for this remains sparse. Further, it remains unclear how much influence PD and intercellular flux have on establishing hormonal gradients during development.

Perhaps the best-known plant hormone is auxin. Its primary effects are promoting cell division and expansion, and auxin signaling has been intensely investigated and described[17]. The local flux of auxin depends on membrane-localized transporters, the AUX1/LAX transporters for influx, the general plasma-membrane-localized ABCB efflux transporters, and the polar PIN-FORMED (PIN) efflux carriers that also mediate auxin recycling within cells and between compartments[18]. These transporters are essential for setting up the auxin gradients through which auxin exerts its effects, as well as regulating auxin homeostasis by subcellular auxin compartmentalization. One puzzle, however, was whether auxin, a small hydrophilic molecule, moved between cells via PD to exert its effects. Indeed, although the genome of the moss *Physcomitrium* (*Physcomitrella*) patens encodes homologs of auxin transporters, auxin moves via PD during lateral branching in the moss gametophore[19] . Exciting recent studies in *Arabidopsis thaliana* confirmed that not only can auxin move via PD in other plants, but that this movement is necessary to complement transporter-mediated auxin flux[17] and is also required to establish tissue-level auxin gradients in the shoot[20]. Indeed, auxin effects on PD include establishing local gradients important for root stem-cell identity[21], lateral root initiation[22], and shoot tropic responses[18]. Further, auxin-mediated callose accumulation at PD is implicated in tropism and lateral root

formation[18,22] . It will be interesting to see how auxin flux is balanced between the genetically encoded transporters and PD, and we anticipate that this will be a question of considerable research interest in the near future.

Studies investigating bud dormancy have been informative for understanding PD–hormone interplay. Bud dormancy and release from dormancy in hybrid aspen and other trees are marked by profound changes to PD and intercellular trafficking in the buds mediated by various hormones. In aspen, PD closure at the onset of dormancy is accomplished by callose accumulation mediated by abscisic acid (ABA), preventing entry of growth-promoting factors like the protein FLOWERING LOCUS T (FT) into the meristem[23] . Release from dormancy is accompanied by removal of callose mediated by gibberellic acid (GA)-inducible β−1,3- glucanases in poplar[24] and hybrid aspen[25] . The gaseous hormone ethylene was also found to mediate PD opening to release dormancy in *Narcissus tazetta*[26] . Gibberellic acid and ABA traffic via PD in *Chara vulgaris* and *P. patens*, respectively[27,28]. In contrast, the defense hormone salicylic acid (SA) does not traffic via the symplast but instead moves in the apoplast[29]. Despite this, SA is well known to regulate plasmodesmata through callose dynamics, acting through the callose synthase enzyme CalS1[30] , PLASMODESMTA LOCATED PROTEINs (PDLPs)[29,31] and modulating lipid organization through the lipid-raft like protein REMORIN to control callose accumulation at PD[32] (Figure 2).

While callose deposition and removal seem to be the primary mechanism through which hormones act to control PD trafficking during development, there are instances where other changes to PD have been observed. Exogenous ABA modified

PD pore size in *P. patens* as application of ABA reduced intercellular trafficking of a fluorescent probe, and although PD in ABA-treated samples were narrower than those in control plants, no increase in PD callose in response to ABA could be detected[28] . Thus, hormones may alter PD ultrastructure other than through callose metabolism, for example, through the cytoskeleton, although this has not been experimentally verified.

As described earlier, there are two major classes of PD that form at different developmental times. The first class is primary PD that form during cytokinesis when strands of ER become trapped in the new cell wall being formed between daughter cells. The second class is the secondary PD which are added to existing cell walls by a mechanism that remains elusive but likely involves cell wall remodeling[4] . Application of the cytokinin benzyladenine (BA) to the shoot apical meristems of *Sinapis alba* induced secondary PD formation, a phenomenon that had previously been observed to occur during the SAM floral transition[33] . This observation along with mutants with increased secondary PD formation could yield new avenues for understanding the intriguing phenomenon of how cell walls are modified coincident with the insertion of plasma membrane and ER to form a new PD.

Given the importance of hormones and intercellular trafficking to plant development, it is surprising that so much remains unknown about how PD and hormones interact to coordinate the production of effective signaling gradients and to allow the non-cell-autonomous effects of hormones. We expect that in the future more comprehensive studies that examine the effects of single hormones and combinations of hormones at physiological concertation on PD will be undertaken. The use of mathematical models to

help explain the effects of PD on hormone gradients and signaling will be a boon to this field, as it has been for studies on auxin[17,20]. Efforts to understand how hormones interact with PD could also provide interesting insights into the cell biology of PD, for example, secondary PD formation and how PD ultrastructure can be altered by factors other than callose. In the long term, understanding and being able to predict the outcome of hormone–PD interactions could provide new tools for approaches that engineer resource allocation for maximizing the proportions of crop photosynthetic output that is available for human consumption[34] (e.g., rice C4 project). Such processes depend on PD for nutrient distribution and manipulating PD may have consequences for hormone signaling and plant development.

## III. REGULATING PLASMODESMATA: CALLOSE

PD function and callose dynamics are controlled by multiple proteins that are involved in response to environmental, metabolic and development signals, as well as stress, and pathogen infection. Thus, callose plays an important role in regulating PD trafficking in response to biotic and abiotic stress as well as during plant growth and development. Callose accumulated at PD can regulate the trafficking of molecules (PD permeability) by controlling the size exclusion limit (SEL) of PD.

Callose is synthesized by the callose synthase enzymes. Genes encoding putative callose synthase such as *CalS* (Callose synthase) and *GSL* (Glucan synthase-like) can synthesize callose in response to wounding and infection by pathogen. Only eight members of the callose synthase family are found in *N. tabacum* while there are twelve in *A. thaliana*[35]. CalS1 and CalS8 are key enzymes involved in regulating plasmodesmal

permeability upon wounding stress and pathogen infections. Overexpression of *CalS1* results in higher levels of callose synthase activity and callose accumulation at PD. CalSs/GSLs also play important roles in pollen development and fertility[36,37]. Plant lipid rafts control callose accumulation at PD, and this is determined by sterol and sphingolipid homeostasis. Sterol reduction results in mislocalization of GPI-anchored PD proteins, PDCBs and PDBGs, that regulated callose deposition by degrading callose at PD. Disruption in lipid rafts impacts other targeting lipid proteins such as Remorins which increase callose levels at PD[38]. Alternations in sphingolipids controls PLASMODESMATA-LOCATED PROTEIN 5 (PDLP5) resulting in callose turnover involving of the SA pathway[38,39]. PDLPs are membrane receptor-like proteins that adjust PD closure and, in some instances, promote cell-to-cell movement of plant viruses. PD closure is observed in overexpression PDLP5 plants whereas loss of function *pdlp5* mutants showed increased PD permeability[31]. As a defense response against powdery mildew infection, modifications of sphingolipids permit the activation of SA, likely through PDLP5, causing PD closure by callose accumulation at PD[29].

Callose removal from PD allows larger molecules than typical to translocate from one cell to another. Callose is removed from the PD in a regulated manner by degradation via β-1,3-glucanases such as BG_ppap, PDBG1, and PDBG2[40,41]. To enhance virus spread, viral genomes encode movement proteins (MPs) that lead to the degradation of callose at the PD neck and increase intracellular trafficking[42,43]. PDCB1 and BG_ppap play important roles in regulating PD callose deposition at SAMs during dormancy. BG_ppap, a glycosylphosphatidylinositol (GPI) lipid-anchored protein that

localizes to the cell membrane, is substantially enriched at PD sites and enables callose degradation atPD[24].

### *Callose at PD: the role of Salicylic Acid*

In the 4th century BC Hippocrates used willow leaves containing salicylate as a pain reliever for women during childbirth[44]. Today salicylates such as aspirin, an acetylsalicylic acid, are common pain relievers. Arylesterases are enzymes found in plant tissues that rapidly convert aspirin to salicylic acid (SA)[44]. Besides its uses in human healthcare, SA is an important phytohormone that is involved in regulating multiple biochemical and physiological processes in plants especially plant growth, defense response against pathogens, and environmental stress. Plant phenolics, such as SA, have been commonly classified as secondary metabolites. High levels of SA have been found in rice, barley, crabgrass, and soybean[44,45]. In *A. thaliana*, barley, and maize, SA is a negative regulator of seed germination under SA-induced oxidative stress[46,47]. However, under abiotic stress, exogenous SA improved *A. thaliana* seed gemination. Plants infected with pathogens have been recorded to have the highest levels of SA. In the model plant *Nicotiana tabacum,* the basal levels of SA are less than 100ng/g fresh weight, compared to induced levels of up to 1 µg/g fresh weight in cucumber stems infected with the *Colletotrichum lagenarium*, anthracnose pathogen[48].

SA plays an important role in plant defense activation in response to pathogen infection. SA has been shown to be derived from two pathways, isochorismate synthase (ICS) and phenylalanine ammonia-lyase (PAL) in the chloroplast[49,50]. SA methyl transferase (SAMT) catalyzes conversion of SA to methyl salicylate (MeSA) which

diffuses into the cytoplasm and is converted back to SA by the esterase activity of salicylic acid binding protein 2, SABP2[51,52]. Many of SA's effects on gene expression are through the activity of the protein NONEXPRESSOR OF PR GENES1 (NPR1). NPR1 is an SA receptor that localizes to the cytoplasm in the absence of SA. On SA binding, the oligomeric NPR1 dissociates into its monomers which can then migrate to the nucleus to activate transcription of SA responsive defense genes including pathogenesis-related genes[51,53,54]. NPR1 is phosphorylated and then sumoylated upon its interaction with WRKY and then TGA transcription factors. Interestingly, proteosome-mediated degradation of modified-NPR1 triggers expression of SA responsive genes, leading to only transient activation of defense gene expression[54].

PLASMODESMATAD-LOCATED PROTEINS (PDLPs) comprise a small family of eight proteins first identified in *A. thaliana* that localize to PD through the secretory pathway and regulate transport and signaling in plants[29,31]. PDLPs have large extracellular domains but very little cytoplasmic structure. Overexpression of some PDLPs promoted the cell-to-cell movement of viruses that use tubule-guided movement (e.g., movement protein (MP) encoded by Tobacco mosaic virus) while overexpression of others led to increased callose accumulation at PD and changes in plant susceptibility to pathogens. Super-resolution imaging revealed that fluorescently tagged PDLP proteins localize to the plasma membrane within plasmodesmatal channels, and studies of these proteins have shown various effects on the regulation of cellular movement of macromolecules and viruses in *Arabidopsis*. Overexpression of PDLP1 shows a decrease in cytosolic GFP trafficking between cells, whereas an

increase of GFP movement between cells was observed in double mutants of PDLP proteins (*pdlp2/3* and *pdlp1/3*). Overexpression of PDLP5 led to an increase in PD trafficking which promotes virus spread, while mutation of *pdlp5* inhibited viral spread. The PDLP family are activated in response to treatments with SA associated with pathogen invasion[55].

PD-facilitated cell-to-cell communication is coordinated with SA signaling pathway through PDLP5. In innate immunity against bacterial pathogens, SA controls PDLP5 to regulate callose by inhibiting PD trafficking[55]. During systemic acquired resistance (SAR), a secondary defense response against early exposure of pathogen, signaling molecules such as azelaic acid (AzA) and glycerol-3-phosphate (G3P) move between cells via the symplast pathway[29,56]. In contrast, SA is transported via the apoplast but uses PDLP1 and PDLP5 for SAR[29]. In Arabidopsis, exogenous application of SA induces callose depositions and closure at PD[55]. In the absence of PDLPs, exogenous SA was not sufficient to induce PD callose responses. Taken together, these findings indicate that PDLP5 and the SA pathway are important for the regulation of PD permeability during a pathogen resistance response. More work is needed to understand the mechanism involved in regulating beneficial interactions, preventing pathogenic invasions, and understanding the virus interaction with SA in a time-dependent manner. Despite considerable efforts PD are poorly understood structures and little is known about how callose is regulated at PD. For example, plant viruses encode movement proteins that modulate cell-to-cell trafficking, possibly through induction of activity of endogenous glucanases to degrade callose, and therefore

increase viral symplastic spread. Further, the importance of callose in regulating molecular diffusion via apoplastic transport at sites away from PD remains unknown.

## IV. TECHNIQUES FOR EXAMING PD

PD play a crucial role in communication which is essential for plant survival, growth, development, and defense. This section addresses the common approaches that have been used to study PD structure and function.

### *Measuring callose*

The level of callose in a tissue can be used to determine the status of PD in that tissue, with high callose levels correlating with low permeability. Staining with the pigment aniline blue is the most commonly used method for measuring callose levels[57], (Figure. 3). It is relatively easy to fix tissues and then apply aniline blue, although care must be taken during tissue isolation to avoid inducing damage and subsequent callose deposition at those sites[57]. Another advantage of aniline blue is that it can be used to examine a relatively large amount of tissue. Measuring callose by immuno-EM using anti-callose antibodies gives greatly improved resolution over aniline blue staining, allowing the visualization of callose at certain positions along pd and the distance from pd to be ascertained[18,58] . Despite these advantages, this approach is not very commonly used, perhaps because of the time, cost of reagents or perceived difficulty and expertise needed for TEM. Despite its widespread use as a proxy for PD permeability, the correlation of callose with PD trafficking is not straightforward, and recent data suggest it is more complicated than previously assumed[59].

In addition, although it is easy to observe callose accumulation, it is harder to measure reductions in callose levels that may be associated with increased permeability. Data on callose levels should be interpreted with caution, and conclusions about PD trafficking should be limited to actual measurements of trafficking. This dissertation will majorly focus on understanding the effect of SA on callose dynamics at PD.

### *Measuring PD trafficking*

Fluorescent dyes were the earliest probes deployed for measuring PD permeability. Small dyes like 5(6)-carboxyfluorescein diacetate (CFDA) can be microinjected into the cytoplasm of cells and the diffusion of the dye beyond the injection site is monitored by fluorescence microscopy (Figure 3). CFDA is a good indicator of symplastic transport because it is membrane impermeant and only on entering the cytoplasm is it cleaved by esterases to liberate the fluorescent CF molecule. The challenge with microinjection is the skill required for delivery into the cytoplasm while avoiding the vacuole which is the bulk of the cell volume in a fully expanded plant cell. CFDA can also be used to measure systemic trafficking via the phloem[60] and it has been widely used for this purpose. More recently, dyes closely

**Figure 3: Experimental approaches used to study PD and intercellular trafficking**. (a) Fluorescent dyes and proteins can be introduced into leaf cells by microinjection. (b) Fluorescently labeled proteins can be transiently expressed in leaf cells by agroinoculation. (c) Fluorescent probes are subsequently imaged by microscopy, and a pattern of cells containing the probes is usually observed when PD permeability allows probe trafficking, with larger areas representing more PD permeability and trafficking. Images show layers of cells into which GFP has moved, with no movement and movement to 3 layers being depicted. Arrows point to nuclei of neighboring cells into which GFP has trafficked. (d) Aniline blue can stain callose at PD (blue dots). I Representation of the distribution of aniline blue around PD, with aniline blue accumulating along the entire length of a pore. (f) PD distribution as revealed by MP30-GFP accumulating in PD at the cell periphery in a confocal micrograph. (g) Thin-section TEM is used to observe complex and simple PD in a cell wall. (h) FIB–SEM combines ion beam milling with an electron beam in one setup. (i) For SBF–SEM, a microtome is mounted inside the microscope to produce serial images of the newly cut surface. (j) TEM tomography Involves the capture of images as a sample is rotated through a tilt series. This was created with BioRender.com.

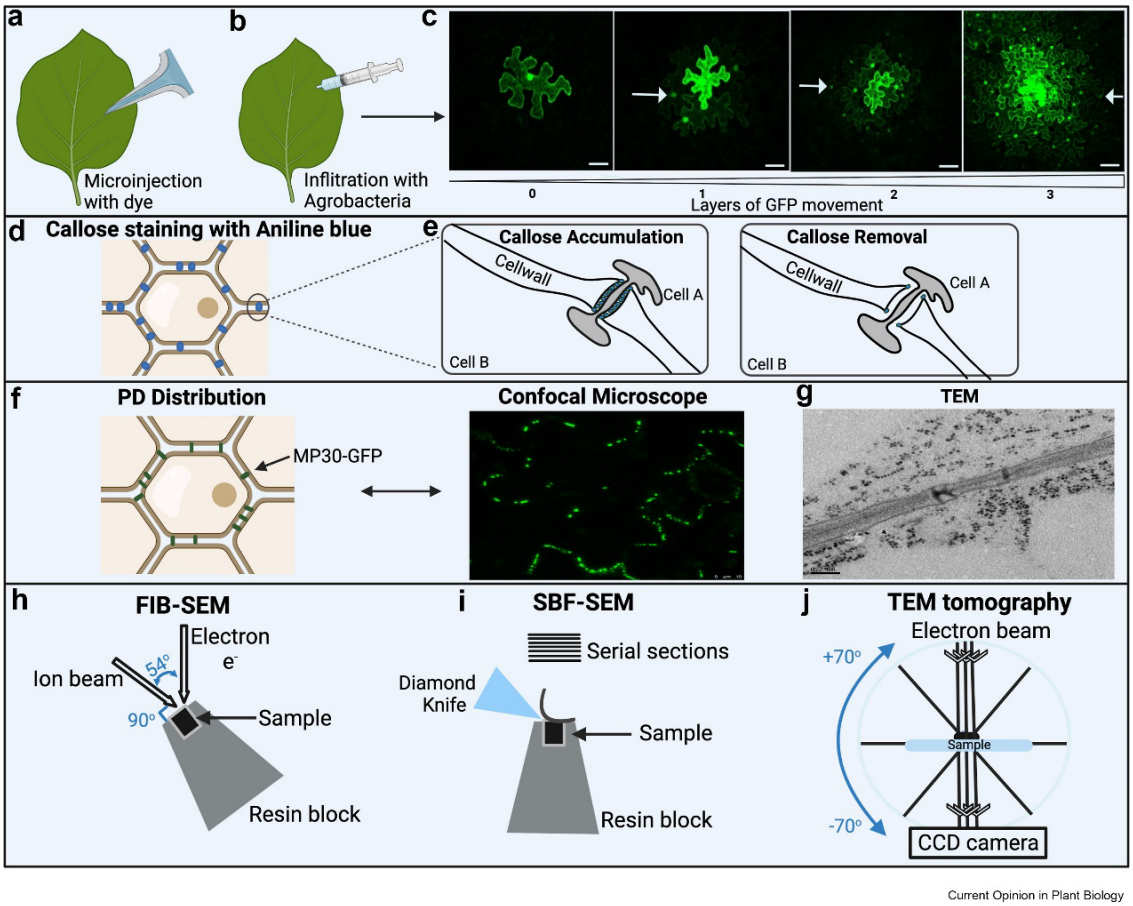
a
b
c
Microinjection with dye
Inflitration with Agrobacteria
0
1
2
3
Layers of GFP movement
d
Callose staining with Aniline blue
e
Callose Accumulation
Cellwall
Cell A
Cell B
Callose Removal
Cellwall
Cell A
Cell B
f
PD Distribution
MP30-GFP
Confocal Microscope
g
TEM
h
FIB-SEM
Electron
e-
Ion beam
54°
90°
Sample
Resin block
i
SBF-SEM
Serial sections
Diamond Knife
Sample
Resin block
j
TEM tomography
Electron beam
+70°
Sample
-70°
CCD camera
Current Opinion in Plant Biology

related to endogenous plant molecules have been adopted for measuring phloem transport[61,62]. In the future these may supplant CFDA as a symplastic tracer. A modern application for CFDA is the Drop-And-See (DANS) assay developed the Lee group[63,64] . Here, a small, measured amount of CFDA is applied to the adaxial leaf surface and the radius of resulting fluorescence, presumably measuring intercellular trafficking, is measured on the abaxial surface. DANS has been used to characterize mutants[65] and measure PD trafficking capacity[2,29]. Other fluorescent molecules that have been used to assess PD permeability include caged fluorescein[66] , 8-hydroxypyrene 1,3,6 trisulfonic acid (HPTS)[67–69] ,
Lucifer Yellow CH (LYCH)[5,70] and fluorescent dextrans of various molecular weights.

Fluorescent proteins have also been widely adopted as probes for measuring PD trafficking. Introduction of GFP-expressing constructs into plant leaves via Agrobacterium has been popular[71] , although bombardment with plasmids for GFP expression is also possible[72] . The soluble cytoplasmic protein (GFP) moves between cells via PD by simple diffusion[72] and GFP movement is used to investigate PD trafficking in response to abiotic and biotic factors, and changes in gene expression[73–75] . GFP can also be stably expressed from tissue-specific promoters. The AtSUC2 promoter is often used for expression of GFP in the phloem[76] ( references therein), which permits GFP to traffic extensively though PD during unloading in the phloem. Tandem copies of GFP (2XGFP or 3XGFP) may also be used as probes, although they do not traffic as extensively as GFP itself[68]. DRONPA and photoactivatable GFP (PA-GFP) are GFP-derived proteins that can yield measurements of high spatial and

temporal resolution[77]. DRONPA can be switched on and off with different wavelengths of light, allowing its movement to be observed in real time. The analysis of data used to assess PD permeability often varies widely between researchers and would benefit from more uniform standards for collection and statistical approaches, as recently proposed[78].

***Determining PD structure and measuring distribution of PD***

Viral movement proteins (MPs) tagged with fluorescent proteins have emerged as excellent probes for PD[3]. Tobacco mosaic virus (TMV) movement protein MP30, although preferring complex PD in some tissues[59,79], can label all types of PD[4] and it has been widely adopted as a PD marker (Figure. 3). MP17 from potato leafroll virus specifically labels complex PD[4,80] and it can therefore be used as a maker for these types of PD. These proteins can be stably expressed in transgenic plants and used in this way to observe PD; however, they often have effects on plant development and metabolism thereby complicating studies[80–82] . It is perhaps more prudent to adopt transient expression by bombardment or Agrobacterium to express these markers, e.g.[74]. In addition to viral MPs, the plant proteins PDLP1 and PD CALLOSE BINDING PROTEIN1 (PDCB1) can also be fluorescently labeled for use as PD markers. An exemplary use of these PD markers to study PD cell biology is the development of a high-throughput imaging platform and accompanying algorithm, PDQUANT, for identifying cells and counting PD[7] . This approach was used to document several features related to the development of complex PD that would otherwise have been recalcitrant to discovery. Unfortunately, such approaches have not seen widespread

adoption, and there remains a need for (semi-)automated imaging and analysis approaches for rapid, reliable and unbiased data collection and analysis.

TEM has a long history as the go-to method for studying PD structure and morphology and measuring PD distribution. Despite its popularity, in thin-section TEM, only a single slice of around 60-70 nm thickness of a 3D structure is visible. This produces a snapshot of PD and usually only a few (or portions thereof) PD in a wall are captured (Figure 3). The details of PD morphology are therefore often obscured and only time and labor-intensive scoring of many sections and PD can give a somewhat reliable estimate of PD form and distribution in a tissue e.g.[12] . Nonetheless, thin sections can be used in interesting ways, e.g., when combined with freeze fracture and fluorescence in a new technique dubbed 3-D immunolocalization confocal microscopy[83] . This technique has been used to measure PD density of PD at the mesophyll-bundle sheath interface in C4 grasses grown under different light regimes and made evident that PD size and distribution are dynamic in response to growth conditions[84] . Detailed analysis of the ultrastructure of the PD nanopores requires use of three-dimensional (3D) approaches, typically TEM tomography (Figure 3). The resulting 3D models allows higher magnification and better resolution of structural components, particularly in the z axis[85]. Ideally, samples are prepared for imaging by high pressure freezing and subsequent freeze substitution[86], the gold standard for preparing plant samples for electron microscopy[87]. Recently, TEM tomography has been used to reveal new forms and structural variants of PD. Type I and Type II PD were discovered by TEM tomography[10], and this technique was also used to identify PD defects in the phloem

unloading modulator (plm) mutant[88]. TEM tomography has also been used to examine the interaction of viruses with PD during infection[89]. Given the power of this technique, TEM tomography should be the gold standard for determining PD (ultra)structure.

Scanning EM (SEM) is typically used to generate images of sample surfaces and does not reveal internal structures; however, combining serial SEM images can be used to produce 3D projections of an object, allowing 3D analysis of larger sample volumes and thicker specimens than TEM tomography. Two approaches for serial SEM-based imaging are serial block face-SEM (SBF-SEM) and focused ion beam-SEM (FIB-SEM), and both have been adopted to analyze PD structure and distribution. Importantly, the same samples that are prepared for thin-section TEM and TEM tomography can be used for 3D SEM [54]. SBF-SEM was used to reveal defective sieve pore formation in the root phloem of the *choline transporter1* (*cher1/clt1*) mutant[90] and to discover funnel PD in the phloem-pole pericycle in the Arabidopsis roots[11]. A pipeline for adopting SBF-SEM for imaging PD distribution and structure has recently become available[91], and we expect that this will lead to wider adoption of the 3D imaging technique for PD analyses. FIB-SEM analysis of *Nicotiana benthamiana* leaves generated a 3D projection of approximately 10 µm of cell wall and the subtending chloroplasts[1]. The presence of pit fields of PD was revealed in this 3D projection, and even with images collected every 20 nm, there was sufficient detail to determine whether individual PD were simple or complex[92]. Any plant tissues can be imaged by FIB-SEM, as demonstrated by examination of PD in the nitrogen-fixing nodules on the roots of a legume (Figure 4).

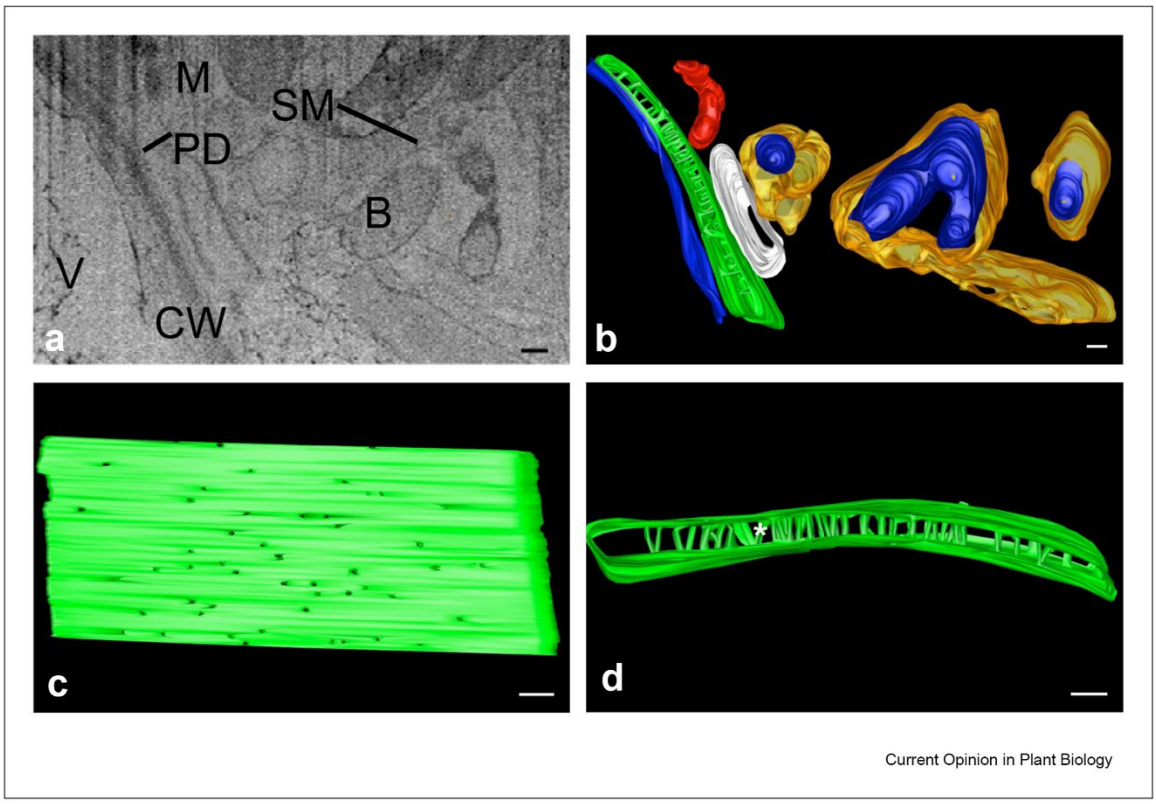


**Figure 4: Focused ion beam–scanning electron microscopy (FIB–SEM) reveals nodule ultrastructure and PD.**

(a) An SEM image of a region of a nitrogen-fixing nodule formed on *Medicago truncatula* roots by *Sinorhizobium meliloti* showing an infected cell and a companion uninfected cell. The image is a single slice of a series of 104 images. (b) Reconstruction of a FIB–SEM tomogram of a *Medicago truncatula* nodule. A total of 104 serial SEM images were combined to generate the 3D model. (c) Many PD span the cell wall shared by the infected and uninfected cell. (d) 3D reconstruction also allows PD structure to be determined; a branched plasmodesma is marked with a white asterisk. Vacuole (V, blue); cell wall (CW, green); mitochondria (M, red); bacterioid (B, dark blue); symbiosome membrane (SM, orange); scale bar = 500 nm.

In summary, there exists a comprehensive suite of resources that can be used to decipher how PD form and function. There are several mutants with defective PD in which these techniques could be applied to examine PD cell biology[93]. Future improvements in these techniques, especially increased temporal and spatial resolution and ease of sample preparation in high-end imaging, will no doubt enhance this research area further.

### *TEM tomography*

TEM tomography reconstructs the internal three-dimensional structure of an object by taking serial-tilting projection images by TEM and back projection of these images[86]. Typically, 100-150 nm-thick sections of resin-embedded fixed samples are examined at 100-120 kV. Images are collected from -70° through +70° of tilt (commonly -65° to +65°) and an image is collected at every degree of tilt or as desired with a CCD camera. For maximal resolution, the sample is rotated 90° and a second tilt series of images is collected to produce a dual axis tomogram. Images are computationally recombined using software like IMOD[94] to produce 3D models. One limitation to TEM tomography for studying large cellular volumes is sample thickness, which is restricted to around 150-200 nm on standard TEMs operating at voltages below 300kV.

### *FIB-SEM*

Focused Ion Beam milling combined with SEM (FIB-SEM) uses a beam of ions (usually gallium) to slice away successive layers of a sample, with the SEM collecting an orthogonal image of each layer uncovered. Samples can be milled in steps as small as

5 nm and the resulting images can be used to generate three-dimensional images of biological cells and tissues with excellent z-axis resolution[95]. Although FIB-SEM produces similar images to TEM, FIB-SEM allows serial reconstructions of larger volumes of tissues to be generated quickly and automatically. One major advantage of FIB-SEM is that the thickness of a sample that can be analyzed is only limited by the time one is willing to spend collecting images.

***SBF-SEM***

Serial block face-scanning electron microscopy (SBF-SEM) uses a diamond knife mounted in the machine to repeatedly cut the sample section by section, generating serial sections that are then imaged by scanning electron microscope. The images are then computationally recombined to enable high resolution 3D imaging of biological samples which have been fixed, stained, and embedded in resin. It is also amenable to other materials that can be sectioned using an ultramicrotome. SBF-SEM can provide nanometer level ultrastructural data over relatively large fields of view and up to several microns in x, y and z axes.

# V. AIMS OF THE DISSERTATION

The central hypothesis of this proposal is that **SA regulates PD in a concentration-dependent manner and with complex temporal dynamics by adjusting callose at PD and changing PD structure through modification of cellular processes involved in secondary PD formation.**

The research presented in this thesis addresses three main questions centered on the role of salicylic acid in regulating plasmodesmata.

1. **Can the detection of plasmodesmal callose be optimized to remove experimental variability and provide a reliable means to examine the SA-callose relationship?**
2. **Are there fine-scale dynamics in the production of callose induced by SA?**
3. **Does SA regulate PD only through callose or are other mechanisms involved?**

These questions were addressed using pharmacological and cell biological approaches in Figure 3. Three methods were evaluated to determine the most effective technique for measuring callose at PD using aniline blue staining (Chapter 2). The effects of SA concentrations, treatment times, PD structure, distribution, and context dependence on intercellular trafficking were determined (Chapter 3). A summary and future directions based on findings are presented (Chapter 4). Materials and methods used are documented (Chapter 5).

# CHAPTER 2

# METHOD OPTIMIZATION; DETECTION AND QUANTIFICATION OF PLASMODESMAL CALLOSE IN *NICOTIANA BENTHAMIANA* LEAVES USING ANILINE BLUE

## Abstract

Callose, a beta-(1,3)-D-glucan polymer, is essential for regulating intercellular trafficking via plasmodesmata (PD). Pathogens manipulate PD-localized proteins to enable intercellular trafficking by removing callose at PD or increasing callose accumulation at PD to limit intercellular trafficking during infection. Plant hosts also use callose to regulate intercellular trafficking during defense against pathogens. Hormones like salicylic acid regulate PD-localized proteins to control PD and intercellular trafficking during innate immune responses. Measuring callose deposition in plants has emerged as a popular parameter for approximating intercellular trafficking and the activity of plant immunity. Despite the popularity of this metric there is no standard for how these measurements should be made. In this study three commonly used methods for identifying and quantifying PD callose using aniline blue staining were evaluated to determine the most effective in the *Nicotiana benthamiana* leaf model. The results reveal that the best method used aniline blue staining and fluorescent microscopy to measure callose deposition in fixed tissue.

## Introduction

In plants, cell-to-cell communication is largely mediated by numerous small pores in the cell wall called plasmodesmata (PD) that directly connect the cytoplasms of neighboring cells [96]. PD are essential for intercellular communication, plant development, and growth. In many instances PD trafficking is regulated by the controlled accumulation of the β-1,3-glucan, callose, in the cell wall surrounding

plasmodesmal pores [97,98]. Callose deposition restricts intercellular trafficking, whereas callose degradation increases intracellular trafficking. The restriction of PD trafficking occurs during defense against pathogens through the physical closure of the PD pore by the accumulation of callose [98,99].

Plant hormones regulate callose levels to influence intercellular trafficking. Exogenous application of salicylic acid (SA) to plants can activate immune responses, concomitant with inducing the accumulation of callose at PD thereby regulating PD-mediated intercellular trafficking. SA regulates PLASMODESMATA LOCATED PROTEIN (PDLP)5 to induce callose accumulation and close PD during innate immune responses [31,100]. Local pathogen infection induced the systemic acquire resistance (SAR) which is linked with the enhanced levels of callose upon secondary pathogen inoculation [101]. Previous studies show an increase in resistance to the necrotrophic fungal pathogen Botrytis cinerea in tomato occurred by callose induction by a mycorrhizal fungus, *Rhizophaus irregularis* [102,103]. PD callose has also been used as a proxy for measuring the number of PD in a cell or tissue. In presence of abscisic acid, PD pore size modified in the *moss P. patens* with PD in ABA-treated samples showing narrower compared to the control plants; no change in PD callose in response to ABA in ABA-treated sample [28].

Aniline blue is an organic compound with five aromatic rings, an amine and three sulfonate groups, and has been widely used as an effective stain for callose in plant tissues including at PD. Aniline blue ($C_{32}H_{25}N_3Na_2O_9S_3$) binds to the cell wall has a molecular formula weight of 737.73g/mole. Over the last few years, it has become fairly

common to measure PD callose levels in response to pathogen infection as a gauge of the plant's response to infection. Callose staining with aniline blue has been tested to efficiently detect and quantify callose at PD, making it a reliable tool to investigate the changes in callose levels using fluorescent microscopy. Because individual PD cannot be resolved by light microscopy, we measured the clusters of callose at PD in pitfields, which are concentrated areas of PD between 0.05 $\mu m^2$ and 4$\mu m^2$ in size. We noticed that protocols for measuring PD callose varied between labs. We therefore set out to determine which protocol was most reliable when used with leaves from *Nicotiana benthamiana*, a widely used model for plant-pathogen interactions [104]. For this, three protocols were tested to identify the most reliable protocol for callose staining with aniline blue in *N. benthamiana* leaves. We found that fixing the tissue before staining with aniline blue (method 1) is the most dependable protocol to effectively detect and quantify callose at PD in *N. benthamiana.*

## Materials and Methods

### *Plant material and callose induction*

The LAB strain of *Nicotiana benthamiana* was used in this study. Seedlings were germinated on soil for 7-10 days before transplanting to individual pots. *N. benthamiana* plants were grow on light carts under long day condition with 16 hours light (120 µmol $m^{-2}$ $s^{-1}$) and 8 hours dark at 25 °C. Miracle Gro All-purpose Plant Food fertilizer was applied after 10-13 days post germination (3 days after transplanting). The leaves of 4-5 weeks old plants were used for callose quantification and salicylic acid treatment

experiments. *N. benthamiana* leaves were infiltrated with 0.05 mM salicylic acid (Sigma-Aldrich) prepared from a 100mM stock solution in DMSO and diluted with distilled water. The SA treatment induces callose accumulation at PD and serves as a positive control to optimize aniline staining method for the quantification of callose depositions in *N. benthamiana* plant.

***Plasmodesmata callose staining and quantification.***

Three methods were evaluated for identifying callose structures. All methods used 1% aniline blue (Ward's Science plus, Rochester NY LOT AD-22103) in 0.01 M $K_3PO_4$, pH 12 buffer. Method 1 was adapted from (Zavaliev and Epel, 2015) to image callose utilizing aniline blue on fixed tissues[57]. Method 2 was adapted from John Innes Center[105] (Aniline blue staining of quantification of plasmodesmal callose (jic.ac.uk)), and Method 3 was adapted from the Lee Lab University of Delaware[35]. For all three methods the 4$^{th}$ and 5$^{th}$ leaves of *N. benthamiana* were directly infiltrated with a 1mL syringe containing 1% aniline blue.

***Method 1: Staining and sample preparation****.*

An entire cut leaf was submerged in 95-96% ethanol in a 500-mL polypropylene jar to bleach the tissue. The petiole was held with forceps to avoid mechanical damage to the leaf. The jar was sealed, and samples were incubated at room temperature on a shaker at 30-40 rpm for at least 5 hours. The ethanol solution was changed to speed up the bleaching after 2 hours incubation. Incubation was continued until the leaves were completely or nearly completely bleached, but less than 6 hours, since plasmolysis occurs at this point, and the resulting separation of the plasma membrane and cell wall

make pitfield identification difficult. Bleached leaves were removed by gently holding by the petiole to avoid breaking the leaf and were placed in a petri dish and cut into 5 mm wide strips with a razor blade. The cut strips were rehydrated in double distilled water (DDW) with 0.01% Tween-20 and incubated at room temperature for 1 hour on a shaker at 30-40 rpm. The tissues were then transferred to a small petri dish (35mm in diameter and 10 mm heights) and submerged in aniline blue solution. The unlidded petri dish was placed in a house vacuum desiccator and vacuumed for approximately 10 minutes followed by slow release of pressure. The petri dish was covered and sealed with foil before shaking at room temperature for 2 hours at 30-40 rpm. No de-staining was necessary. The samples were then imaged with confocal microscopy.

***Method 2: Callose staining in unfixed tissue.***

The $4^{th}$ and $5^{th}$ leaves of 4- to 5-weeks-old *N. benthamiana* plants were infiltrated with 1% aniline blue using a 1-mL needleless syringe. Leaves were then cut into 3-5mm strips and placed on a microscope slide for confocal microscopy.

***Method 3: One hour aniline blue staining on unfixed tissue***

The leaves of 4-5 weeks old *N. benthamiana* plants were cut into 5mm strips and incubated in 1% aniline blue in 0.01 M $K_3PO_4$, pH 12 buffer in the dark for 30-60 minutes. Aluminum foil was used to cover the petri dish containing the cut leaves and 1% aniline blue solution. After submerging leaf tissues in a staining solution, they were vacuumed gently for 10 minutes.

### *Confocal microscopy*

A Leica SP8 laser scanning confocal scanning microscope (Leica, Whetzlar, Germany) was used to imaged callose deposits from the abaxial side of the leave tissues using a 40x/1.10 water immersion objective (HC PL APO CS2 40x/1.10 WATER). The excitation for aniline blue was with a 405-nm laser, UV (0.5-1%) and emission was captured from 415 nm-525 nm. Z-stacks were collected from multiple regions of interest (ROI) (approximately 23-25 ROIs per leaf) were collected. Z stacks were collected using the system optimized step size (<1 µm). All three methods were analyzed using ImageJ to quantify aniline blue-stained callose at plasmodesmata.

### *Scanning parameters and Acquisition settings*

Frame scanning mode: XYZ

Frame size: 1024 x 1024

Zoom factor: 5

Line average: 1

Pixel depth: 8 bit

Scan speed: 400 Hz

To observe as many PD as possible, the pinhole aperture was initially set to open. Laser intensity and gain were adjusted to optimize the PD fluorescence against the background signal, while being careful to avoid oversaturation of callose sites. Saturation of the stomata was permitted. 23-25 Z-stacks were imaged using the same settings of image acquisition in the independent experiments.

### *ImageJ analyses*

For image analysis, the raw files were converted into max intensity Z-projections in ImageJ [106,107]. Images were converted into 8-bit grayscale, inverted, and threshold adjusted to identify pixels of pitfields and to reduce background noise for better analysis. Connected components in a binary image were separated by watershed separation. An automatic particle analysis was performed to obtain information on PD-associated callose particles. Pitfields per 100 $\mu m^2$ cell wall were calculated using Microsoft Excel.

### *Statistical analyses*

Interquartile analysis was done in Excel by using the interquartile range method to remove outliers. Data were analyzed using GraphPad Prism 9 (version 9.5.0) and presented as Box & Whiskers plots with all pitfields values. Plots display the middle line representing the median, 1-4 quartiles with the minimum and maximum values within the interquartile range. Pitfields per 100 $\mu m^2$ cell wall were normalized to untreated control. An unequal variances Welch's t-test was conducted for each plot.

### *CalloseQuant and quantification*

Semi-automated quantification of pitfields was performed using the CalloseQuant plugin developed by *C. Huang et al.* 2022. Images captured using confocal microscopy were first auto-scaled and converted into .tiff format using FIJI ImageJ[108]. Depending on the nature of the confocal micrograph, the peak prominence values range were between 25-45μm, and the measurement radius was maintained at 5.5 for Method A. For method B, the rolling ball radius range was used with 6-8 pixels, and the mean filter radius was

kept at 2 pixels. The images were thresholded using Bremsen's technique at a radius of 50. Due to programming errors in Method B, the thresholded particles were manually analyzed at a micron size of 0.02-infinity with a circularity range of 0.00-1.00. All the data collected were manually checked for the elimination of signals and data points outside of the region of interest (ROI).

## Results

Aniline blue staining  is commonly use in numerous studies to determine the distribution of PD in several different tissues during plant development[18,58]. Here, we measured PD that are distributed in clusters called pitfields. We tested three different staining protocols and collected multiple z-stacks using confocal microscopy to determine which method gave the most reliable outcomes for measuring plasmodesmata. PD density was measured in the epidermal cell walls of *N. benthamiana*, a model plant for studying PD. Details of each method is presented in the Materials and Methods. Method 1 involved fixing the tissue before staining the callose with aniline blue. Representative images obtained in maximum intensity z-stack projections from confocal microscopy of the untreated control and SA treatment are shown in Figure 5A. The control shows multiple pitfields in the cell wall, and other artifacts that are not within the cell wall (marked with white arrows). Method 2 for staining involved direct infiltration of aniline blue into leaves while they were still attached to the plants.  A representative maximum intensity projection of a z-stack is shown in Figure 5b. Aniline blue foci representing PD were clearly observed in the cell wall, and staining of other structures were rarely observed.

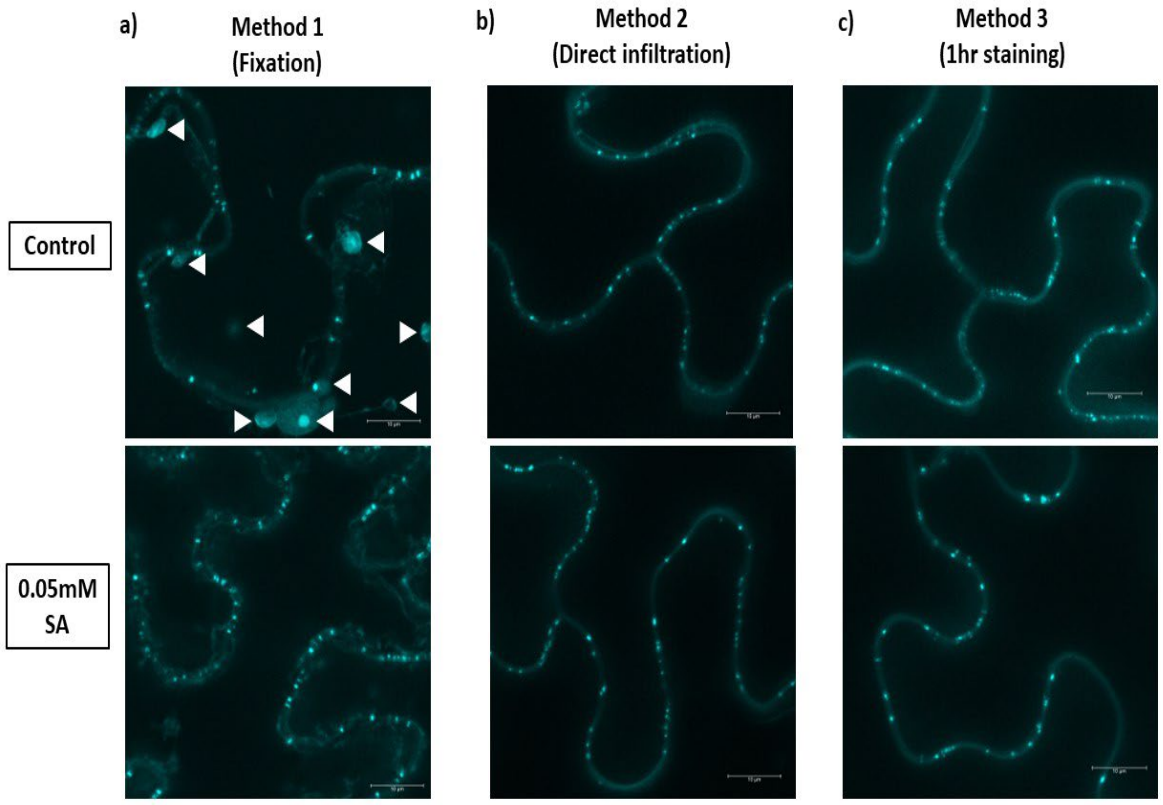


**Figure 5: Three methods of aniline blue staining for plasmodesmata pitfield imaging.**

*N. benthamiana* leaf epidermal cells with staining of plasmodesmata (PD)-associated callose using 1% Aniline blue concentration. Representative images are shown for three different callose staining methods, both for untreated and SA treated plants. Panels corresponding to the three methods of aniline blue staining: a) fixed tissue, b) non-fixed tissue directly infiltrated with aniline blue, and c) non-fixed tissue stained with aniline blue for 30-60 minutes. Images are maximum projections of Z-stacks of images collected by confocal fluorescence microscopy and were used for the quantification of aniline blue-stained plasmodesmata (PD) pitfields. Scale bar = 10μm

Method 3 involved treating detached, unfixed leaves with aniline blue for 1 hour before imaging. A representative image is shown in Figure 5c. Like with Method 2, aniline blue foci were only detected in the cell wall and there were few, if any, other structures stained.

To determine the average density of PD pitfields, at least 25 z-sacks were collected from each of three to four biological replicates for analysis using ImageJ Fiji [106,107]. Pitfields were quantified per 100um$^2$ of cell wall for a region of interest. The workflow of the analysis for identification of callose deposition at PD is shown in Figure 9. To describe the analysis pipeline, the dataset used to generate Figure 5A is used. The maximum intensity projection (Figure 9a) was converted to 8-bit (Figure 9b). The image was then inverted to perform inverse binary thresholding to measure the area of pitfields shown in red spots (Figure 9c-9f). Cell-wall lengths were measured by tracing the cell wall in the region of interest (Figure 9h). Only the total number of pitfields within the traced cell wall was calculated (Figure 9g) within each region of interest as pitfields/unit area. More details on the analysis of the pitfields/unit area can be found in the Materials and Methods of this chapter. Figure 6 shows the result of method comparison on the control *N. benthamiana* plant with all data values. The colors represent each biological replicate with the same experimental conditions but with different batches of plants. An interquartile range (IQR) analysis was used to overcome the sensitivity to extreme data values. To determine if the median pitfield densities were significantly different between the three methods, the data for the untreated controls were analyzed with and without IQR analysis. For the IQR analysis, outlier data points

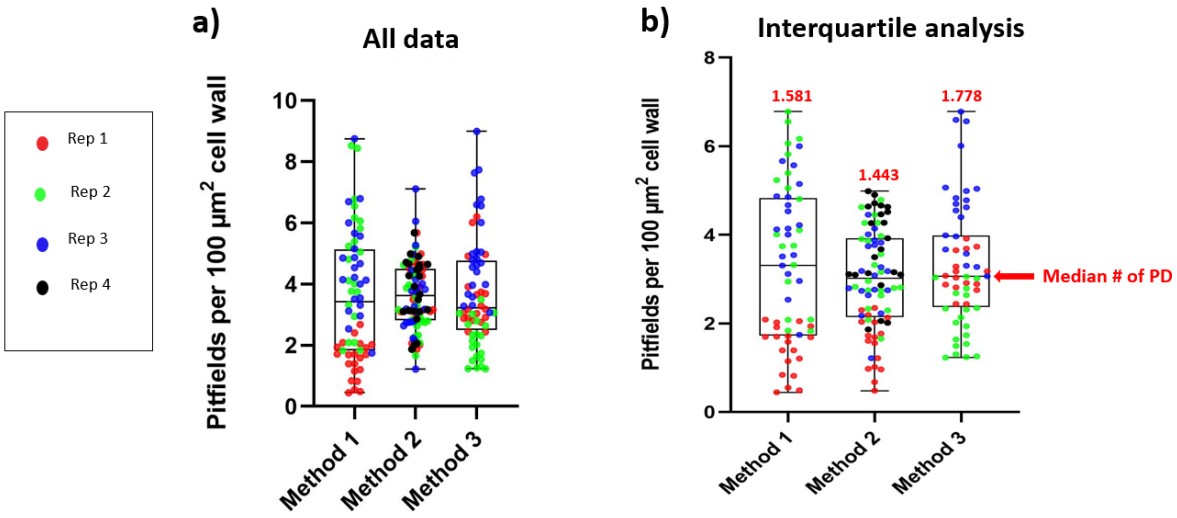


**Figure 6: Reproducibility of pitfield quantification across methods**

Pitfield quantification data from 3-4 biological replicates using each method were combined and are plotted using different colors. a) The medians are shown using a box and whisker plot. B) The same data is replotted using an interquartile analysis to remove outliers from each replicate. Median values are displayed above each plot in pitfields per 100 $\mu m^2$ of cell wall. Medians from all methods are not significantly different based on the Tukey's multiple comparisons test. P-values for method 1 vs. method 2 combination are 0.5037; method 1 vs. method 3 contain a p-value of 0.9915 and method 2 vs method 3 contain a p-value of 0.4271.

more than 1.5 times the interquartile range were excluded. The median within the interquartile range shows Method 1 untreated has a median of 1.581, Method 2 has a median of 1.443, and Method 3 has a median of 1.778 pitfields per 100 $um^2$ cell wall, and none were significantly different from each other (Figure 6b). All three methods display similar medians in the control plants, so that does not give us a clear determination of which method is best for callose quantification at PD.

Salicylic acid reduces intercellular trafficking via PD during innate immune response against pathogens [109]. Treatment with SA induced the accumulation of callose at PD in *Arabidopsis thaliana* plants exposed to the elicitor flg22 [110,111] or pathogen-associated molecular pattern (PAMP) derived from bacterial flagellin protein [112]. To determine which method would best reflect the accumulation of callose at PD induced by SA, *N. benthamiana* leaves were treated with 0.05 mM SA, and 12 hours later the leaves were stained with aniline blue using each of the previously described methods. We analyzed multiple datasets of images from 0.05 mM SA-treated *N. benthamiana* plants along with the control. Figure 7 shows all data values and the interquartile analysis of the various methods in treated and untreated controls. For Method 1, each replicate showed an increase in PD callose, reflected as an increase in PD density (Figure 7a and Figure 11). The median pitfield density increased from 3.417 to 5.731 on treatment with SA ($p<0.0005$) (Figure 10a). For method 2, however, the individual replicates did not consistently reveal increased callose at PD in response to SA treatment (Figure 7b and Figure 10b). This is best exemplified by Rep 2 (green dots) and Rep 4 (black dots), which show no change and a decrease in pitfield density on SA

**Figure 7: Quantification of PD-associated callose in *N. benthamiana* leaves treated with 0.05 mM salicylic acid (SA) to induce callose.**

Pitfield densities were quantified for at least 23 regions of interest (ROIs) for 3 biological replicates of fixed (a) and 1hr staining (c; red, blue, and orange pitfields) and 4 biological replicates of direct infiltrated aniline blue (b; red, blue, orange, and black pitfields). Fold induction by SA for all three methods is shown (d), along with the standard deviation, standard error and range. Statistical significance was determined by the Welch's t-test ($p<0.0001$).

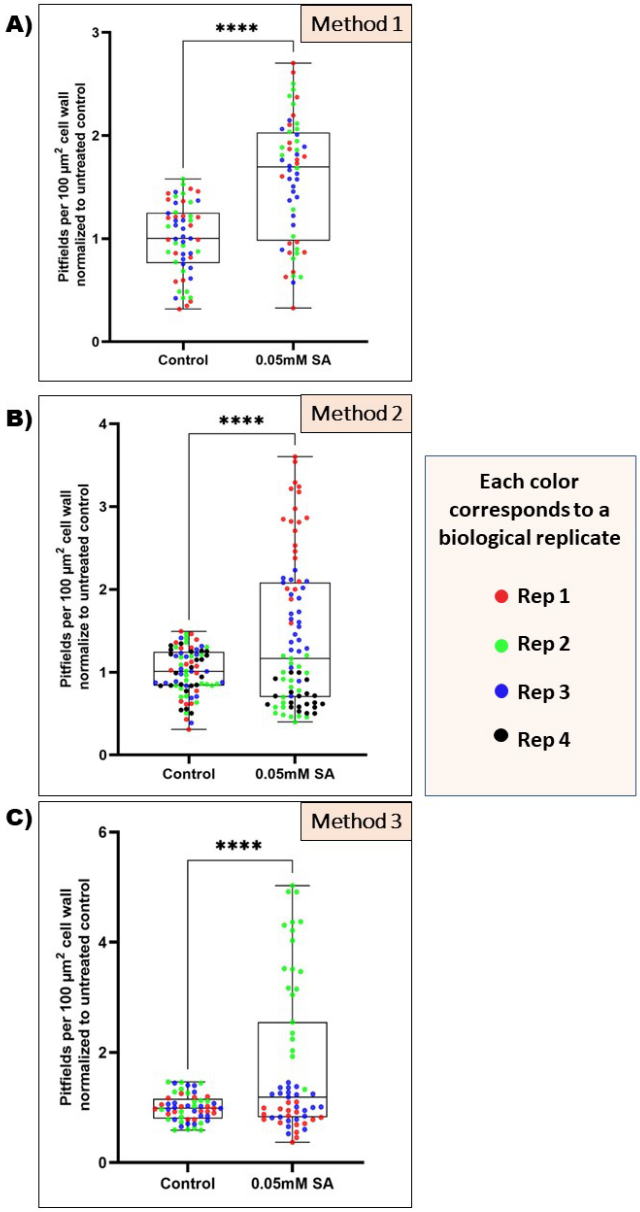


d)

| | Fold induction by SA | Std. Deviation | Std. Error of Mean | Range of SA | Difference in Range |
|---|---|---|---|---|---|
| **Method 1** | 1.58 | 0.5959 | 0.07963 | 0.326 - 2.703 | 2.377 |
| **Method 2** | 1.44 | 0.8896 | 0.09765 | 0.397 - 3.602 | 3.205 |
| **Method 3** | 1.78 | 1.361 | 0.1772 | 0.373 - 5.031 | 4.658 |

application, respectively. While method 2 shows no significant differences in the control and SA treatment, method 3 revealed significant differences in the control and SA treated plants (Figure 7c and Figure 10c). The median pitfield density increased from 3.226 to 4.613 on treatment with SA ($p<0.0005$) (Figure 10c). However, the individual data reproducibility of each method clarifies that method 1 generated similar experimental results for each biological replicate (Figure 11.). In contrast, in our testing, method 2 and method 3 showed problems with high variability between replicates (Figure 12 and 13). Applying the IQR analysis for both the control and SA treatment datasets led to method 2 going from no significant difference to statistically significant difference between the control and SA treatment (Figure 10b and Figure 7b). In order to combine all replicates, despite the variability between each replicate, we normalized the treatment to the average control group within each replicate. Figure 7 shows normalized data of the three methods along with the fold induction, the range, and standard deviation. Method 1 has the smallest range (0.326 to 2.703) with the lowest standard deviation error of 0.08. Data points from each replicate are spread evenly on method 1, whereas methods 2 and 3 show data points for each replicate are separated and not evenly spread between the ranges in the treated plants (Figure 7b and 7c). In Figure 8, we compared manual analysis data from method 1 to the CalloseQuant, a plug-in for semi-automated image analysis that is described to be a simple and fast in vivo staining procedure for the image and quantification of callose at PD[108]. The CalloseQuant plug-in comes with two methods; method A is highly sensitive to fluorescence intensity whereas method B has a low sensitivity to fluorescence due to thresholding [108]. Both

**Figure 8: Pitfield deposition quantification using manual and automated (CalloseQuant) methods in ImageJ.**

Callose-stained images using Method 1 (fixation) a) were quantified using manual counting, CalloseQuant A, and CalloseQuant B, both for SA treated and untreated samples. Three biological replicates are shown using different colors. Fold induction in response to SA treatment, standard deviation, standard error and range are shown (b).

**A)**

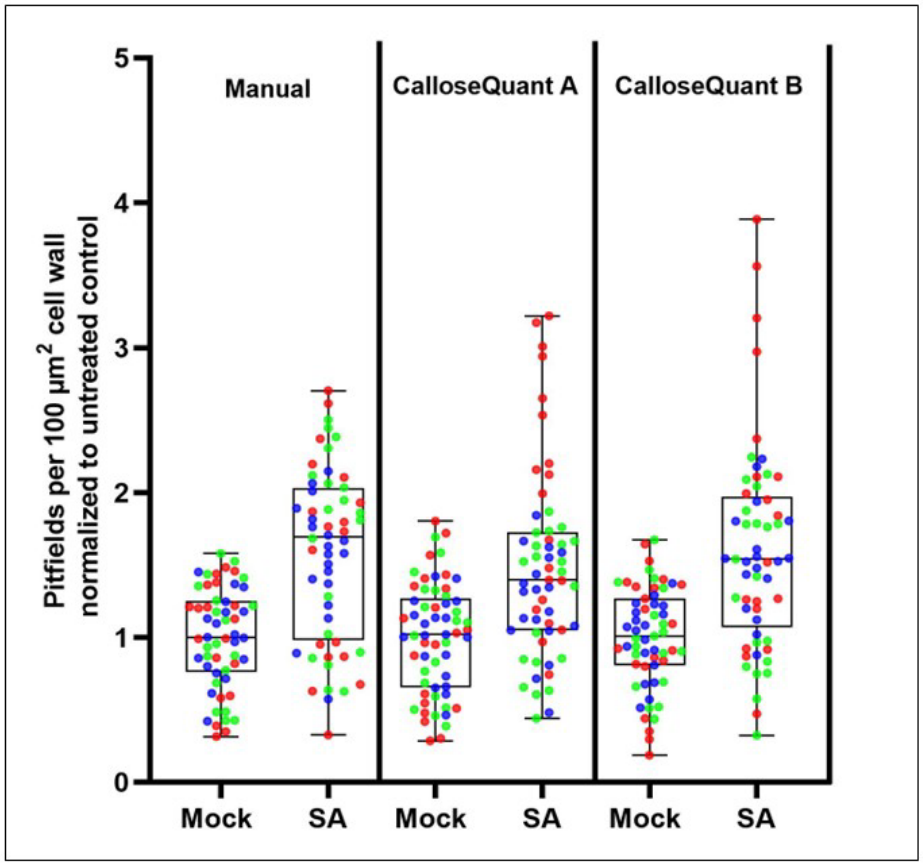


**B)**

| | Fold induction by SA | Std. Deviation | Std. Error of Mean | Range |
|---|---|---|---|---|
| **Manual** | 1.58 | 0.5959 | 0.07963 | 0.326 - 2.703 |
| **CalloseQuant A** | 1.48 | 0.6451 | 0.08398 | 0.441 - 3.221 |
| **CalloseQuant B** | 1.60 | 0.7086 | 0.09386 | 0.325 - 3.885 |

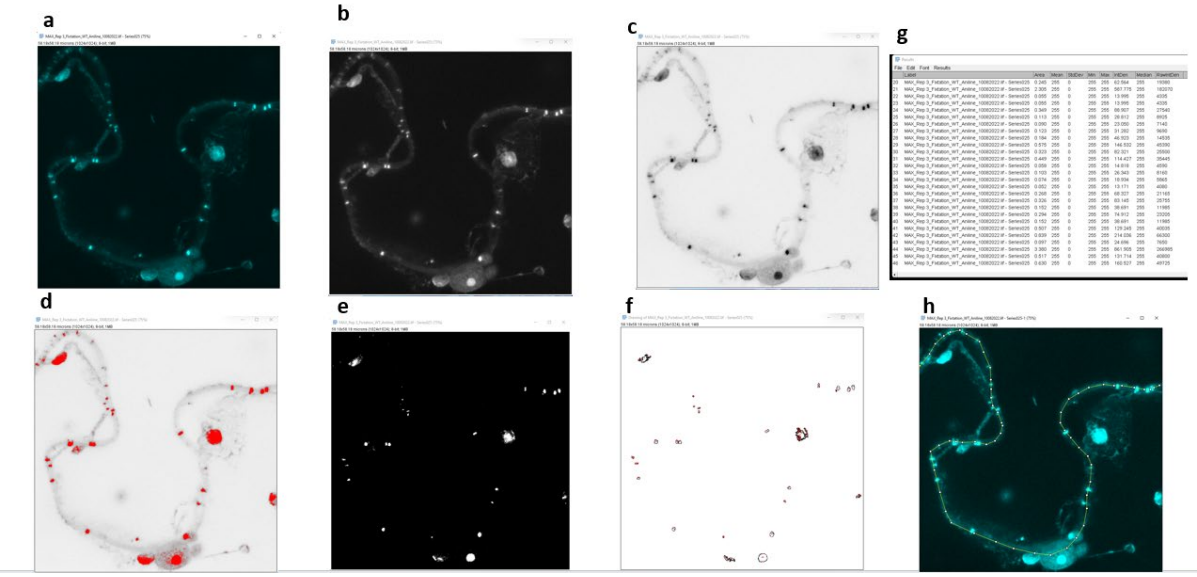


**Figure 9: Using FIJI to quantify the number of pitfields and measure the cell length (area)**

Maximum intensity projections of a Z-stack of images (a) are converted to 8 bits (b), inverted (c), and a threshold is set to select callose staining (red; d) along the cell wall. Adjoining foci are separated into distinct bodies using binary watershed (e). Any signal that is not along the cell wall is manually excluded (f, g). Lastly, the length of cell wall within ROI is measured using the segmented line tool (h).

**Figure 10: Pitfield quantifications for each method using all data, without interquartile analysis.**

Quantification of staining of callose depositions with 1% aniline blue in untreated leaves and after 12 hours salicylic acid (SA) treatment. Method 1 (a) shows a significant difference (p=0.0001), method 2 (b) is not significant (p=0.0705), and method 3 (c) shows a significant difference (p=0.0014) using the Welch's t-test (ns, p>0.05; *, p≤0.05; **, p≤0.01; ***, p≤0.001; p< ****, p<0.0001).

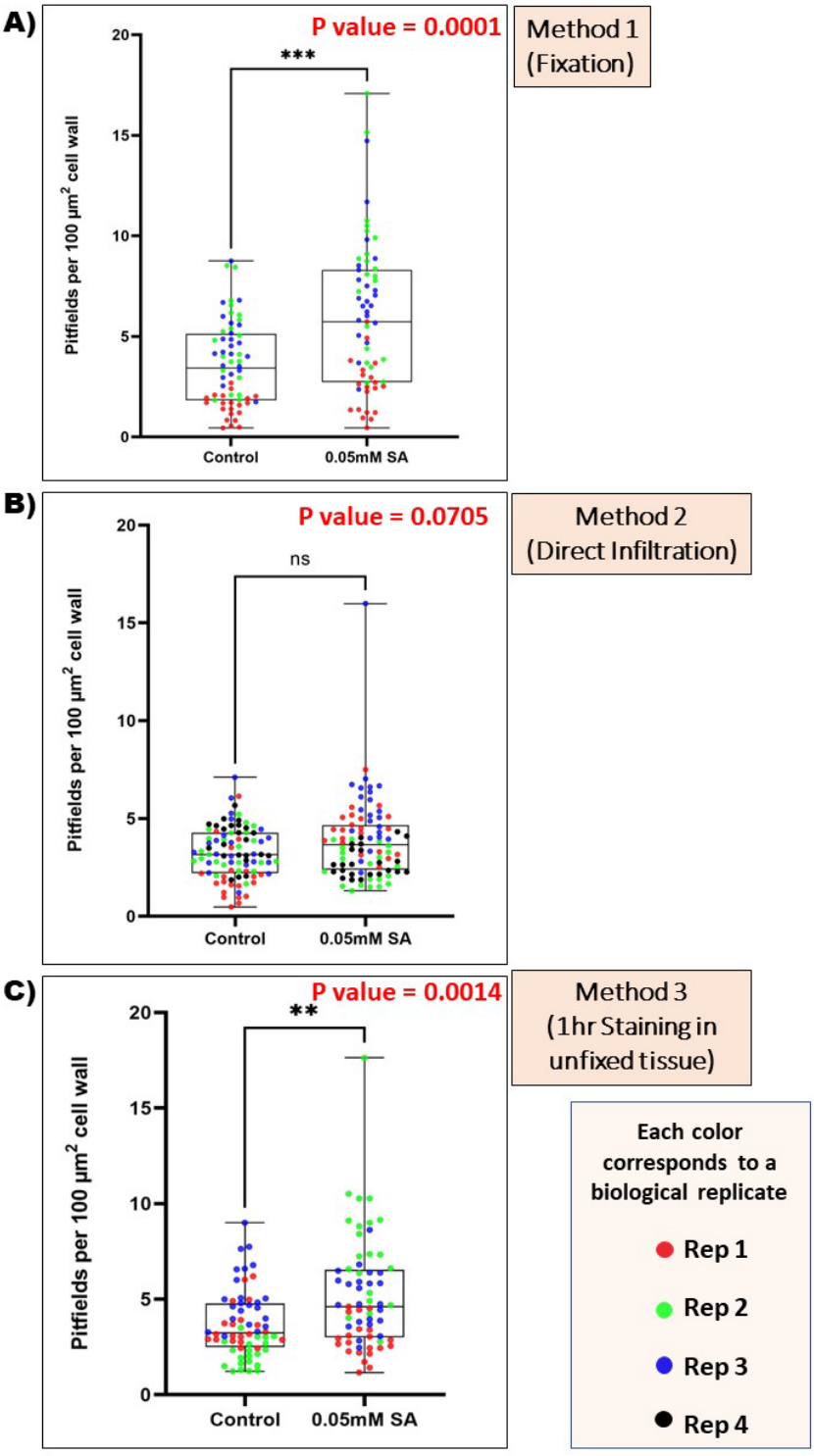
A)
P value = 0.0001
***
Pitfields per 100 µm² cell wall
20
15
10
5
0
Control
0.05mM SA
Method 1
(Fixation)
B)
P value = 0.0705
ns
Pitfields per 100 µm² cell wall
20
15
10
5
0
Control
0.05mM SA
Method 2
(Direct Infiltration)
C)
P value = 0.0014
**
Pitfields per 100 µm² cell wall
20
15
10
5
0
Control
0.05mM SA
Method 3
(1hr Staining in
unfixed tissue)
Each color
corresponds to a
biological replicate
Rep 1
Rep 2
Rep 3
Rep 4

**Figure 11: Reproducibility of pitfield quantifications aniline blue staining method 1**.

Pitfields were quantified using method 1 with each of 3 biological replicates plotted independently, along with their fold changes (control:SA treatment). Statistical significance between untreated and SA treated are shown (Welch's t-test; ns, $p>0.05$; *, $p\leq0.05$; **, $p\leq0.01$; ***, $p\leq0.001$; p< ****, $p<0.0001$)

Method 1
(Fixation)

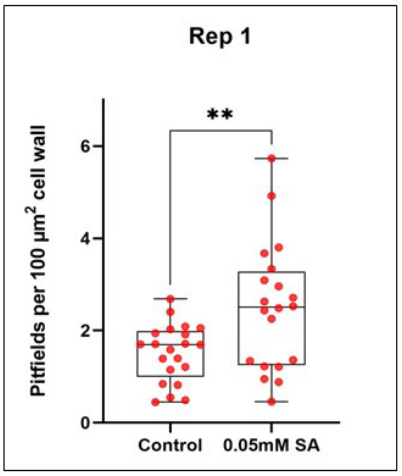


**Fold change:**

**0.55**

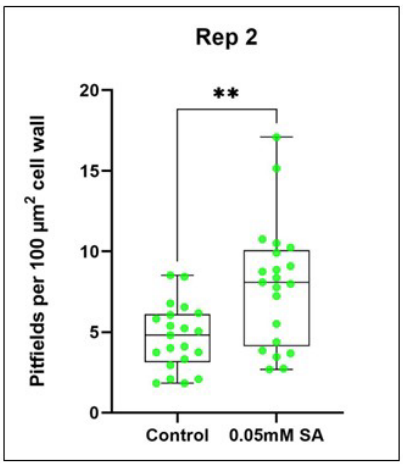


**0.64**

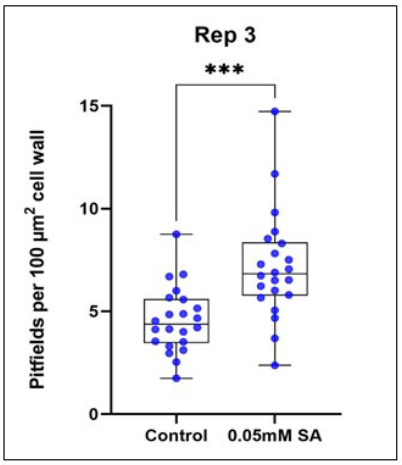


**0.55**

**Figure 12: Reproducibility of pitfield quantifications aniline blue staining method 2.**

Pitfields were quantified using method 2 with each of 4 biological replicates plotted independently, along with their fold changes (control:SA treatment). Statistical significance between untreated and SA treated are shown (Welch's t-test; ns, $p>0.05$; *, $p\leq0.05$; **, $p\leq0.01$; ***, $p\leq0.001$; p< ****, $p<0.0001$).

Method 2
(Direct Infiltration)

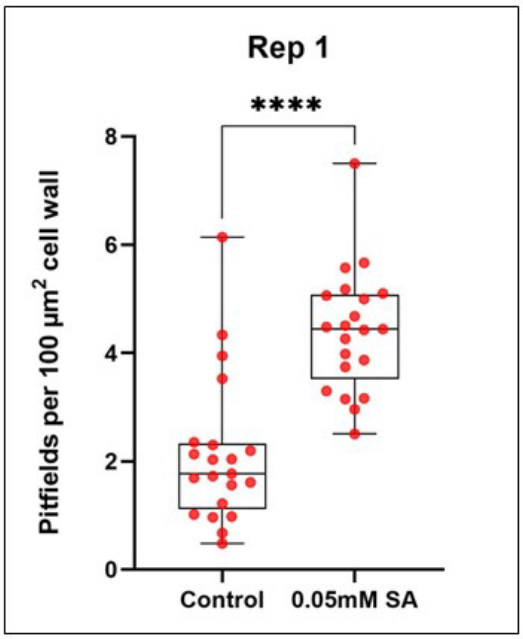


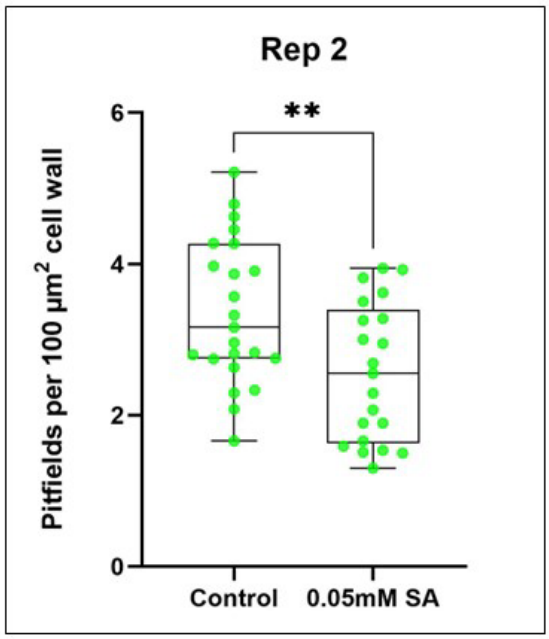


**Fold change: 1.70**

**-0.22**

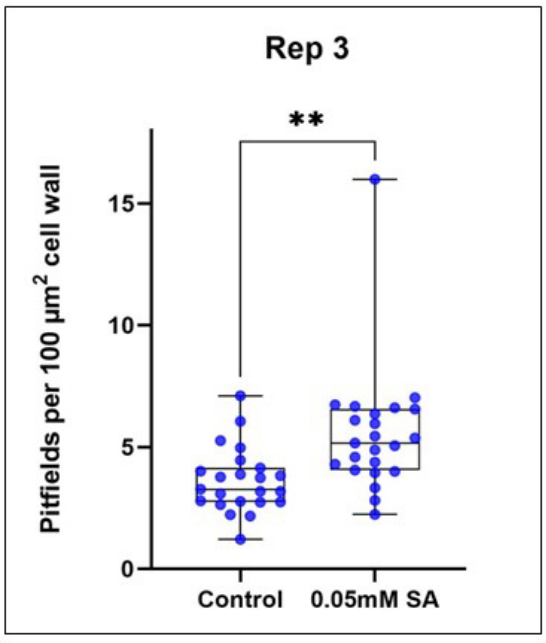


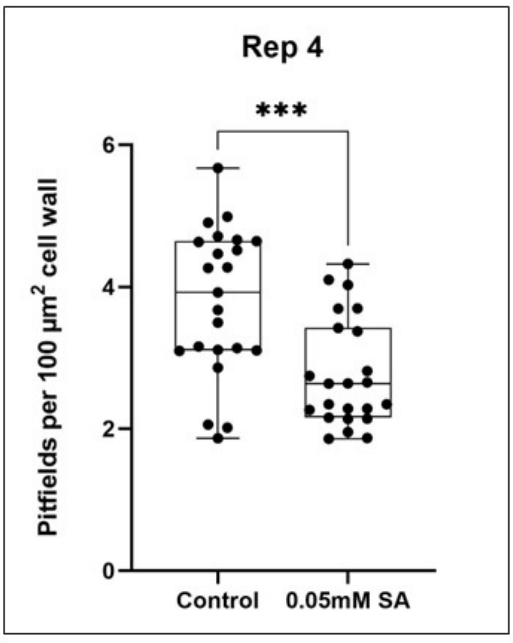


**0.61**

**-0.31**

**Figure 13: Reproducibility of pitfield quantifications aniline blue staining method 3.**

Pitfields were quantified using method 3, with each of 3 biological replicates plotted independently, along with their fold changes (control:SA treatment). Statistical significance between untreated and SA treated are shown (Welch's t-test; ns, $p>0.05$; *, $p\leq0.05$; **, $p\leq0.01$; ***, $p\leq0.001$; p< ****, $p<0.0001$).

Method 3
(1hr Staining in unfixed tissue)

**Fold change:**

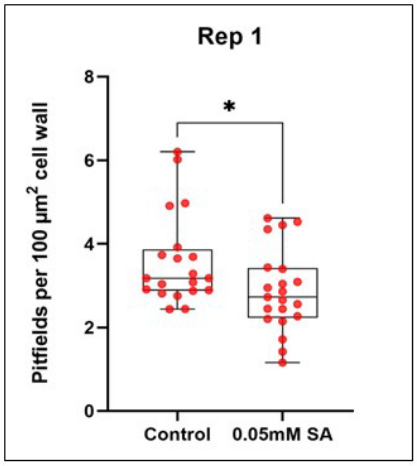


**-0.20**

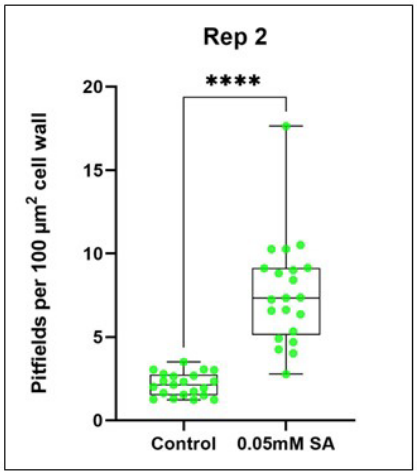


**2.42**

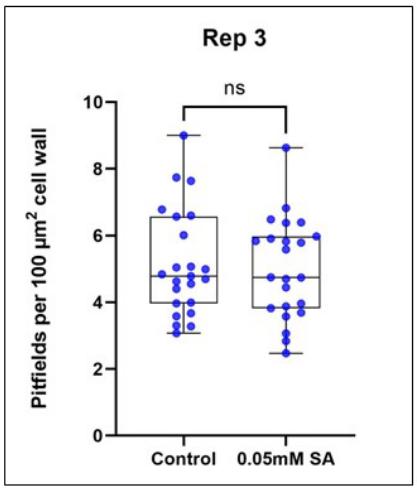


**0.036**

approaches were used with the callosequant.ijm plugin to measure the pitfields and callose quantity of confocal images of method 1. While the manual analysis showed the smallest range compared to CalloseQuant A and B, the fold induction by the SA was similar in all three approaches (Figure 8). If CalloseQuant A is said to be highly sensitive to fluorescence, we expected to see higher ranges of pitfields compared to CalloseQuant B (Figure 8b).

## DISCUSSION

Callose dynamics plays an important role in allowing or limiting trafficking of signal molecules through PD. Callose accumulation at PD restricts intercellular trafficking whereas the removal of callose increases cell-to-cell trafficking of molecules. The well-known defense hormone salicylic acid is preferentially transported via the apoplast pathway and restricts intercellular trafficking through the deposition of callose at PD, making it a useful tool for inducing callose deposition and facilitating PD detection by aniline blue staining. Because of its ability to fluorescently stain callose (β 1,3 glucan), cellulose, and related polysaccharides in the cell walls, aniline blue has been widely adopted for visualization of callose deposition at PD. At present different methods are used to administer this aniline blue staining, and without a rigorous comparison of these methods, it is difficult to make direct comparisons between studies. In this study, we compared the results and reproducibility of three methods for PD staining using aniline blue. We found that fixation of *N. benthamiana* leaf tissue prior to aniline blue staining produced the most reproducible results with similar fold changes and was better able to detect significant differences in our experiment (Figure 11). We

also compared the more manual quantification of the resulting images described here and a promising new semi-automated pitfield counting plugin. The CalloseQuant plugin (*Callosequant.ijm*) developed by Hung, Mutterer, & Heinlein is primarily used for quantifying callose accumulation at PD as well as measuring the pitfields per unit length of cell wall[108]. For high-throughput studies, an automated PD quantification tool will clearly benefit the field. In our hands, CalloseQuant showed similar medians in our PD quantifications, although the range was wider (Figure 8).

CalloseQuant A is highly sensitive to fluorescence intensity whereas CalloseQuant B has low sensitivity because of thresholding, which makes it especially susceptible to the presence of high fluorescence bodies (organelles) outside the ROI and outside the cell wall area. 2D images with lower magnification are recommended for use with CalloseQuant. However, z-stacks (3D) images give more details on pitfields in the z-axis and binary watershed segmentation which separates closely adjacent foci given the correct value for callose deposition at PD. Lower magnification images of aniline blue staining would be more likely show multiple fluorescent bodies as one, reducing quantifications. Conversely, the absence of any step to exclude non-cell wall-associated signal would inflate quantifications, a concern since aniline blue stains other cellular components. As a result, using individual ROIs at higher magnification to analyze callose deposition may produce more accurate counts. Accordingly, the range and standard deviation/error were higher for CalloseQuant quantifications than the manual method. Notably, the fixation method of aniline blue staining which performed the best in our testing, also contains more artifactual signals due to the ethanol fixation.

The quantification method used here excludes such signals when not localized to the cell wall, so the semiautomated approach should be evaluated with the methods (2 and 3) containing little to no signal outside the cell wall (Figure 5). However, these potential shortcomings may well be less meaningful at higher sample sizes, and being able to reliably and reproducibly show relative changes between treatments at high throughput is more important than absolute quantifications, both of which are beyond the scope of this study to evaluate.

# CHAPTER 3

# SALICYLIC ACID, INTERCELLULAR TRAFFICKING, AND PD DISTRIBUTION

## INTRODUCTION

### *3.1 The importance of plasmodesmata: intercellular trafficking and communication in plants.*

Pores in plant cell walls, plasmodesmata (PD), directly connect neighboring cells allowing the intercellular trafficking of small molecules like metabolites and hormones, as well as macromolecules like small RNAs and protein transcription factors that act as signaling molecules during development and defense. Thus, PD are indispensable for signaling and communication between plant cells. PD are structurally complex yet diverse, and transmission electron microscopy (TEM) reveals that they are usually 30-50 nm in diameter and can consist of a single opening or multiple openings connected to each other via a central cavity[4]. The desmotubule at the center of the PD consists of compressed endoplasmic reticulum (ER) and thus allows ER continuity between cells. The desmotubule is tethered to the plasma membrane (PM) of PD by PD-regulatory proteins synaptotagmin A (SYTA/SYT1), suggesting that PD are specialized ER-PM contact sites[96]. The major conduit for cell-to-cell trafficking is likely the cytoplasmic sleeve, the cytoplasm-filled space between the desmotubule and the PMs of the connected cells. PD trafficking is often regulated by the controlled accumulation of the β-1,3-glucan callose in the cell wall surrounding a plasmodesmal pore[97] (Figure 2). Callose deposition reduces intercellular trafficking while the converse occurs when callose is removed[98].

### *3.2 Intercellular trafficking via plasmodesmata is important for plant defense and is regulated by hormones.*

Beyond their roles in development, PD are also critical for defense against pathogen infection[113]. Plants are not passive in the face of pathogen intrusion, and they have evolved to limit pathogen ingress via PD. One major strategy is to limit trafficking of pathogen-derived molecules (effectors) or pathogens themselves (viruses, some fungi, and oomycetes) through PD. The restriction of PD trafficking capacity during development or in defense against pathogens is usually accomplished through the physical occlusion of the PD pore by the accumulation callose. In both instances, the regulated accumulation of callose is mediated by hormones[98]. Another function of PD during defense is facilitating the systemic distribution of signaling molecules including hormones that initiate defense responses distal from the initial infection sites, especially during systemic acquired resistance (SAR)[99].

### *3.3 Salicylic acid (SA) regulates PD trafficking in response to pathogen infection.*

In plants, the small molecule salicylic acid (SA) plays an important physiological role growth, development, and defense against biotrophic pathogens[109]. As a hormone, SA acts by increasing the plant's response to biotic stress conditions and is essential for the whole-plant defense response termed SAR. Endogenous SA is produced through two distinct but related pathways, the isochorismate synthase (ICS) pathway and the phenylalanine ammonia-lyase (PAL) pathway[114]. To produce SA, both pathways require the primary metabolite chorismite, the product of the shikimate pathway of the plastid. Exogenous application of SA in plants can trigger immune responses[31]. SA can regulate

intercellular trafficking through plasmodesmata, and exogenous application of SA decreased intercellular flux via PD[31]. SA regulates plasmodesmata through callose dynamics, acting through the callose synthase enzyme CalS1[30] , PLASMODESMATA LOCATED PROTEINs (PDLPs)[29,31] and modulating lipid metabolism through the lipid-raft like protein REMORIN to control callose accumulation at PD[32] . SA application also accelerated the formation of complex PD[7].

Considering the importance of PD to pathogen infection, pathogens have evolved to counteract the effects of SA on PD. This is exemplified by plant viruses. SA induces plant defense against viruses[50,50,115] and one of its effects is callose accumulation at PD and reduced PD trafficking[116]. Plant viruses often, however, increase intercellular trafficking in a well-known process termed gating[3,117,118]. This suggests that the relationship between PD and SA is not straightforward but instead dynamic and complex. SAR is one form of long-lasting, broad-spectrum resistance that is induced in distal parts of a plant in response to a localized infection[99]. Several mobile chemical signals are involved in SAR[99]. Recent research shows that the methylated derivative of SA, methyl salicylate (MeSA), serves as a crucial phloem-mobile SAR signal, although MeSA is not itself necessary for SAR in distal tissues[99]. In contrast, SA does not traffic via the symplast but instead moves outside the cell in the apoplast[29]. Besides SA, other plant hormones can act non-cell-autonomously. Jasmonic acid (JA) is a lipid-derived hormone that is well known for its important role in defense against necrotrophic pathogens[119]. Experimental evidence suggests that JA and its derivatives, especially JA-conjugated to isoleucine (JA-Ile), can move systemically in plants although many

questions about the identity of the mobile molecule in JA signaling remain[120]. The effect of JA on PD has not been clearly described, although one report suggests that treatment with JA stimulated export of photoassimilate (sugar) from source leaves, suggesting altered PD trafficking[121]. While SA and JA are two of the major defense hormones, their signaling pathways are antagonistic to each other[122,123]. Given the importance of these hormones in mediating defense responses, the effects of these hormones on PD and intercellular trafficking should be clarified.

### *3.4 The effect of hormones on PD structure*

While callose deposition and removal seem to be the primary mechanism through which hormones act to control PD trafficking during development, there are instances where other changes to PD have been observed. Exogenous application of another plant hormone abscisic acid (ABA) modified PD pore size in the moss *P. patens*, with PD in ABA-treated samples being narrower than those in control plants, and no increase in PD callose in response to ABA was detected[28]. There are two major classes of PD that form at different times in development. The first class is primary PD that form during cytokinesis when strands of ER become trapped in the nascent cell wall forming between daughter cells. The second class is the secondary PD which are added to existing cell walls by a mechanism that remains elusive but must involve cell wall remodeling[4]. Exogenous application of SA induced the formation of secondary PD in Arabidopsis leaves, causing the leaves to change from simple pores to branched structures[7]. Thus, hormones may alter PD ultrastructure by means other than callose

metabolism, although this has not been experimentally verified. This possibility was investigated in the proposed research[124].

***3.5 Central Hypothesis:*** As important players for signaling between plant cells and tissues, PD and hormones are intimately connected. Several recent studies have addressed the role of the hormones, auxin[17,20] and cytokinin[75] in regulating PD during development. Further, the trafficking of auxin via PD is an exciting emerging field in plant physiology[125,126]. Regulated intercellular trafficking via PD is an important aspect of plant-pathogen interactions. Despite the importance of PD-hormone interplay in plants, **how hormones influence PD remains poorly understood**, and only now is the role of PD in mediating hormonal and signaling flux being investigated. Based on the seemingly contradictory effects of viruses on SA and PD interactions, the central hypothesis of this work is that **SA regulates PD in a concentration dependent manner, and with complex temporal dynamics, by changing PD structure and formation through modification of cellular processes involved in secondary PD formation.** By using pharmacological and cell biological approaches (Figure 3), we determined and measured the effects of different SA concentrations and treatments on PD trafficking and, determined the effects of SA on PD structure, distribution, and number. We discovered SA regulate PD trafficking though callose dynamic in a time and dose manners.

# RESULTS

### *Optimizing exogenous application of SA to Nicotiana benthamiana leaves*

Arabidopsis carries five paralogs of *NONEXPRESSOR OF PATHOGENESIS-RELATED GENES 1* (*NPR1*), which are required for SA response and serve as markers for SA signaling. *PR1*, *PR2*, and *PR5* are considered markers for SA-dependent SAR[127]. Quantitative PCR (qPCR) was used to measure expression of the accumulation SA marker gene in *Nicotiana benthamiana*, *NbPR5,* in response to exogenous application of SA under our experimental protocols. SA at varying concentrations was introduced into leaves of 4-week-old *N. benthamiana* plants by infiltration with a needleless syringe. *N. benthamiana* was used in these experiments because it is used as a model host for studying many plant-pathogen interactions and because its large leaves and ease of transformation by *Agrobacterium tumefaciens* make it well suited for cell biology investigations like microscopy.

Induction of *NbPR5* expression was interpreted as indicating the activation of SA defense signaling pathways (Figure 14). Treatment with 100 uM SA(Sigma-Aldrich) induced expression of *PR5* almost 30-fold. In contrast, 5mM of SA infiltrated into leaves resulted in a lower *NbPR5* induction, with only 6-fold induction. It was also observed that 5 mM SA damaged the infiltrated leaves leading to necrosis, and this damage could account for the lower measurements of induction by qPCR.

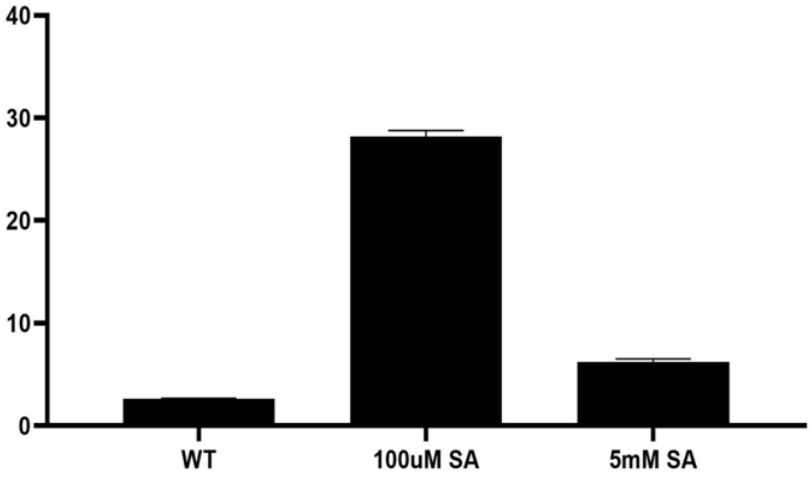


**Figure 14: qPCR results for *NbPR5* expression after SA infiltration.**

*NbPR5* mRNA accumulation was quantified following two infiltrations with a solution containing 100 µM SA, 5 mM SA, or mock treatment (WT). Data are normalized to the untreated wild type (WT) sample. Error bars are represented as mean SD (n=3). Data shows high accumulation of SA-induced transcript level with 100uM of SA.

***Measure the effect of SA concentration, treatment time and context dependence on intercellular trafficking.***

A very low inoculum of *A. tumefaciens* cells ($OD_{600}$=0.0002) carrying a plasmid for expression of plant-optimized monomeric *GFP* was infiltrated into *N. benthamiana* leaves with needleless syringes so that individual epidermal cells would be transformed to express monomeric GFP. Twenty-four hours later, 100 µM (0.1mM) SA was infiltrated into the same leaves. Intercellular trafficking of GFP to neighboring epidermal cells was then quantified 48 hours after infiltration of *A. tumefaciens* (24 hours after infiltration of SA). An example GFP movement between epidermal cells is shown in Figure 3c. Movement was scored by counting the number of neighboring layers of cells into which GFP has moved (light green) from the transformed cell (bright green) (Figure 3c). Traditionally, studies of the effects of hormones on PD have relied on a single-concentration dose and the collection of data at a single time point after application. This methodology can be expected to produce a single increase/decrease answer without the nuance of how hormone levels fluctuate in a cell over time or during a defense response. The length of exposure to the hormone stimulant is another variable that could determine the observed effects on PD. Short treatment times could report on the immediate effects of SA while longer times could allow the induction of secondary signaling pathways, e.g., those of other hormones, induced by SA. To determine whether there is a dose-dependent response, we therefore conducted movement assays at various times after application of SA. Further, defense responses typically involve multiple hormones interacting with complex dynamics. We therefore determined

the effects of SA on PD at different concentrations and times after application. Experiments that examine the effects of SA on plants use a wide range of concentrations, from 0.01 to 5 mM[109] although 1 mM is often used for studies on defense[128]. A variety of concentrations was used to determine the sensitivity of PD to varying amounts of SA. A minimum of three biological replicates were completed for each concentration and each replicate contained at least 20 foci of GFP movement. Our data show long treatment with SA (12 or 24 hours) reduces intercellular trafficking via plasmodesmata, consistent with previous literature. Interestingly, short treatment with SA modifies intercellular trafficking in unexpected ways (Figure 15 and 16). While treatment with SA for one hour reduced intercellular trafficking of the GFP probe, four hours of SA treatment increased PD permeability (Figure 15 and 16). The effect of SA on intercellular trafficking was concentration dependent with the 0.1 mM concentration inducing stronger changes in permeability at four and 24 hours of treatment (Figure 15 and 16). Our data suggest that SA has effects on PD other than inhibiting trafficking and support the hypothesis that SA effects may be time and concentration dependent.

***Determine the effects of SA on PD number and structure.***

This experiment was followed by measuring callose accumulation and degradation at PD using aniline blue staining and fluorescent microscopy. We investigated the correlation between cell-to-cell trafficking via movement assay and the staining of callose deposition with 1% aniline blue in untreated leaves and after various lengths of (1, 4, 12hrs) SA treatment (Figure 17). We observed a strong correlation between PD relative permeability and callose deposition in the presence of 0.05mM SA (Figure 18),

**Figure 15: The effect of SA on intercellular trafficking is concentration dependent and long treatment with SA reduces intercellular trafficking.**

A) 24-hrs treatment of SA reduces cell-to-cell movement at both 0.05 mM and 0.1mM concentrations (n = 94) compared to the untreated control (WT), with 0.1 mM showing a greater reduction. B) 12-hrs treatment of SA reduces cell-to-cell movement for 0.05 mM and 0.1 mM SA treatments, with 0.05 mM showing the greater reduction (n = 115). C) 4-hrs treatment of SA increases cell-to-cell movement (n = 108) for 0.05 mM and 0.1 mM treatments, with 0.1 mM showing the greater increase. D) 1-hr treatment of SA reduces cell-to-cell movement for both concentrations tested (n = 103) with 0.05 mM showing a greater increase.

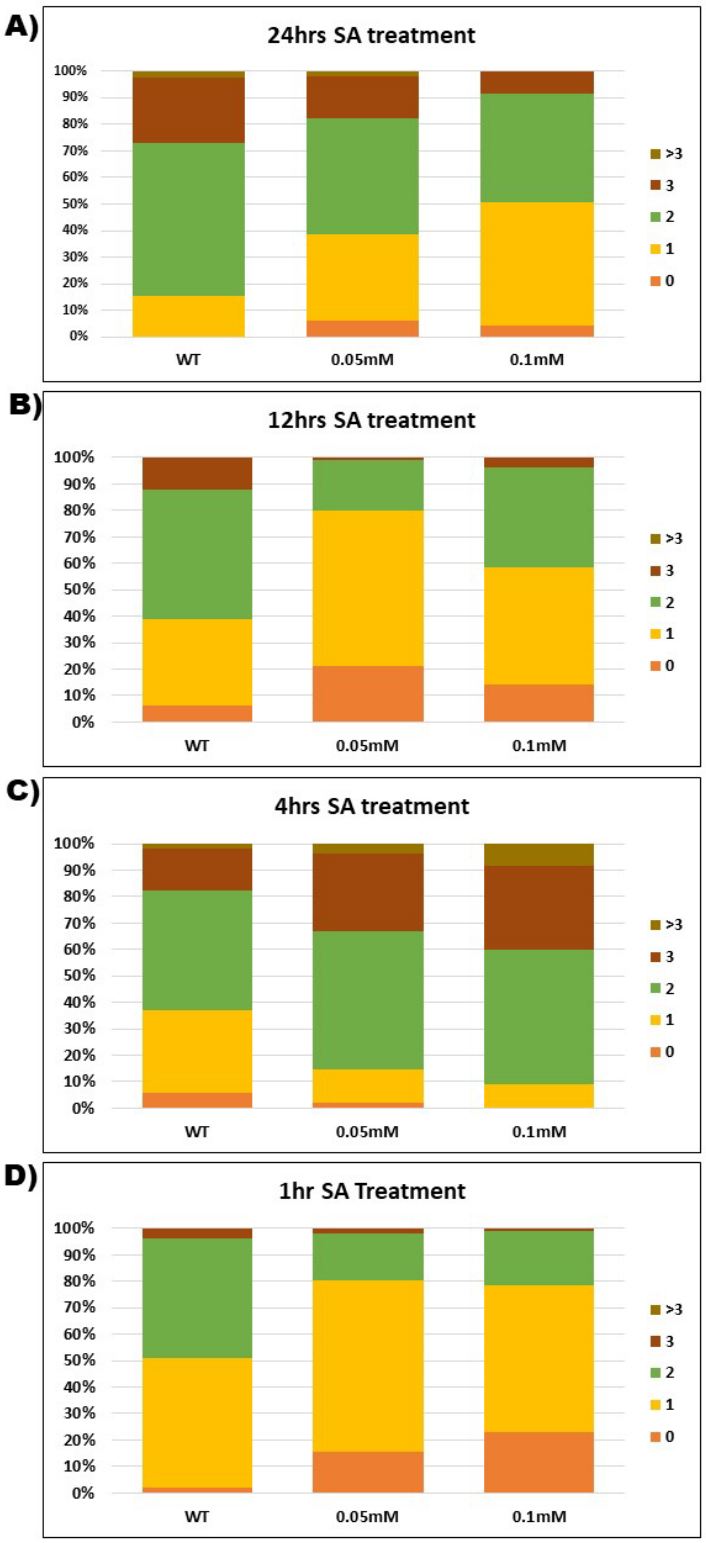
A)
24hrs SA treatment
100%
90%
80%
70%
60%
50%
40%
30%
20%
10%
0%
WT
0.05mM
0.1mM
>3
3
2
1
0
B)
12hrs SA treatment
C)
4hrs SA treatment
D)
1hr SA Treatment

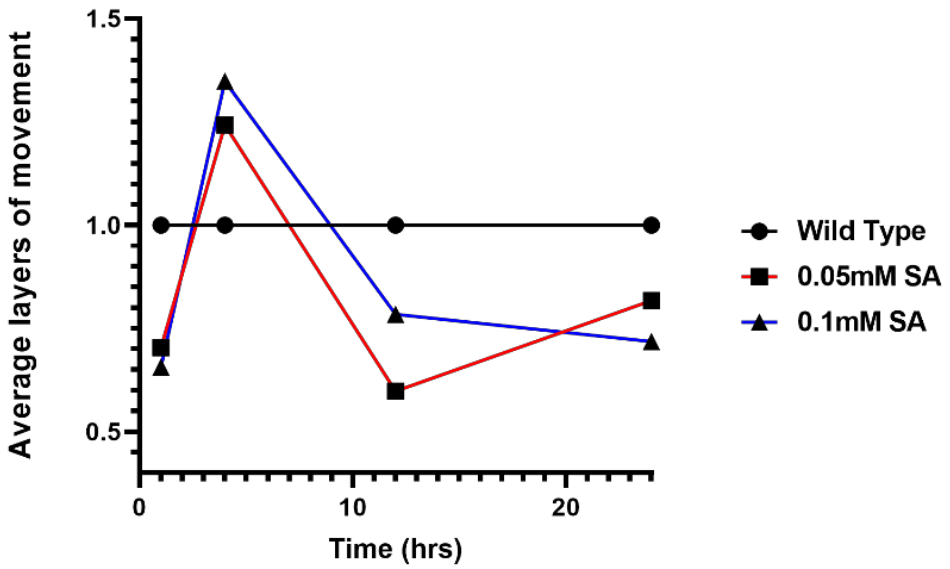


**Figure 16: SA changes PD permeability in a time-dependent manner.**

Data shows the fold chance in the average number of layers of movement in movement assay over a 24 h time course, for untreated (WT; black), 0.05 mM SA (red) and 0.1 mM SA (blue), relative to untreated. The result shows that SA has complex time-dependent and dose-dependent effect on movement.

**Figure 17: Quantification of PD-associated callose in fixed *N. benthamiana* leaves treated with 0.05mM salicylic acid using the fixation method of aniline blue staining (Method 1).**

Data show the number of pitfields per 100 $\mu m^2$ of cell wall. A) 12 hours of SA treatment show significant increase of pitfields in the treated plants. B) 4-hour SA treatment shows significant decrease in pitfields in the treated plants. C) 1 hours SA treatment shows increase in pitfield in the treated plants compared to the untreated control. Significant differences were determined using the Welch's t-test (ns, $p>0.05$; *, $p\leq0.05$; **, $p\leq0.01$; ***, $p\leq0.001$; p< ****, $p<0.0001$). n= 68 – 96 for each treatment across the three experiments.

A)

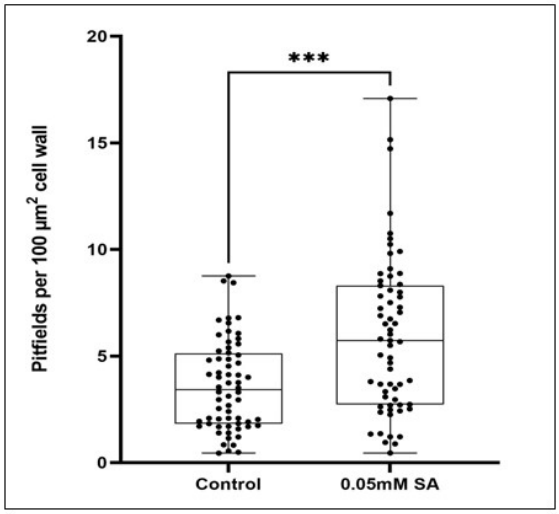


12 hours SA treatment

B)

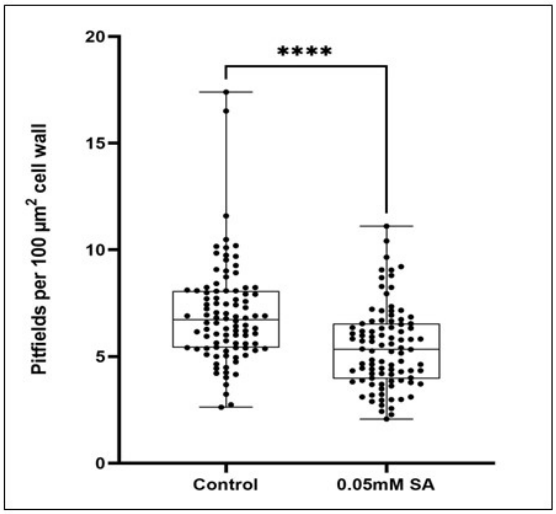


4 hours SA treatment

C)

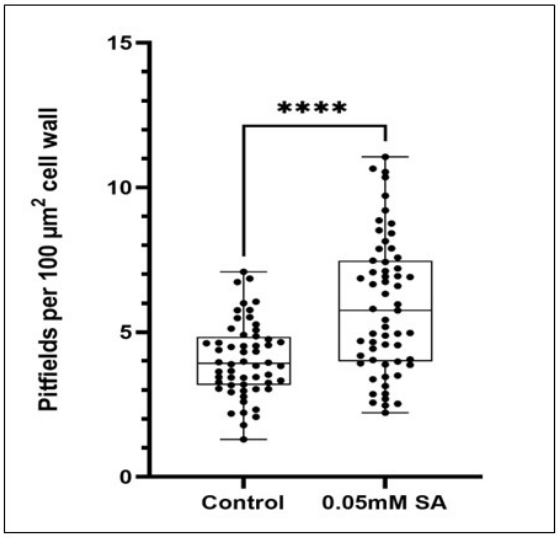


1 hour SA treatment

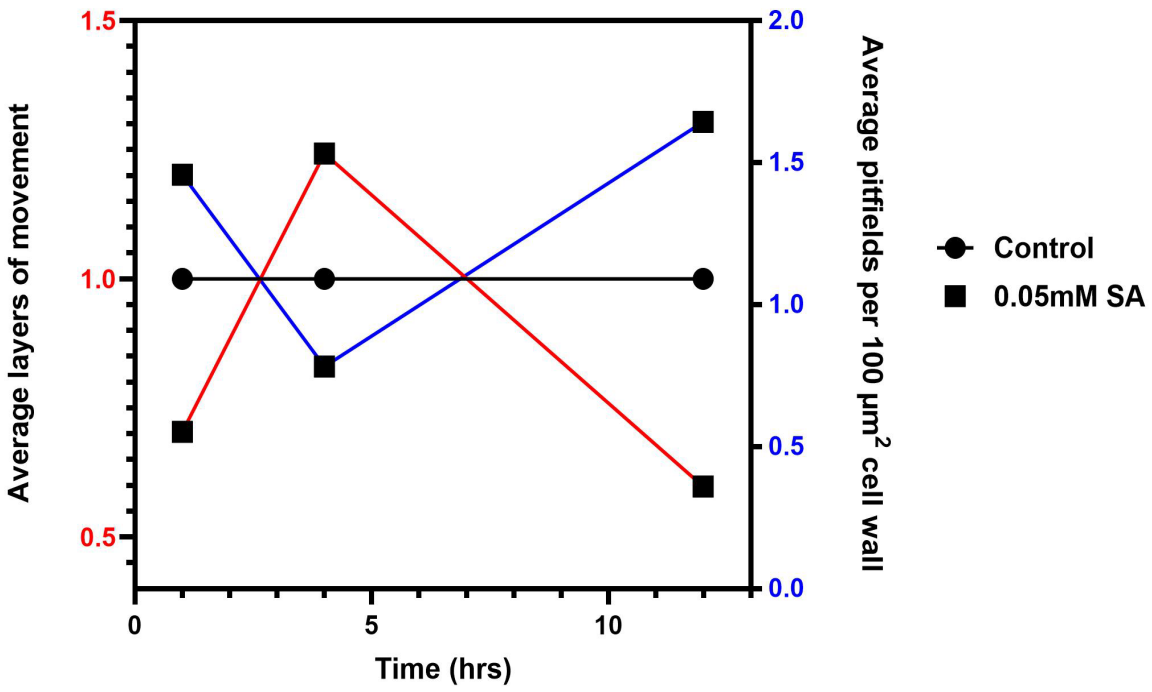


**Figure 18: Quantification of PD-associated callose in fixed *N. benthamiana* leaves treatment with 0.05mM salicylic acid to verify the correlation between callose deposition and PD movement by callose staining with aniline blue.**

The dynamic callose turnover by callose synthases and degradation at the cell well (blue plot) is correlated with the layers of movement data in (red plot). Callose accumulates in the cell wall of 1 hour and 12 hours of SA treated plants compared to the untreated control. However, the dynamics of the callose response is different at 4hrs of SA treatment which shows reduced accumulation of callose at the PD compared to the untreated control. n= 68 – 96 for each treatment time experiment.

which raises many intriguing questions, including the mechanisms that are involved in modifying intercellular trafficking at the different treatment times.

### *Measuring PD distribution in SA-treated tissue*

SA has been reported to inhibit PD by inducing callose accumulation at PD through the action of members of the PDLP family[29,31,55]. PDLPs have large extracellular domains but very little cytoplasmic structure and when tagged with fluorescent proteins they are used as markers for the presence of PD[7,74]. PD are diverse and can be roughly grouped into three different morphological forms: simple, twinned, branched or complex[4]. Simple PD can be modified into complex PD as during the sink to source transition in leaves[8]. SA accelerated the formation of complex (secondary PD) in Arabidopsis leaves[7]. No other effects of SA on PD structure or formation have been reported. We therefore set out to determine whether SA has effects on PD in addition to callose accumulation. Increased numbers of PD are correlated with increased intercellular trafficking in *N. benthamiana* leaves and the opposite was also observed for decreased trafficking[74], and our preliminary data suggest that some concentrations of SA may increase intercellular trafficking.

To measure whether SA increases or inhibits trafficking by modifying the numbers of PD in leaves we used the fluorescently labeled marker, PDLP1-GFP. Confocal images were used to determine the localization of PD along the cell junctions of *N. benthamiana* epidermal cells (Figure 3f). Leaves of 4-5 weeks old *N. benthamiana* plants was infiltrated with *A. tumefaciens* carrying a plasmid construct for expression of *PDLP1-GFP*. Twenty-four (24) hours after agroinfiltration, SA was infiltrated into the

same leaves. Data were collected by confocal fluorescence microscopy on the Danforth Center's Leica SP8-X instrument and PD was scored using our previously described approach based on semi-automated image processing in ImageJ[74,129]. Tissue treated with vehicle only were served as the negative control and data were collected from three biological replicates each of which allowed scoring of at least 30 fields of view of cells. The SA concentrations and treat times used were determined by experiments described above. Unexpectedly, we observed SA concentrations and treatment times do not affect secondary PD formation, we saw no changes in the number of PDLP1-GFP foci in the SA-treated compared to the control (Figure 19). Since the number of observed PDLP1-GFP foci remains unchanged, we concluded that SA does not affect secondary PD formation in our system.

### *Determining structural changes to PD in response to SA by transmission electron microscopy*

Transmission electron microscopy (TEM) is used to obtain detailed images of the internal structures of cells and thus, allowed us to visualize the ultrastructure of PD[124] (Figure 3). The Burch-Smith lab has developed a consistent protocol that produces high quality samples for TEM[87]. Leaf tissues treated with SA in the same protocol as described in above and in Fitzgibbon *et al* 2013 were prepared for TEM by high pressure freezing followed by freeze substitution and our standard lab protocol[87]. Observed PD were classified into structural forms according to Burch-Smith *et al* 2010, and the density of PD (total and by structural form) was determined per 100 $\mu m^2$ of cell wall as described previously[12]. Our lab previously used PFLP1-GFP to measure PD

**Figure 19: Quantification of PD density in *N. benthamiana* using the PD marker PDLP1-GFP to measure PD distribution in SA-treated tissue and check for secondary Pd formation.**

Pitfields per 100 μm$^2$ of cell wall are plotted as previously described. Quantifications are for 0.05 mM SA treated and untreated control after 12 hours (A), 4 hours (B), and 1 hour (C). No significant differences were observed in the untreated control and treated SA plants regardless of the treatment time. n = 69 for each time treatment experiment. Significant differences were determined using the Welch's t-test (ns, $p>0.05$; *, $p\leq0.05$; **, $p\leq0.01$; ***, $p\leq0.001$; p< ****, $p<0.0001$).

A)

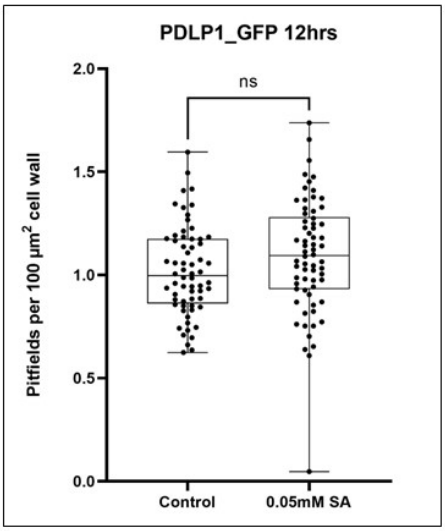


PDLP-GFP foci after 12 hours SA Treatment

B)

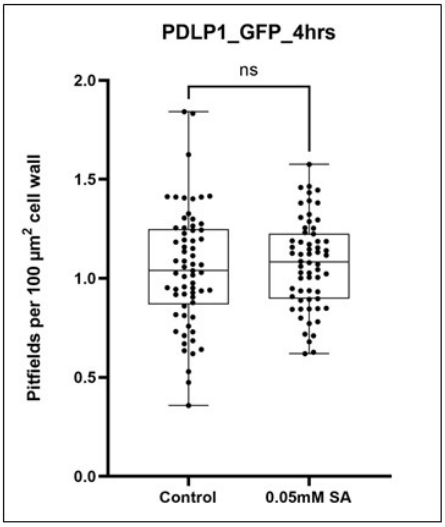


PDLP-GFP foci after 4 hours SA Treatment

C)

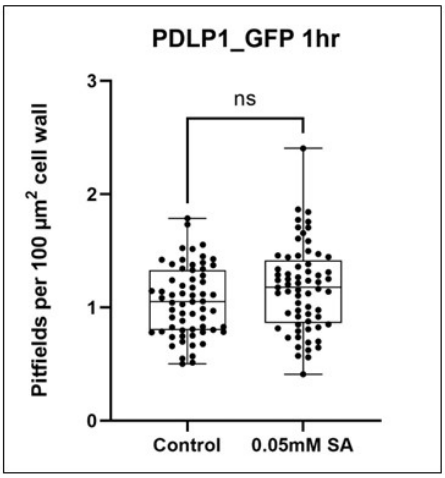


PDLP-GFP foci after 1 hour SA Treatment

density[74]. It is possible, however, that SA could influence the trafficking of PDLP1-GFP to the PD and that interpretation of data could be complicated by the involvement of PDLP proteins in mediating SA effects on PD. The use of TEM imaging of PD was complementing the use of PDLP1-GFP as a marker and confirm observations with PDLP1-GFP. Thin-section TEM imaging is known to undercount PD in a sample and is therefore inferior to whole-volume 3D-imaging techniques like serial block face-scanning electron microscopy (SBF-SEM) and focused ion beam-SEM (FIB-SEM)[92] (Figure 3). However, the 3D techniques require specialized instrumentation that is currently unavailable at the Danforth Center. Since the sample blocks prepared for thin-section TEM can be used for 3D SEM-based imaging, we used these 3D imaging approaches should they become available.

## Discussion

It is surprising that much remains unknown about the interplay between hormones and PD given the importance of both in plant development. The overarching goal of this project is to elucidate how the important defense hormone SA changes PD to control intercellular flux of signaling and defense molecules, as well as pathogen-associated molecules. It has been long known that SA plays an important role in plant defense signaling and therefore decreases cell-to-cell trafficking. While SA does not transport via PD, it uses PD-localized proteins such as (PDLP5) to induce callose at PD and block trafficking. Some bacterial pathogens use effectors that pass through PD to block the

systemic acquired resistance response and therefore keep PD open, allowing the spread of pathogens.

To investigate the time-dependent and concentration-dependent effects of SA on PD, we first determined the best method to apply the exogenous SA to *N. benthamiana* leaves. We found that 100 μM SA infiltrated into *N. benthamiana* leaves successfully showed upregulation of the pathogenesis-related gene 5 (PR5) by qPCR (Figure 14). We then measured the layers of movement in SA-treated plants and untreated controls. We observed a significant difference in movement of the untreated control vs the SA-treated plants at various time points (1, 4, 12, and 24 hrs) (Figure 15). Consistent with the literature, we observed a decrease in cell-to-cell trafficking at 24 hours, 12 hours, and 1 hour of SA treatment, supporting that the experimental protocol was successful. Fascinatingly, we discovered an increase in movement at 4 hours of SA treatment (Figure 15 and 16). This finding, together with the simultaneous reduction in callose staining (Figure 17 and Figure 18), suggests that at 4 hours SA regulates PD trafficking by degradation of callose at PD. This finding could represent an important new detail about how plants balance the need to restrict pathogen movement through PD with their own need to use intercellular communication to coordinate defense. While this finding is yet to be experimentally explored, we speculate that this brief opening of PD 4 hours after activation of the SA-induced defense response could function to facilitate the trafficking of important mobile RNA necessary to fight against pathogens, including antiviral siRNA.

While callose deposition or degradation at PD can dynamically control PD permeability, it is also possible that PD number could change in response to SA. We observed no significant change in the pitfield density between untreated controls and SA-treated plants at all tested time points (1, 4, and 12 hours) (Figure 20). From this finding we conclude that SA regulates PD through callose dynamics by using PD localized proteins to close (1hr), open (4hrs), and then again close (12hrs) PD. At 1 hour SA treatment, SA most likely to activate PD-localized proteins (such as PDLP 5) to deposit callose at PD and therefore restrict intercellular trafficking. At 4 hours of SA treatment, the cell wall signals the nucleus to activate glucanases which results in callose degradation at PD. At longer treatment time, SA activates the systemic responses to induce callose synthases and therefore decrease cell to cell trafficking.

These findings regarding the dynamic closing and opening of PD by SA may be applicable to other hormones such as cytokinins, abscisic acid, auxins, and jasmonic acid[97] etc.; other hormones could be tested In the long term, understanding and being able to predict the outcome of hormone-PD interactions provide new tools for approaches that can enable the engineering of resource allocation, such as for maximizing the proportions of crop photosynthetic output that is available for human consumption, e.g., the rice C4 project[34]. Improved crops could improve human health and nutrition.

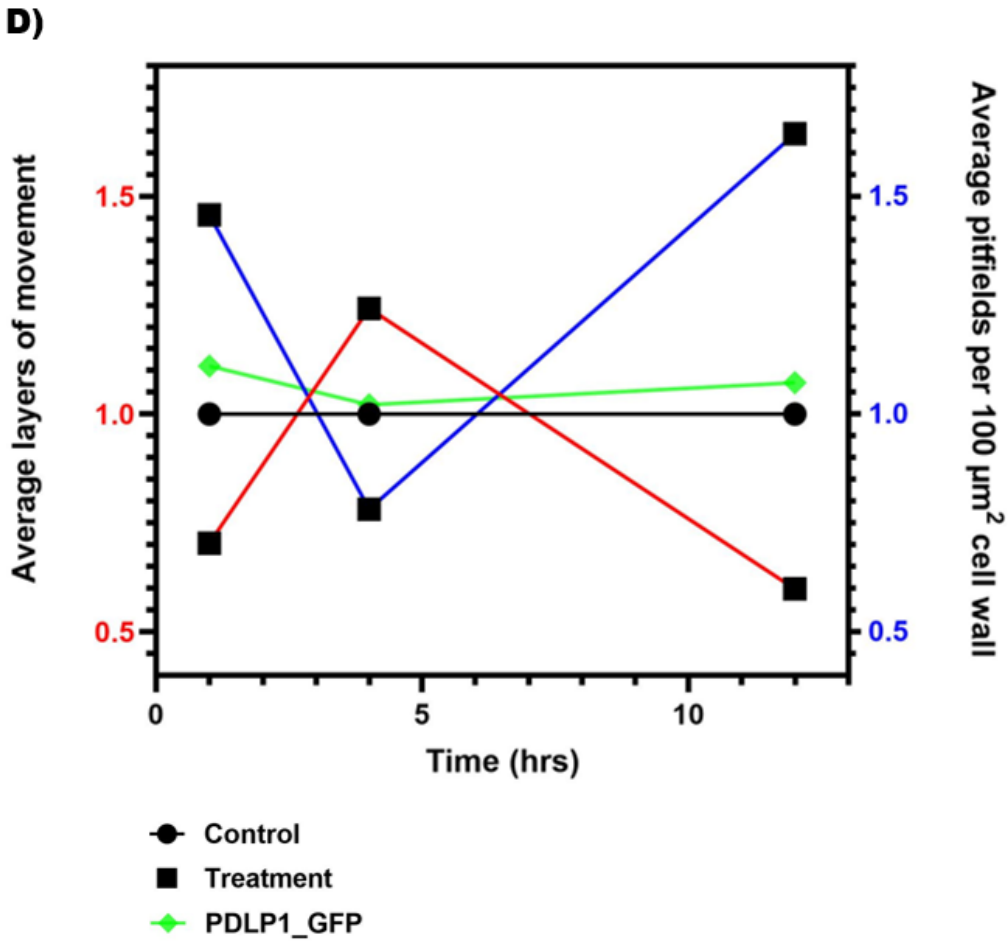


**Figure 20: Summary of SA-induced PD density quantification and movement**

Following 0.05 mM SA treatment, average fold change in layers of movement relative to untreated is shown (red), along with the average pitfield number per 100 µm$^2$ of cell wall as determined by aniline blue callose staining (blue) or using the PD marker PDLP1-GFP (green) in *N. benthamiana*. Data shows a clear negative correlation between the movement (red) and callose-staining of PD (blue), while the total number of PD pitfields remains unchanged (green).

# CHAPTER 4

# OVERALL DISCUSSION ON THE TIME-DEPENDENT SA-INDUCED CHANGES IN PD CALLOSE

Plants are multicellular organisms and communication between cells is critical for the survival of individual plants. However, plant cells have the added challenge of having cellulosic cell walls between cells, which imposes a physical spacing that limits direct cell-to-cell contact of cell surface components. Plasmodesmata (PD) are pores that connect one plant cell to another, allowing them to have passages between cells that traverse the cell wall barrier. PD are plasma membrane-lined pores in the plant cell walls which allow trafficking of small molecules and macromolecules including metabolites and signaling molecules from one plant cell to neighboring cells. Plants have evolved to use PD transportation for regulators of development and function. Several hormones also traffic between cells via PD. Interestingly, while salicylic acid (SA) does not traffic via PD, but rather through the cell wall (apoplast), it can influence PD trafficking functions. Indeed, SA is a critical hormonal signal that regulates cell-to-cell permeability in response to pathogen infection. Previous studies have shown SA to regulate plasmodesmata through callose dynamics. SA has long been known to increase plant responses to biotic stress conditions by potentiating systemic acquired resistance (SAR). SAR is a secondary immune response that acts against pathogens in plants. Because PD are very important for plant growth, development, and defense, I sought to understand the molecular mechanisms involved in PD regulation and trafficking. The cellular mechanisms of how SA, a PD regulator, could directly or indirectly regulate intercellular trafficking by adjusting PD permeability were investigated in the body of work described in this dissertation.

PD trafficking is often regulated by the controlled accumulation of the β-1,3-glucan callose in the cell wall surrounding a plasmodesmal pore. Callose deposition reduces intercellular trafficking while the converse occurs when callose is removed. The restriction of PD trafficking capacity during development or in defense against pathogens is usually accomplished through the physical occlusion of the PD pore by the accumulation of callose. In both instances, the regulated accumulation of callose is mediated by hormones. Hormones have varying effects on PD-mediated trafficking**.** Hormones such as cytokinin-benzyladenine (BA) and gibberellic acid (GA) promote the removal of callose at PD to allow intercellular trafficking. In contrast, auxin, abscisic acid (ABA), and salicylic acid (SA) cause the deposition of callose at PD, restricting intercellular trafficking. Plants use salicylic acid (SA) as a signaling molecule to mediate responses to pathogen invasion and stop the infection process. SA is therefore a well-studied defense hormone that regulates PD, and its mode of action is usually thought to be by restricting trafficking of signaling molecules through callose accumulation at PD.

A well-known defense hormone, SA is preferentially transported from cell-to-cell via the apoplast pathway and yet, intriguingly, it restricts intercellular trafficking via the symplast through the deposition of callose at PD. During pathogen infection, plants respond by sending mobile signals through the apoplast to neighboring plant cells, which then develop a systemic response that includes adjusting callose accumulation at PD usually resulting in pore closure. The role of PD during defense is complex.  Some bacterial effectors that inhibit defenses and promote infection also hijack PD-located

innate immune responses to increase PD permeability and enable the movement of the bacterial effector from cell-to-cell. When SA is involved, recognition of effectors triggers the intercellular movement of the systemic signals azelaic acid (AzA) and glycerol-3-phosphate (G3P). These two metabolites are associated with PD-LOCATED PROTEINs (PDLPs) that can regulate PD permeability by inducing callose at the PD. The central hypothesis of this work is that PD and hormones are intimately connected, as they are important players in signaling between plant cells and tissues. This project investigated the effects of salicylic acid on PD and intercellular trafficking given its importance in mediating defense responses. Understanding how plasmodesmata regulate communication during development can potentially open avenues to engineering crops with greater yield for the growing population, and better understanding PD may similarly help limit infection by plant pathogens including viruses, which cause considerable economic losses and are a threat for sustainable agriculture.

Fluorescent dyes are the most common and easy method for measuring intercellular trafficking. Movement can be observed using low-pressure bombardment to transfect cells to produce GFP. Alternatively, microinjection with small dyes like CFDA can also be used to measure trafficking. In this project, we measure cell-to-cell trafficking using agrobacteria carrying a tag-free GFP construct. Movement of free GFP from the transfected cell through PD to neighboring epidermal cell layers is quantified. If GFP is only observable in the transfected cell nucleus this is quantified as zero movement, i.e. the GFP is in the zero layer (Figure 3C). If GFP is observed in nuclei of immediately adjacent cells, this is described as one layer of movement, and so forth for

the two and three layers of movement. The effect of SA on PD trafficking was measured after the exogenous application of SA at 0mM, 0.05mM, and 0.1mM concentrations for different treatment times. I discovered that the effects of SA depend on the treatment time. Previous studies showed longer SA treatment times lead to severe reductions in intercellular trafficking. For instance, SA was shown to increase PD callose using the callose synthase enzyme CalS1[30] and PDLPs[29,128], and also by callose-independent mechanisms[108]. I found that long treatment (12 hours and 24 hours) with SA reduces intercellular trafficking whereas short time SA treatment modifies intercellular trafficking in unexpected ways. One hour of SA treatment reduced cell-to-cell movement (Chapter 3). I also discovered that the effect of SA on intercellular trafficking was also concentration dependent. Interestingly, at four hours and 12 hours of SA treatment, I observed an increase in trafficking at 0.1mM compared to 0.05mM. in contrast, I observed a decrease in trafficking at 0.1mM compared to 0.05mM at 1 hour and 24 hours SA treatment. I also investigated the correlation between callose deposition and PD movement using callose staining with aniline blue on fixed tissue. I observed a strong negative correlation between PD relative permeability and callose deposition at PD. To test whether SA increases or decreases trafficking by modifying the numbers of PD in *N. benthamiana*, I measured the pitfield distribution using the PD marker PDLP1-GFP to determine whether SA causes secondary PD formation, perhaps explaining the increasing cell-to-cell trafficking we observed at 4 hours of SA treatment. Our results showed no statistically significant effect on plasmodesmatal distribution which indicates

that SA does not regulate PD formation and only regulates PD through callose dynamics.

This novel finding raises many intriguing questions such as what mechanisms involved in PD trafficking to decrease at one hour of treatment, increase after four hours of treatment, and decrease at 12 hours. Are there any specific gene expression changes between these timepoints? This could be addressed by comparing gene expressions in plants treated with SA for 4 or 12 hours using RNAseq. Another question is what effect does endogenous SA accumulation have on cell-to-cell trafficking? This can be addressed by preforming virus-induced gene silencing (VIGS) of the *SERINE PALMITAYTRANSFERASE* (*SPT*) gene whose silencing activated the SA signaling pathway[130]. SPT catalyzes the first reaction in long-chain base (LCB) synthesis. LCBs act as bioactive molecules in the immune response. Plant immunity was affected as *SPT*-silenced plants accumulated SA, constitutively expressed the SA-inducible *NbPR-1* gene and showed increased susceptibility to the necrotroph *A.alternata f. sp. lycopersici.* VIGS of *SPT* profoundly affected *N. benthamiana* development as well as LCB composition of sphingolipids. Alternatively, transgenic plants expressing the bacterial salicylate hydroxylase gene *NahG* that degrades SA and are incapable of mounting SAR. This can be used to address how low levels of SA influence cell-to-cell trafficking when compared to *NahG* plants treated with 0.05mM SA at 4- and 12-hours treatment time. Understanding the relationship between PD and hormones is a complex and exciting focus in plant physiology and my research findings open new avenues for future research.

In summary, we discussed the importance of cellular communication and cellular coordination to proper plant functioning and survival. The mechanism of how hormones like SA are connected, correlated, or regulated PD transports remains unclear. This dissertation contributes to understanding of the patterns of PD-hormone interactions through callose dynamics and the cellular mechanisms that drive the regulations of hormones and PD in *N. benthamiana* leaves. PD regulation is an important component of plant defense and development and provides essential cell-to cell trafficking for effective response to pathogens or biotic stress in a timely manner (Figure 21). An increase in cell-to-cell trafficking after 4 hours of SA raises an intriguing question regarding what mobile RNAs or signal molecules are transported via PD during this brief transport window. With optimized and more uniform methods for the study of PD, researchers will be able to efficiently investigate the mechanistic details underlying the regulation of PD permeability.

**Figure 21: Working model of time-dependent SA-induced changes in PD callose.**

1 hour of exogenous application of SA activates PD-localized callose synthases proteins (PDLP5, AZA, GP3, etc.) and restricts intercellular trafficking. Cell wall signals nucleus to activate glucanases to temporarily open PD at 4 hours of SA treatment. At 12 hours, SA activates the SAR inducing callose synthases to restrict intercellular trafficking.

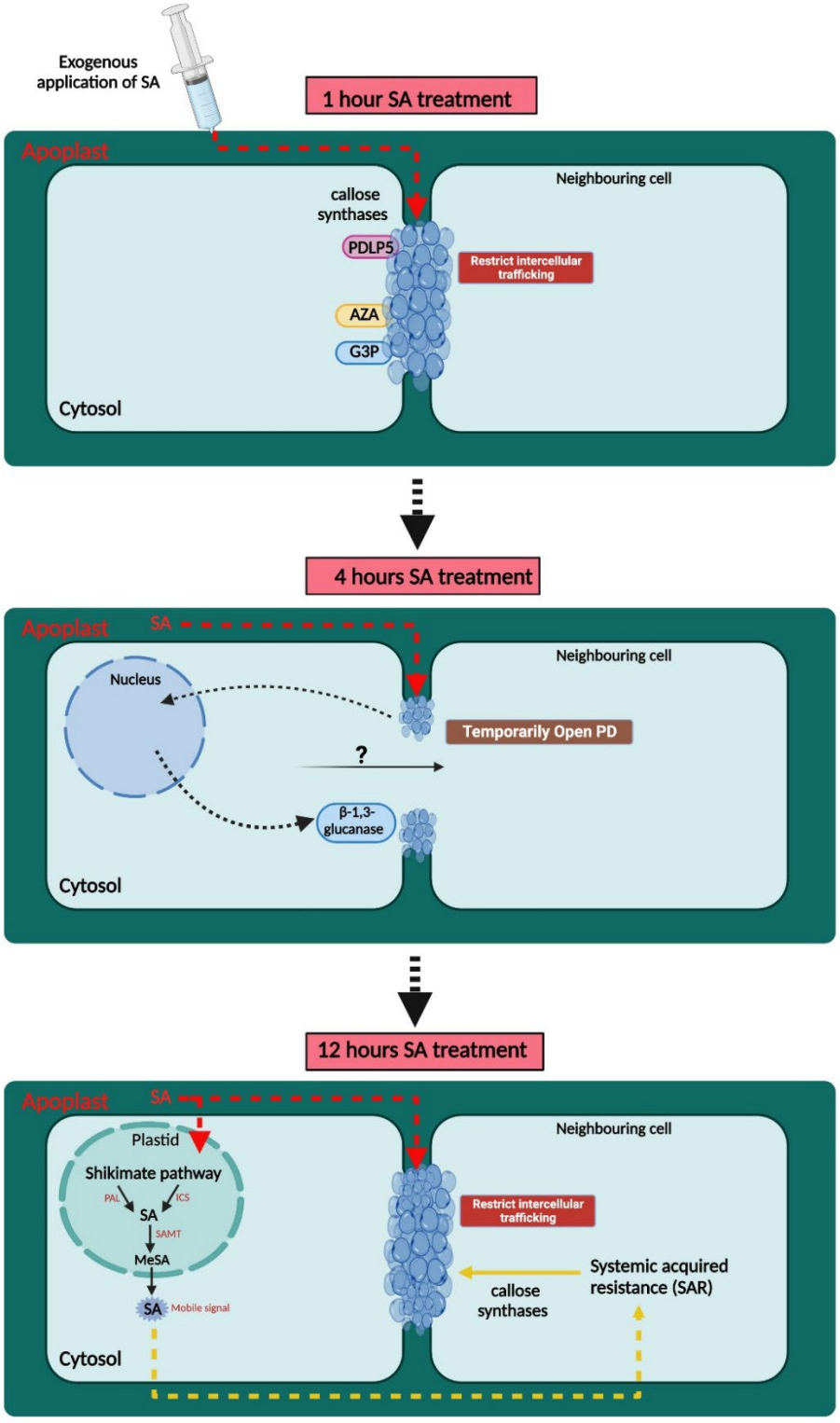
Exogenous application of SA
1 hour SA treatment
Apoplast
Neighbouring cell
callose synthases
PDLP5
Restrict intercellular trafficking
AZA
G3P
Cytosol
4 hours SA treatment
Apoplast
SA
Neighbouring cell
Nucleus
Temporarily Open PD
?
β-1,3-glucanase
Cytosol
12 hours SA treatment
Apoplast
SA
Neighbouring cell
Plastid
Shikimate pathway
PAL
ICS
SA
SAMT
MeSA
SA
Mobile signal
Restrict intercellular trafficking
Systemic acquired resistance (SAR)
callose synthases
Cytosol

# Future direction

### *Measuring PD trafficking in the presence of Virus and SA*

Our lab previously hypothesized that SA regulates secondary PD formation. However, my findings instead revealed that SA alone does not affect plasmodesmata distribution, suggesting that the previous observation may be due to viral regulation. This raises a new question. Does virus infection show the same time-dependent dynamics in PD permeability as observed with the SA treatment? This experiment can be addressed using the protocols for measuring cell-to-cell trafficking though movement assay as previously described. Another important question is what is the function of the brief increase in PD permeability at 4 hours following SA treatment? It is possible transient increase in intercellular trafficking is to enable the spread of defense signals like AzA and G3P which mediate SAR. In the case of a viral infection, transient increases in intercellular trafficking could allow antiviral siRNA or mobile mRNA to spread for systemic defense, and the virus usurps this phenomenon for its own spread. This leads to another question: does PD trafficking have a different response to the viral infection at various time points? This can be addressed by performing movement assay to measure changes in trafficking and also measuring pitfield distribution using the PDLP1-GFP marker at carefully selected time points. We can also determine what structural changes in PD in response to virus and SA using TEM.

***Measuring PD trafficking in the presence of SA and another defense hormone***

Besides SA, other plant hormones can act non-cell-autonomously. Jasmonic acid (JA) is a lipid-derived hormone that is well known for its important role in defense against necrotrophic pathogens[119]. Experimental evidence suggests that JA and its derivatives, especially JA-conjugated to isoleucine (JA-Ile), can move systemically in plants although many questions about the identity of the mobile molecule in JA signaling remain[120]. The effect of JA on PD has not been clearly described, although one report suggests that treatment with JA stimulated export of photoassimilate (sugar) from source leaves, suggesting altered PD trafficking[121]. While SA and JA are two of the major defense hormones, their signaling pathways are antagonistic to each other[122,123]. Given the importance of these hormones in mediating defense responses, the effects of these hormones on PD and intercellular trafficking should be clarified.

To investigate the effects of the hormone JA on PD, leaves will be treated with JA, SA, JA+SA or vehicle only and then quantitative GFP movement assays will be performed. JA will initially be used at a concentration of 0.25 mM as reported in the literature[131] and adjusted as needed. Optimal SA concentrations and treatment times will be based on my results from Chapter 3. If JA and SA are antagonistic to each other with respect to PD, we expect to see opposite effects on intercellular trafficking with JA increasing intercellular trafficking at 0.25mM.

***Measure the effects of different SA concentrations and treatments on PD trafficking and compare the effects of SA in combination with JA.***

Another direction the research could take is to determine the effect that SA has on endocytosis and endoplasmic reticulum-plasma membrane (ER-PM) contact sites. In various organisms, membrane contact sites allow communication between organelles to coordinate metabolism[132]. PD contain appressed ER internally and the PM establishes their external limits, and these membranes and their composition are essential for PD structure and function[133–135]. PD can be viewed as specialized ER-PM contact sites[96]. Endocytosis is important for regulating PD function, especially in connection with virus infection[136,137]. SA negatively regulates clathrin-mediated endocytosis in plants[138,139], and we therefore predict that changes in endocytosis will occur with SA treatments. In plants, members of the SYNAPTOTAGMIN (SYT) family act as ER-PM tethers[137], and some SYTs protein localize near PD[140]. SYT proteins have been found to be important for virus infection[137,141,142]. We hypothesize that ER-PM contact sites could serve as sites for new PD formation or modification in response to SA treatment.

One could therefore investigate how endocytosis and ER-PM contact sites are involved in SA-mediated effects on PD. We expect the coordination of the ER-PM contact sites, endocytosis, and cell wall modification to maintain the architecture and conductivity of PD. The effects of SA on endocytosis can be probed by using confocal and super resolution microscopy to measure endocytosis in plant cells in the absence or presence of SA. The rates of endocytosis in untreated cells will be measured using the dye FM4-64 to label the plasma membrane and endocytic vesicles. Although other

probes are now used to measure endocytosis in yeast and mammalian systems, FM4-64 is still a common marker for endocytosis in plants[143]. *N. benthamiana* leaves will be treated with SA or vehicle control for the length of time and concentrations determined in Chapter 3. If reduced rates of endocytosis are observed in tissues treated with SA concentrations or durations that reduce intercellular trafficking and secondary PD formation, this will support the hypothesis that endocytosis is required for PD formation. If reduced rates of endocytosis are observed when either PD function or formation alone is disturbed, then the role of SA in regulating PD trafficking will be further clarified.

In plants, fluorescently tagged SYT proteins serve as markers for ER-PM contact sites[144]. To investigate the dynamics of ER-PM contact sites we could treat plants with SA as previously described, and image the number of SYT foci per unit of cell wall. PDLP1-RFP will be used as a PD marker to colocalize PD and ER-PM contact sites in these studies. We expect that changes in PD formation caused by SA may be observed as changes in the number and distribution of ER-PM contact sites.

# CHAPTER 5

# MATERIALS AND METHODS

**5:1 Plant growth conditions and transfection**

*Nicotiana benthamiana* seeds were germinated in Professional Growing Mix soil (Jolly Gardener PRO-LINE Custom Growing Mix) for 7-10 days before transplanting to individual pots (15x11x12.2 cm). Plants were grown on light carts under long day conditions with 16 hours light and 8 hours dark (120 µmol $m^{-2}$ $s^{-1}$) at 25 degrees Celsius. Miracle Gro All-purpose Plant Food fertilizer was applied 10-13 days post germination (3 days after transplanting). *N. benthamiana* at 4-5 weeks old were used for transfections. *Agrobacterium tumefaciens* strain GV3101[145] (Koncz *et al*. 1968) was grown on LB agar plants supplemented with 50µg/mL gentamycin, 50µg/mL rifampicin and either 50µg/mL spectinomycin (for PDLP1-GFP) or 50µg/mL kanamycin (for XM82). Single colonies were used to inoculate liquid LB medium, and the cultures were incubated for 48 hours on a 28°C shaking incubator. *A. tumefaciens* cultures were collected by centrifugation at 3,000 x g for 10 minutes and pellets were resuspended in infiltration medium (10 mM $MgCl_2$, 10mM MES-NaOH, pH 5.7 and 200 µM acetosyringone). The optical density of the resuspended cultures was measured by spectrophotometry (absorbance at 600 nm light; $OD_{600}$). The cultures were then diluted with infiltration solution to $OD_{600}$ = 0.0001 (for XM82) and $OD_{600}$ = 0.001 (for PDLP1-GFP). Diluted cultures were placed in a slow shaker for approximately 2-3 hours while the acetosyringone activated the expression of virulence genes. Transfection was performed by agroinfiltration of *N. benthamiana* plants as previously described[71] (Brunkard *et al*. 2015). The adaxial side of the leaf was infiltrated with a needless

syringe until the infiltration solution spread across the leaf. After infiltration, plants were placed on the light until imaging.

### 5:2 Method optimization: Callose quantification and salicylic acid treatment experiments

*N. benthamiana* leaves were infiltrated with 0.05 mM salicylic acid to induce callose formation. An entire cut leaf was submerged in a 500 mL polypropylene jar containing 95-96% ethanol to bleach the tissue. The petiole was held with forceps to avoid mechanical damage to the leaf. The jar was sealed and incubated at room temperature on a shaker at 30-40 rpm for at least 5 hours. The ethanol solution was changed to speed up the bleaching after 2 hours incubation. Incubation was continued until the leaves were completely or nearly completely bleached, but less than 6 hours, since plasmolysis occurs at this point, and the resulting separation of the plasma membrane and cell wall make pitfield identification difficult. Bleached leaves were removed by gently holding by the petiole to avoid breaking the leaf and were placed in a petri dish and cut into 5 mm wide strips with a razor blade. The cut strips were rehydrated in double distilled water (DDW) with 0.01% Tween-20 and incubated at room temperature for 1 hour on a shaker at 30-40 rpm. The tissues were then transferred to a small petri dish filled with 1/3 (v/v) of 1% aniline blue in 0.01 M $K_3PO_4$, pH 12 buffer. The unlidded petri dish was placed in a house vacuum desiccator and vacuum applied for approximately 10 minutes followed by slow release of pressure. The petri dish was covered with foil before shaking at room temperature for 2 hours at 30-40 rpm. No de-staining was necessary. The samples were then imaged by confocal microscopy.

### 5:3 Confocal microscopy for aniline blue staining experiment

A Leica SP8 laser scanning confocal microscope (Leica, Whetzlar, Germany) was used to imaged callose deposits from the abaxial side of *N. benthamiana leaf* tissues using a 40x, 1.10 numerical aperture water immersion objective (HC PL APO CS2 40x/1.10 WATER). Aniline blue was excited with a 405 nm laser, and emission was captured from 415 nm-525 nm. Z-stacks were collected from multiple regions of interest (ROI) (approximately 23-25 ROIs per leaf)

*Scanning parameters and Acquisition settings*

Frame scanning mode: XYZ

Frame size: 1024 x 1024

Zoom factor: 5

Line average: 1

Pixel depth: 8 bit

Scan speed: 400 Hz

To observe as many PD as possible, the pinhole aperture was initially set to open. Laser intensity and gain were adjusted to optimize the plasmodesmata fluorescence against the background signal, while being careful to avoid oversaturation of callose sites. Saturation of the stomata was permitted. Z-stacks for 23-25 ROIs were captured for each replicate using the same image acquisition settings.

### 5:4 ImageJ analyses for pitfields distribution

For image analysis, the raw files were converted into max intensity Z-projections in ImageJ 1.53t[107,129,146]. Images were converted into 8-bit grayscale, inverted, and

threshold adjusted to produce a binary image which reduced background noise and identified pixels of pitfields. Connected components in a binary image were separated by watershed separation. A built-in automatic particle analysis was performed to obtain information on PD-associated callose particles. Pitfields per 100 $\mu m^2$ cell wall were calculated using Microsoft Excel. Refer to Chapter 2 for more details as the entire chapter analysis focuses entirely on image analysis for callose-associated pitfields distribution.

### 5:5 Statistical analyses for pitfields distribution

Interquartile analysis was done in Excel by using the interquartile range method to remove outliers. Data were analyzed using GraphPad Prism 9 (version 9.5.0) and presented as Box & Whiskers plots with all pitfields values. Plots display the middle line representing the median, 1-4 quartiles with the minimum and maximum values within the interquartile range. Pitfields per 100 $\mu m^2$ cell wall were normalized to untreated control. An unequal variances Welch's t-test was conducted for each plot.

### 5:6 CalloseQuant and quantification for pitfields distribution

Semi-automated quantification of pitfields was performed using the calloseQuant plugin developed by Hung and coworkers (*Huang et al.* 2022). Images captured using confocal microscopy were first auto-scaled and converted into .tiff format using FIJI ImageJ[108]. Depending on the nature of the confocal micrograph, the peak prominence value ranges were between 25-45 µm, and the measurement radius was maintained at 5.5 for Method A. For method B, the rolling ball radius range was used with 6-8 pixels,

and the mean filter radius was kept at 2 pixels. The images were thresholded using Bremsen's technique at a radius of 50. To avoid programming errors inherent in Method B, the thresholded particles were manually analyzed at a micron size of 0.02-infinity and with a circularity range of 0.00-1.00. All the data collected were manually checked for the elimination of signals and data points outside of the region of interest (ROI).

### 5:7 RNA extraction and cDNA synthesis for quantitative polymerase chain reaction (qPCR)

Wild type or treated *N. benthamiana* tissues were collected and frozen in liquid nitrogen. A QIAprep® Spin Miniprep Kit (QIAGEN, cat. Nas 27104 and 27106) was used to collect RNA from three biologically independent samples according to the manufacturer's protocol. DNAase-free DNA removal kit (Invitrogen, Carlsbad, CA) was used to digest genomic DNA. cDNA was synthesized using M-MLV reverse transcriptase and the oligo-dT primers in accordance with the manufacturer's protocol, (Promega, Madison, WI). The manufacturer's protocol was used for first strand cDNA synthesis, which was then used for quantitative-PCR.

cDNA obtained from SA-treated and untreated control plants were diluted to 1:5 with nuclease-free water. qPCR was performed using a commercial SYBR Green master mix on a 364 well format LightCycler 480 real-time PCR system (Roche, IN, USA) with the following thermal cycling settling:

Step 1: 95 °C for 10 minutes

Step 2: 40 cycles of 95 °C for 10 seconds

Step 3: 59 °C for 10 seconds

Step 4: 72 °C for 20 seconds.

Raw qPCR data was used to analyze the cycle threshold values and normalized to the expression of EF1 alpha as a reference gene along with the untreated control[74].

### 5:8 Measuring the effects of SA: Movement assay to measure intercellular trafficking via plasmodesmata

To measure intercellular trafficking via plasmodesmata, movement assays were performed as described in chapter 3. A low inoculum of *A. tumefaciens* cells ($OD_{600}$=0.0001) carrying a plasmid for expression of plant-optimized monomeric GFP was infiltrated into *N. benthamiana* leaves with needleless syringes so that individual epidermal cells would be transformed to express monomeric GFP. 24 hours after infiltrating *A. tumefaciens*, 50 µM and 100 µM salicylic acid (SA) were infiltrated into different locations within the same leaves, and then plants were placed on light cart for another 24 hours. The spread of GFP to neighboring epidermal cells was quantified 48 hours after infiltration of *A. tumefaciens* (and 24 hours after infiltration of SA)**.** This procedure was repeated for the other SA treatment times (12 hours, 4 hours and 1 hour), but the SA infiltration time was adjusted for each such that analysis occurred 48 hours after agrobacterial infiltration for all treatments. Z-stacks of GFP foci were collected by confocal fluorescence microscopy on the Leica SP8-X instrument with a 20x objective. Z-stacks were reconstructed and processed in ImageJ. To quantify the movement, the number of layers of cells in the epidermis surrounding the transformed cell were scored with the highest movement layer recorded. Movement assays were performed for at least 3-4 biological replicates. Each replicate included at least 40 foci.

Statistical significance between treated and untreated samples was determined using the Mann Whitney U test ($p<0.05$) compared.

### 5:9 Measuring PD density using PDLP-GFP expression

To measure pitfield density along the cell wall, *N. benthamiana* PDLP1-GFP was transiently expressed in the leaves of untreated and SA treated leaves. *A. tumefaciens* infiltration was performed as previously described using an $OD_{600}$ =0.001. Following agroinfiltration, SA was infiltrated at different timepoints. For instance, 12 hours of SA treatment corresponded to SA infiltration 60 hours after agroinfiltration. Images were collected at 72 hours after infiltrations with a Lecia SP8-X confocal microscope with white light laser using a 25x water immersion objective and 4x zoom setting. The same laser power and gain settings were used to collect 15 µm z-stacks of epidermal cells expressing PDLP-GFP at a step size of 1 µm. A total of approximately 68-70 stacks were collected across three biological replicates for the control and treatment plants.

### 5:10 Image analysis using ImageJ for measuring pitfield distribution.

The total number of GFP puncta (pitfields) in each image were collected using the maximum intensity projection for each z-stack. Images were converted into 8-bit images and inverted. Thresholding was performed on the binary images to adjust the threshold of intensity. The total number of pitfields were collected using the particle analyzer function on Image J which counts the total number of GFP punctate. Cell wall lengths were measured by tracing the cell wall in the region of interest. The total number of PD within each region of interest was calculated as the following: Pitfields/unit area

(Pitfields/100 $\mu m^2$ cell wall). Statistical significance was determined by the Welch's t-test ($p<0.0001$).

**5:12 Transmission electron microscopy of N. benthamiana leaf tissues**

*N. benthamina* plants were grown in 16 hours of light and 8 hours of darkness at 25 °C. SA-treated and untreated control tissues were collected at the different treatment time points (1hr, 4hrs, and 12 hrs). Tissues were then subjected to high-pressure freezing and freeze substitution with $OsO_4$ following the protocol from Burch-Smith and Zambryski, 2010 for TEM sample preparation[12].

**5:13 High pressure Freezing and Freeze substitution.**

High pressure freezing was performed using a Leica EM ICE high pressure freezer and a Leica EM AFS2-FSP, located at the Danforth Center microscopy core facility, and used for automated freeze substitution for sample preparation, along with Thermo Scientific Talos L120C G2 with a Ceta 16M 4k x 4k CMOS camera for TEM.
Freeze substitution was performed by using 3 mL from a 100 mL acetone bottle and combining with 3mL water, and stored in –80 °C. Two ampules of 1 g OsO4 was added to the acetone bottle and stored in –80 °C. 5 mL of 2% uranyl acetate (Uac) in methanol (0.1 g Uac in 5 mL methanol) was dissolved and chilled in –80 °C and added to the substitution fluid (2% OsO4 + 3% H2O + 0.1% Uac in acetone). The substitution fluid was stored in –80 °C.

### 5:12 Chemical Fixation

The procedure for chemical fixation requires 9 days. To ensure this procedure is clear to the reader, the procedure is broken down into actions performed on each individual day, which includes both the actions and reagents used.

**Step 1: Day 1**

Approximately 5 mm of leaf samples were collected and placed in the primary fixative solution (2% paraformaldehyde + 2% glutaraldehyde + 0.01% Tween20 + 0.05% Malachite green in 0.1 M sodium cacodylate buffer; Table XX). Vacuum infiltration of samples with fixative was performed for 30 mins before gentle agitation on a shaker for two hours. Samples were then exchanged with secondary fixation buffer (2% paraformaldehyde + 2% glutaraldehyde in Sodium cacodylate buffer; Table 1) and incubated overnight at 4 °C.

**Step 2: Day 2**

The leaf pieces were transferred into vials filled with 0.1 M sodium cacodylate buffer. Samples were washed in 0.1 M sodium cacodylate Buffer 4x (changed every 10 min). Next, 2 mL of Postfix in 2% Osmium tetroxide was added to each vial and incubated for 4 hours on the shaker at room temperature. The leaf samples in vials were rinsed with water three times, for 10 minutes each. *En bloc* staining was used for TEM imaging to view thin sections without additional post staining. One mL of 1% aqueous uranyl acetate was added to vials and placed at 4°C overnight to *en bloc* uranyl acetate.

**Table 1**

| Stock | Final concentration | Volume needed (Vt=40 mL) |
|---|---|---|
| 16% Paraformaldehyde aqueous | 2% | 5 mL |
| 8% Glutaraldehyde aqueous | 2% | 10 mL |
| 1% Tween-20 | 0.01% | 0.4 mL |
| 1% Malachite green | 0.05% | 2 mL |
| 0.2 M Sodium cacodylate buffer | 0.1 M | 20 mL |
| Water | - | 2.6 mL |
| 16% Paraformaldehyde aqueous | 2% | 5 mL |
| 8% Glutaraldehyde aqueous | 2% | 10 mL |
| 0.2 M Sodium cacodylate buffer | 0.1 M | 20 mL |
| Water | - | 5 mL |

**Step 3: Day 3**

*Note: Transferred freeze substituted samples from –80°C to -20°C*

Samples were incubated in uranyl acetate (described above) at 50°C for 2 hours. The sample temperature was then lowered to room temperature, and this 50°C to room temperature cycling was repeated three times. Samples were then rinsed with water three times for 15 mins each.

En bloc lead

0.04 g L-aspartic acid (Sigma A-8949) was dissolved in 10 ml water and warmed up to 60°C in solution. 0.066 g lead nitrate (Aldrich 203580-10G) was added and adjusted to a pH of 5.5 using 350 µl of 1 M sodium hydroxide. The solution was maintained at 60°C prior to staining. Lead aspartate was added and placed in the oven at 50°C for 2 hrs and then cooled down to room temperature. Samples were rinsed three times with 15 mins incubation.

Dehydration steps

Dehydration was performed as below in room temperature with slow agitation on the shaker:

25% cold acetone 30 min

50% cold acetone 30 min

75% cold acetone 30 mins

Incubate overnight with fresh 75% cold acetone at room temperature on the shaker.

**Figure 22: Fixed samples for TEM images**

A disk of filter paper was added on top to keep the leaf pieces submerged as imaged above.

**Day 4:**

Place freeze substituted samples in 4°C in the morning, then perform the following washes:

95% cold acetone 30 min

100% cold acetone 30 min

100% cold acetone 30 min

Rinse freeze-substituted samples in acetone ~4 times. They will be processed together with the chemically fixed samples from now on.

Propylene oxide treatment

100% propylene oxide was added and incubated for 30 mins on the shaker at 50 rpm. Repeated two times and each time make sure caps are tightened. A lid of a pipette tips box was used to keep the vials standing.

*Note:* This step is carcinogenic and volatile. Double gloves and long sleeves/lab coat were used. Experiment work was done in the fume hood with sash lowered; the required amount was carefully poured into a small beaker and used a glass pipette to transfer.

Infiltration with propylene oxide + quetol (without DMP30)

3:1 Propylene oxide: quetol incubated overnight at room temperature on shaker, 50 rpm.

**Day 5:**

Sample were replaced with 2:1 propylene oxide:quetol in the morning and 1:1

propylene oxide:quetol in the afternoon and then incubated over the weekend on shaker.

**Day 6**

Samples were replaced with 1:2 propylene oxide:quetol (fresh quetol) in the morning and 1:3 propylene oxide: quetol in the afternoon and incubated overnight on shaker.

**Day 7:**

Samples were replaced with 100% quetol w/o DMP30 in the morning. Mojst of the quetol was removed and the vials were left in the hood without lids for 2 hours to air dry. 100% quetol w/o DMP30 was added to vials in afternoon and then incubated overnight on shaker.

**Day 8:**

Vials solutions were replaced with 100% quetol+DMP30 in the morning and replaced with 100% quetol+DMP30 in the afternoon. Samples were incubated overnight at room temperature.

**Day 9:**

Samples were exchanged with 100% quetol+DMP30 (fresh batch of quetol) in the morning and then proceeded to embed at midday. Samples were placed in the oven at 50°C for 48 hours.

Blocks sample preparation before TEM

Blocks were trimmed with an ultra-microtome, at the Danforth Center, to expose plant tissue. This provided a smooth surface area for imaging using TEM.

# REFERENCES


1. Reagan, B.C., Ganusova, E.E., Fernandez, J.C., McCray, T.N., and Burch-Smith, T.M. (2018). RNA on the move: The plasmodesmata perspective. Plant Science *275*, 1–10. 10.1016/j.plantsci.2018.07.001.

2. Yosef, F., Ronald J. Myers JR., Deana G. Grant, and Ron Mittler (2021). Plasmodesmata-localized proteins and ROS orchestrate light-induced rapid systemic signaling in Arabidopsis. Science Signaling.

3. Reagan, B.C., and Burch-Smith, T.M. (2020). Viruses Reveal the Secrets of Plasmodesmal Cell Biology. MPMI *33*, 26–39. 10.1094/MPMI-07-19-0212-FI.

4. Burch-Smith, T.M., Stonebloom, S., Xu, M., and Zambryski, P.C. (2011). Plasmodesmata during development: re-examination of the importance of primary, secondary, and branched plasmodesmata structure versus function. Protoplasma *248*, 61–74.

5. Ehlers, K., and Kollmann, R. (2001). Primary and secondary plasmodesmata: structure, origin, and functioning. Protoplasma *216*, 1–30.

6. Faulkner, C., Akman, O.E., Bell, K., Jeffree, C., and Oparka, K. (2008). Peeking into Pit Fields: A Multiple Twinning Model of Secondary Plasmodesmata Formation in Tobacco. The Plant Cell *20*, 1504–1518. 10.1105/tpc.107.056903.

7. Fitzgibbon, J., Beck, M., Zhou, J., Faulkner, C., Robatzek, S., and Oparka, K. (2013). A Developmental Framework for Complex Plasmodesmata Formation Revealed by Large-Scale Imaging of the Arabidopsis Leaf Epidermis. The Plant Cell *25*, 57–70. 10.1105/tpc.112.105890.

8. Oparka, K.J., Roberts, A.G., Boevink, P., Cruz, S.S., Roberts, I., Pradel, K.S., Imlau, A., Kotlizky, G., Sauer, N., and Epel, B. (1999). Simple, but Not Branched, Plasmodesmata Allow the Nonspecific Trafficking of Proteins in Developing Tobacco Leaves. Cell *97*, 743–754. 10.1016/S0092-8674(00)80786-2.

9. Ehlers, K., and van Bel, A.J.E. (2010). Dynamics of plasmodesmal connectivity in successive interfaces of the cambial zone. Planta *231*, 371–385. 10.1007/s00425-009-1046-8.

10. Nicolas, W.J., Grison, M.S., Trépout, S., Gaston, A., Fouché, M., Cordelières, F.P., Oparka, K., Tilsner, J., Brocard, L., and Bayer, E.M. (2017). Architecture and permeability of post-cytokinesis plasmodesmata lacking cytoplasmic sleeves. Nature Plants *3*, 1–11. 10.1038/nplants.2017.82.

11. Ross-Elliott, T.J., Jensen, K.H., Haaning, K.S., Wager, B.M., Knoblauch, J., Howell, A.H., Mullendore, D.L., Monteith, A.G., Paultre, D., Yan, D., et al. (2017). Phloem unloading in Arabidopsis roots is convective and regulated by the phloem-pole pericycle. eLife *6*, e24125. 10.7554/eLife.24125.

12. Burch-Smith, T.M., and Zambryski, P.C. (2010). Loss of INCREASED SIZE EXCLUSION LIMIT (ISE) 1 or ISE2 increases the formation of secondary plasmodesmata. Current Biology *20*, 989–993.

13. Gunning, B.E., and Robards, A. (2012). Intercellular communication in plants: studies on plasmodesmata (Springer Science & Business Media).

14. Levy, A., Guenoune-Gelbart, D., and Epel, B.L. (2007). β-1, 3-Glucanases: plasmodesmal gate keepers for intercellular communication. Plant Signaling & Behavior *2*, 404–407.

15. Levy, A., Erlanger, M., Rosenthal, M., and Epel, B.L. (2007). A plasmodesmata-associated β-1, 3-glucanase in Arabidopsis. The Plant Journal *49*, 669–682.

16. Vatén, A., Dettmer, J., Wu, S., Stierhof, Y.-D., Miyashima, S., Yadav, S.R., Roberts, C.J., Campilho, A., Bulone, V., and Lichtenberger, R. (2011). Callose biosynthesis regulates symplastic trafficking during root development. Developmental cell *21*, 1144–1155.

17. Mellor, N.L., Voß, U., Janes, G., Bennett, M.J., Wells, D.M., and Band, L.R. (2020). Auxin fluxes through plasmodesmata modify root-tip auxin distribution. Development *147*, dev181669.

18. Han, X., Hyun, T.K., Zhang, M., Kumar, R., Koh, E., Kang, B.-H., Lucas, W.J., and Kim, J.-Y. (2014). Auxin-callose-mediated plasmodesmal gating is essential for tropic auxin gradient formation and signaling. Developmental cell *28*, 132–146.

19. Coudert, Y., Palubicki, W., Ljung, K., Novak, O., Leyser, O., and Harrison, C.J. (2015). Three ancient hormonal cues co-ordinate shoot branching in a moss. Elife *4*, e06808.

20. Gao, C., Liu, X., De Storme, N., Jensen, K.H., Xu, Q., Yang, J., Liu, X., Chen, S., Martens, H.J., and Schulz, A. (2020). Directionality of plasmodesmata-mediated transport in Arabidopsis leaves supports auxin channeling. Current Biology *30*, 1970–1977.

21. Liu, Y., Xu, M., Liang, N., Zheng, Y., Yu, Q., and Wu, S. (2017). Symplastic communication spatially directs local auxin biosynthesis to maintain root stem cell niche in Arabidopsis. Proceedings of the National Academy of Sciences *114*, 4005–4010.

22. Sager, R., Wang, X., Hill, K., Yoo, B.-C., Caplan, J., Nedo, A., Tran, T., Bennett, M.J., and Lee, J.-Y. (2020). Auxin-dependent control of a plasmodesmal regulator creates a negative feedback loop modulating lateral root emergence. Nature Communications *11*, 364.

23. Tylewicz, S., Petterle, A., Marttila, S., Miskolczi, P., Azeez, A., Singh, R.K., Immanen, J., Mähler, N., Hvidsten, T.R., and Eklund, D.M. (2018). Photoperiodic control of seasonal growth is mediated by ABA acting on cell-cell communication. Science *360*, 212–215.

24. Rinne, P.L., Welling, A., Vahala, J., Ripel, L., Ruonala, R., Kangasjärvi, J., and van der Schoot, C. (2011). Chilling of dormant buds hyperinduces FLOWERING LOCUS T and recruits GA-inducible 1, 3-β-glucanases to reopen signal conduits and release dormancy in Populus. The Plant Cell *23*, 130–146.

25. Singh, R.K., Miskolczi, P., Maurya, J.P., and Bhalerao, R.P. (2019). A tree ortholog of SHORT VEGETATIVE PHASE floral repressor mediates photoperiodic control of bud dormancy. Current Biology *29*, 128–133.

26. Li, X.-F., Shao, X.-H., Deng, X.-J., Wang, Y., Zhang, X.-P., Jia, L.-Y., Xu, J., Zhang, D.-M., Sun, Y., and Xu, L. (2012). Necessity of high temperature for the dormancy release of Narcissus tazetta var. chinensis. Journal of plant physiology *169*, 1340–1347.

27. Autoradiographic studies on the role of plasmodesmata in the transport of gibberellin | SpringerLink https://link.springer.com/article/10.1007/BF00197801.

28. Kitagawa, M., Tomoi, T., Fukushima, T., Sakata, Y., Sato, M., Toyooka, K., Fujita, T., and Sakakibara, H. (2019). Abscisic acid acts as a regulator of molecular trafficking through plasmodesmata in the moss Physcomitrella patens. Plant and Cell Physiology *60*, 738–751.

29. Lim, G.-H., Shine, M.B., de Lorenzo, L., Yu, K., Cui, W., Navarre, D., Hunt, A.G., Lee, J.-Y., Kachroo, A., and Kachroo, P. (2016). Plasmodesmata localizing proteins regulate transport and signaling during systemic acquired immunity in plants. Cell host & microbe *19*, 541–549.

30. Dong, X., Hong, Z., Chatterjee, J., Kim, S., and Verma, D.P.S. (2008). Expression of callose synthase genes and its connection with Npr1 signaling pathway during pathogen infection. Planta *229*, 87–98.

31. Lee, J.-Y., Wang, X., Cui, W., Sager, R., Modla, S., Czymmek, K., Zybaliov, B., van Wijk, K., Zhang, C., and Lu, H. (2011). A plasmodesmata-localized protein mediates crosstalk between cell-to-cell communication and innate immunity in Arabidopsis. The Plant Cell *23*, 3353–3373.

32. Huang, D., Sun, Y., Ma, Z., Ke, M., Cui, Y., Chen, Z., Chen, C., Ji, C., Tran, T.M., and Yang, L. (2019). Salicylic acid-mediated plasmodesmal closure via Remorin-dependent lipid organization. Proceedings of the National Academy of Sciences *116*, 21274–21284.

33. Ormenese, S., Bernier, G., and Périlleux, C. (2006). Cytokinin application to the shoot apical meristem of Sinapis alba enhances secondary plasmodesmata formation. Planta *224*, 1481–1484.

34. Ermakova, M., Danila, F.R., Furbank, R.T., and von Caemmerer, S. (2020). On the road to C4 rice: advances and perspectives. The Plant Journal *101*, 940–950.

35. Cui, W., and Lee, J.-Y. (2016). Arabidopsis callose synthases CalS1/8 regulate plasmodesmal permeability during stress. Nature plants *2*, 1–9.

36. Chen, X.-Y., and Kim, J.-Y. (2009). Callose synthesis in higher plants. Plant signaling & behavior *4*, 489–492.

37. Shi, X., Sun, X., Zhang, Z., Feng, D., Zhang, Q., Han, L., Wu, J., and Lu, T. (2015). GLUCAN SYNTHASE-LIKE 5 (GSL5) plays an essential role in male fertility by regulating

callose metabolism during microsporogenesis in rice. Plant and Cell Physiology *56*, 497–509.

38. Iswanto, A.B.B., and Kim, J.-Y. (2017). Lipid Raft, Regulator of Plasmodesmal Callose Homeostasis. Plants (Basel) *6*, 15. 10.3390/plants6020015.

39. German, L., Yeshvekar, R., and Benitez-Alfonso, Y. (2023). Callose metabolism and the regulation of cell walls and plasmodesmata during plant mutualistic and pathogenic interactions. Plant, Cell & Environment *46*, 391–404. 10.1111/pce.14510.

40. Wu, S.-W., Kumar, R., Iswanto, A.B.B., and Kim, J.-Y. (2018). Callose balancing at plasmodesmata. Journal of experimental botany *69*, 5325–5339.

41. Han, X., Huang, L.-J., Feng, D., Jiang, W., Miu, W., and Li, N. (2019). Plasmodesmata-related structural and functional proteins: the long sought-after secrets of a cytoplasmic channel in plant cell walls. International Journal of Molecular Sciences *20*, 2946.

42. Oparka, K.J. (2004). Getting the message across: how do plant cells exchange macromolecular complexes? Trends in plant science *9*, 33–41.

43. Lucas, W.J. (2006). Plant viral movement proteins: agents for cell-to-cell trafficking of viral genomes. Virology *344*, 169–184.

44. Raskin, I. (1992). Role of Salicylic Acid in Plants. Annual Review of Plant Physiology and Plant Molecular Biology *43*, 439–463. 10.1146/annurev.pp.43.060192.002255.

45. Hayat, S., Ali, B., and Ahmad, A. (2007). Salicylic acid: biosynthesis, metabolism and physiological role in plants. Salicylic acid: A plant hormone, 1–14.

46. Krantev, A., Yordanova, R., Janda, T., Szalai, G., and Popova, L. (2008). Treatment with salicylic acid decreases the effect of cadmium on photosynthesis in maize plants. Journal of plant physiology *165*, 920–931.

47. Popova, L.P., Maslenkova, L.T., Yordanova, R.Y., Ivanova, A.P., Krantev, A.P., Szalai, G., and Janda, T. (2009). Exogenous treatment with salicylic acid attenuates cadmium toxicity in pea seedlings. Plant Physiology and Biochemistry *47*, 224–231.

48. Kubota, M., and Nishi, K. (2006). Salicylic acid accumulates in the roots and hypocotyl after inoculation of cucumber leaves with Colletotrichum lagenarium. Journal of Plant Physiology *163*, 1111–1117. 10.1016/j.jplph.2005.09.005.

49. Lefevere, H., Bauters, L., and Gheysen, G. (2020). Salicylic acid biosynthesis in plants. Frontiers in plant science *11*, 338.

50. Zhong, Q., Hu, H., Fan, B., Zhu, C., and Chen, Z. (2021). Biosynthesis and roles of salicylic acid in balancing stress response and growth in plants. International Journal of Molecular Sciences *22*, 11672.

51. Loake, G., and Grant, M. (2007). Salicylic acid in plant defence—the players and protagonists. Current opinion in plant biology *10*, 466–472.

52. Ding, P., and Ding, Y. (2020). Stories of salicylic acid: a plant defense hormone. Trends in plant science *25*, 549–565.

53. Kumar, D. (2014). Salicylic acid signaling in disease resistance. Plant Science *228*, 127–134.

54. Soares, J.M., Weber, K.C., Qiu, W., Mahmoud, L.M., Grosser, J.W., and Dutt, M. (2022). Overexpression of the salicylic acid binding protein 2 (SABP2) from tobacco enhances tolerance against Huanglongbing in transgenic citrus. Plant Cell Reports *41*, 2305–2320.

55. Wang, X., Sager, R., Cui, W., Zhang, C., Lu, H., and Lee, J.-Y. (2013). Salicylic acid regulates plasmodesmata closure during innate immune responses in Arabidopsis. The Plant Cell *25*, 2315–2329.

56. Kachroo, A., Liu, H., Yuan, X., Kurokawa, T., and Kachroo, P. (2022). Systemic acquired resistance-associated transport and metabolic regulation of salicylic acid and glycerol-3-phosphate. Essays in Biochemistry *66*, 673–681.

57. Imaging Callose at Plasmodesmata Using Aniline Blue: Quantitative Confocal Microscopy (2015). (Springer), pp. 105–119.

58. Koh, E.-J., Zhou, L., Williams, D.S., Park, J., Ding, N., Duan, Y.-P., and Kang, B.-H. (2012). Callose deposition in the phloem plasmodesmata and inhibition of phloem transport in citrus leaves infected with “Candidatus Liberibacter asiaticus.” Protoplasma *249*, 687–697.

59. Abou-Saleh, R.H., Hernandez-Gomez, M.C., Amsbury, S., Paniagua, C., Bourdon, M., Miyashima, S., Helariutta, Y., Fuller, M., Budtova, T., Connell, S.D., et al. (2018). Interactions between callose and cellulose revealed through the analysis of biopolymer mixtures. Nat Commun *9*, 4538. 10.1038/s41467-018-06820-y.

60. Grignon, N., Touraine, B., and Durand, M. (1989). 6 (5) Carboxyfluorescein as a tracer of phloem sap translocation. American Journal of Botany *76*, 871–877.

61. Knoblauch, M., Vendrell, M., de Leau, E., Paterlini, A., Knox, K., Ross-Elliot, T., Reinders, A., Brockman, S.A., Ward, J., and Oparka, K. (2015). Multispectral Phloem-Mobile Probes: Properties and Applications. Plant Physiology *167*, 1211–1220. 10.1104/pp.114.255414.

62. Mehdi, R., Lamm, C.E., Bodampalli Anjanappa, R., Müdsam, C., Saeed, M., Klima, J., Kraner, M.E., Ludewig, F., Knoblauch, M., Gruissem, W., et al. (2019). Symplasmic phloem unloading and radial post-phloem transport via vascular rays in tuberous roots of Manihot esculenta. Journal of Experimental Botany *70*, 5559–5573. 10.1093/jxb/erz297.

63. Cui, W., Wang, X., and Lee, J.-Y. (2015). Drop-ANd-See: A Simple, Real-Time, and Noninvasive Technique for Assaying Plasmodesmal Permeability. In Plasmodesmata:

Methods and Protocols Methods in Molecular Biology., M. Heinlein, ed. (Springer), pp. 149–156. 10.1007/978-1-4939-1523-1_10.

64. Wang, X., Sager, R., and Lee, J.-Y. (2020). Chapter 6 - Evaluating molecular movement through plasmodesmata. In Methods in Cell Biology Plant Cell Biology., C. T. Anderson, E. S. Haswell, and R. Dixit, eds. (Academic Press), pp. 99–117. 10.1016/bs.mcb.2020.04.008.

65. Yang, X., Lu, Y., Wang, F., Chen, Y., Tian, Y., Jiang, L., Peng, J., Zheng, H., Lin, L., Yan, C., et al. (2020). Involvement of the chloroplast gene ferredoxin 1 in multiple responses of Nicotiana benthamiana to Potato virus X infection. Journal of Experimental Botany *71*, 2142–2156. 10.1093/jxb/erz565.

66. Martens, H.J., Hansen, M., and Schulz, A. (2004). Caged probes: a novel tool in studying symplasmic transport in plant tissues. Protoplasma *223*, 63–66. 10.1007/s00709-003-0029-z.

67. Gisel, A., Barella, S., Hempel, F.D., and Zambryski, P.C. (1999). Temporal and spatial regulation of symplastic trafficking during development in *Arabidopsis thaliana* apices. Development *126*, 1879–1889. 10.1242/dev.126.9.1879.

68. Kim, I., Hempel, F.D., Sha, K., Pfluger, J., and Zambryski, P.C. (2002). Identification of a developmental transition in plasmodesmatal function during embryogenesis in Arabidopsis thaliana. Development *129*, 1261–1272. 10.1242/dev.129.5.1261.

69. Grzyb, M., Wróbel-Marek, J., Kurczyńska, E., Sobczak, M., and Mikuła, A. (2020). Symplasmic Isolation Contributes to Somatic Embryo Induction and Development in the Tree Fern Cyathea delgadii Sternb. Plant and Cell Physiology *61*, 1273–1284. 10.1093/pcp/pcaa058.

70. Oparka, K.J., and Prior, D.A.M. (1988). Movement of Lucifer Yellow CH in potato tuber storage tissues: A comparison of symplastic and apoplastic transport. Planta *176*, 533–540. 10.1007/BF00397661.

71. Brunkard, J.O., Burch-Smith, T.M., Runkel, A.M., and Zambryski, P. (2015). Investigating Plasmodesmata Genetics with Virus-Induced Gene Silencing and an Agrobacterium-Mediated GFP Movement Assay. In Plasmodesmata: Methods and Protocols Methods in Molecular Biology., M. Heinlein, ed. (Springer), pp. 185–198. 10.1007/978-1-4939-1523-1_13.

72. Crawford, K.M., and Zambryski, P.C. (2000). Subcellular localization determines the availability of non-targeted proteins to plasmodesmatal transport. Current Biology *10*, 1032–1040. 10.1016/S0960-9822(00)00657-6.

73. Brunkard, J.O., and Zambryski, P. (2019). Plant Cell-Cell Transport via Plasmodesmata Is Regulated by Light and the Circadian Clock. Plant Physiol. *181*, 1459–1467. 10.1104/pp.19.00460.

74. Ganusova, E.E., Reagan, B.C., Fernandez, J.C., Azim, M.F., Sankoh, A.F., Freeman, K.M., McCray, T.N., Patterson, K., Kim, C., and Burch-Smith, T.M. (2020). Chloroplast-to-nucleus retrograde signalling controls intercellular trafficking via plasmodesmata formation. Philosophical Transactions of the Royal Society B: Biological Sciences *375*, 20190408. 10.1098/rstb.2019.0408.

75. Horner, W., and Brunkard, J.O. (2021). Cytokinins Stimulate Plasmodesmatal Transport in Leaves. Frontiers in Plant Science *12*.

76. Stadler, R., and Sauer, N. (2019). The AtSUC2 Promoter: A Powerful Tool to Study Phloem Physiology and Development. In Phloem: Methods and Protocols Methods in Molecular Biology., J. Liesche, ed. (Springer), pp. 267–287. 10.1007/978-1-4939-9562-2_22.

77. Gerlitz, N., Gerum, R., Sauer, N., and Stadler, R. (2018). Photoinducible DRONPA-s: a new tool for investigating cell–cell connectivity. The Plant Journal *94*, 751–766. 10.1111/tpj.13918.

78. Johnston, M.G., and Faulkner, C. (2021). A bootstrap approach is a superior statistical method for the comparison of non-normal data with differing variances. New Phytol *230*, 23–26. 10.1111/nph.17159.

79. Dlng, B., Haudenshield, J.S., Hll, J., and Lucbs', W.J. Secondary Plasmodesmata Are Specific Sites of Localization of the Tobacco Mosaic Virus Movement Protein in Transgenic Tobacco Plants.

80. Fitzgibbon, J., Bell, K., King, E., and Oparka, K. (2010). Super-Resolution Imaging of Plasmodesmata Using Three-Dimensional Structured Illumination Microscopy. Plant Physiology *153*, 1453–1463. 10.1104/pp.110.157941.

81. Hofius, D., Herbers, K., Melzer, M., Omid, A., Tacke, E., Wolf, S., and Sonnewald, U. (2001). Evidence for expression level-dependent modulation of carbohydrate status and viral resistance by the potato leafroll virus movement protein in transgenic tobacco plants. The Plant Journal *28*, 529–543. 10.1046/j.1365-313X.2001.01179.x.

82. Olesinski, A.A., Almon, E., Navot, N., Perl, A., Galun, E., Lucas, W.J., and Wolf, S. (1996). Tissue-Specific Expression of the Tobacco Mosaic Virus Movement Protein in Transgenic Potato Plants Alters Plasmodesmal Function and Carbohydrate Partitioning. Plant Physiology *111*, 541–550. 10.1104/pp.111.2.541.

83. Rinne, P.L.H., Boogaard, R. van den, Mensink, M.G.J., Kopperud, C., Kormelink, R., Goldbach, R., and Schoot, C. van der (2005). Tobacco plants respond to the constitutive expression of the tospovirus movement protein NSM with a heat-reversible sealing of plasmodesmata that impairs development. The Plant Journal *43*, 688–707. 10.1111/j.1365-313X.2005.02489.x.

84. Danila, F.R., Quick, W.P., White, R.G., Furbank, R.T., and von Caemmerer, S. (2016). The Metabolite Pathway between Bundle Sheath and Mesophyll: Quantification of

Plasmodesmata in Leaves of C $_3$ and C $_4$ Monocots. Plant Cell *28*, 1461–1471. 10.1105/tpc.16.00155.

85. Danila, F.R., Quick, W.P., White, R.G., von Caemmerer, S., and Furbank, R.T. (2019). Response of plasmodesmata formation in leaves of C4 grasses to growth irradiance. Plant, Cell & Environment *42*, 2482–2494. 10.1111/pce.13558.

86. Miranda, K., Girard-Dias, W., Attias, M., de Souza, W., and Ramos, I. (2015). Three dimensional reconstruction by electron microscopy in the life sciences: An introduction for cell and tissue biologists. Molecular Reproduction and Development *82*, 530–547. 10.1002/mrd.22455.

87. Bobik, K., Dunlap, J.R., and Burch-Smith, T.M. (2014). Tandem High-pressure Freezing and Quick Freeze Substitution of Plant Tissues for Transmission Electron Microscopy. JoVE (Journal of Visualized Experiments), e51844. 10.3791/51844.

88. McDonald, K.L. (2014). Out with the old and in with the new: rapid specimen preparation procedures for electron microscopy of sectioned biological material. Protoplasma *251*, 429–448. 10.1007/s00709-013-0575-y.

89. Yan, D., Yadav, S.R., Paterlini, A., Nicolas, W.J., Petit, J.D., Brocard, L., Belevich, I., Grison, M.S., Vaten, A., Karami, L., et al. (2019). Sphingolipid biosynthesis modulates plasmodesmal ultrastructure and phloem unloading. Nat. Plants *5*, 604–615. 10.1038/s41477-019-0429-5.

90. Dettmer, J., Ursache, R., Campilho, A., Miyashima, S., Belevich, I., O'Regan, S., Mullendore, D.L., Yadav, S.R., Lanz, C., Beverina, L., et al. (2014). CHOLINE TRANSPORTER-LIKE1 is required for sieve plate development to mediate long-distance cell-to-cell communication. Nat Commun *5*, 4276. 10.1038/ncomms5276.

91. Paterlini, A., Belevich, I., Jokitalo, E., and Helariutta, Y. (2020). Computational Tools for Serial Block Electron Microscopy Reveal Plasmodesmata Distributions and Wall Environments. Plant Physiol. *184*, 53–64. 10.1104/pp.20.00396.

92. Brandon C. Reagan, Paul J. -Y. Kim, Preston D. Perry, John R. Dunlap, and Tessa M. Burch-Smith (2017). Spatial distribution of organelles in leaf cells and soybean root nodules revealed by focused ion beam-scanning electron microscopy. Functional Plant Biology *45(2)*, 180–191. https://doi.org/10.1071/FP16347.

93. Azim, M.F., and Burch-Smith, T.M. (2020). Organelles-nucleus-plasmodesmata signaling (ONPS): an update on its roles in plant physiology, metabolism and stress responses. Current Opinion in Plant Biology *58*, 48–59.

94. Kremer, J.R., Mastronarde, D.N., and McIntosh, J.R. (1996). Computer Visualization of Three-Dimensional Image Data Using IMOD. Journal of Structural Biology *116*, 71–76. 10.1006/jsbi.1996.0013.

95. Kittelmann M., M., Hawes, C., and Hughes, L. (2016). Serial block face scanning electron microscopy and the reconstruction of plant cell membrane systems. Journal of Microscopy *263*, 200–211. 10.1111/jmi.12424.

96. Tilsner, J., Nicolas, W., Rosado, A., and Bayer, E.M. (2016). Staying tight: plasmodesmal membrane contact sites and the control of cell-to-cell connectivity in plants. Annual review of plant biology *67*, 337–364.

97. Sankoh, A.F., and Burch-Smith, T.M. (2021). Plasmodesmata and hormones: pathways for plant development. American Journal of Botany *108*.

98. Zavaliev, R., Ueki, S., Epel, B.L., and Citovsky, V. (2011). Biology of callose (β-1,3-glucan) turnover at plasmodesmata. Protoplasma *248*, 117–130. 10.1007/s00709-010-0247-0.

99. Singh, A., Lim, G.-H., and Kachroo, P. (2017). Transport of chemical signals in systemic acquired resistance. Journal of integrative plant biology *59*, 336–344.

100. Lee, J.-Y., and Lu, H. (2011). Plasmodesmata: the battleground against intruders. Trends in plant science *16*, 201–210.

101. Conrath, U. (2006). Systemic acquired resistance. Plant signaling & behavior *1*, 179–184.

102. Pérez-de-Luque, A., Tille, S., Johnson, I., Pascual-Pardo, D., Ton, J., and Cameron, D.D. (2017). The interactive effects of arbuscular mycorrhiza and plant growth-promoting rhizobacteria synergistically enhance host plant defences against pathogens. Scientific reports *7*, 16409.

103. Sanmartín, N., Pastor, V., Pastor-Fernández, J., Flors, V., Pozo, M.J., and Sánchez-Bel, P. (2020). Role and mechanisms of callose priming in mycorrhiza-induced resistance. Journal of Experimental Botany *71*, 2769–2781.

104. Goodin, M.M., Zaitlin, D., Naidu, R.A., and Lommel, S.A. (2008). Nicotiana benthamiana: its history and future as a model for plant–pathogen interactions. Molecular plant-microbe interactions *21*, 1015–1026.

105. Aniline blue staining of quanatification of plasmodesmal callose John Innes Centre. https://www.jic.ac.uk/research-impact/aniline-blue-staining-of-qunatification-of-plasmodesmal-callose/.

106. Rueden, C.T., and Eliceiri, K.W. (2019). ImageJ for the next generation of scientific image data. Microscopy and microanalysis *25*, 142–143.

107. Schindelin, J., Arganda-Carreras, I., Frise, E., Kaynig, V., Longair, M., Pietzsch, T., Preibisch, S., Rueden, C., Saalfeld, S., and Schmid, B. (2012). Fiji: an open-source platform for biological-image analysis. Nature methods *9*, 676–682.

108. Huang, C., Mutterer, J., and Heinlein, M. (2022). In Vivo Aniline Blue Staining and Semiautomated Quantification of Callose Deposition at Plasmodesmata. In Plasmodesmata: Methods and Protocols (Springer), pp. 151–165.

109. Koo, Y.M., Heo, A.Y., and Choi, H.W. (2020). Salicylic acid as a safe plant protector and growth regulator. The plant pathology journal *36*, 1.

110. Wang, Y., Li, X., Fan, B., Zhu, C., and Chen, Z. (2021). Regulation and function of defense-related callose deposition in plants. International Journal of Molecular Sciences *22*, 2393.

111. Yi, S.Y., Shirasu, K., Moon, J.S., Lee, S.-G., and Kwon, S.-Y. (2014). The activated SA and JA signaling pathways have an influence on flg22-triggered oxidative burst and callose deposition. PloS one *9*, e88951.

112. Mason, K.N., Ekanayake, G., and Heese, A. (2020). Staining and automated image quantification of callose in Arabidopsis cotyledons and leaves. In Methods in cell biology (Elsevier), pp. 181–199.

113. Ganusova, E.E., Rice, J.H., Carlew, T.S., Patel, A., Perrodin-Njoku, E., Hewezi, T., and Burch-Smith, T.M. (2017). Altered expression of a chloroplast protein affects the outcome of virus and nematode infection. Molecular Plant-Microbe Interactions *30*, 478–488.

114. Hartmann, M., and Zeier, J. (2019). N-hydroxypipecolic acid and salicylic acid: a metabolic duo for systemic acquired resistance. Current opinion in plant biology *50*, 44–57.

115. White, R.F. (1979). Acetylsalicylic acid (aspirin) induces resistance to tobacco mosaic virus in tobacco. Virology *99*, 410–412.

116. Jiang, Y., Zheng, W., Li, J., Liu, P., Zhong, K., Jin, P., Xu, M., Yang, J., and Chen, J. (2021). NbWRKY40 positively regulates the response of Nicotiana benthamiana to tomato mosaic virus via salicylic acid signaling. Frontiers in Plant Science *11*, 603518.

117. Epel, B.L. (2009). Plant viruses spread by diffusion on ER-associated movement-protein-rafts through plasmodesmata gated by viral induced host β-1, 3-glucanases. In Seminars in cell & developmental biology (Elsevier), pp. 1074–1081.

118. Wolf, S., Lucas, W.J., Deom, C.M., and Beachy, R.N. (1989). Movement protein of tobacco mosaic virus modifies plasmodesmatal size exclusion limit. Science *246*, 377–379.

119. Han, G.-Z. (2017). Evolution of jasmonate biosynthesis and signaling mechanisms. Journal of experimental botany *68*, 1323–1331.

120. Oelmüller, R. (2021). Threat at one end of the plant: what travels to inform the other parts? International Journal of Molecular Sciences *22*, 3152.

121. Babst, B.A., Ferrieri, R.A., Gray, D.W., Lerdau, M., Schlyer, D.J., Schueller, M., Thorpe, M.R., and Orians, C.M. (2005). Jasmonic acid induces rapid changes in carbon transport and partitioning in Populus. New phytologist *167*, 63–72.

122. Aerts, N., Pereira Mendes, M., and Van Wees, S.C. (2021). Multiple levels of crosstalk in hormone networks regulating plant defense. The Plant Journal *105*, 489–504.

123. Thaler, J.S., Humphrey, P.T., and Whiteman, N.K. (2012). Evolution of jasmonate and salicylate signal crosstalk. Trends in plant science *17*, 260–270.

124. Sankoh, A.F., and Burch-Smith, T.M. (2021). Approaches for investigating plasmodesmata and effective communication. Current Opinion in Plant Biology *64*, 102143. 10.1016/j.pbi.2021.102143.

125. Winnicki, K., Polit, J.T., Żabka, A., and Maszewski, J. (2021). Do plasmodesmata play a prominent role in regulation of auxin-dependent genes at early stages of embryogenesis? Cells *10*, 733.

126. Band, L.R. (2021). Auxin fluxes through plasmodesmata. New Phytologist *231*, 1686–1692.

127. Ryals, J.A., Neuenschwander, U.H., Willits, M.G., Molina, A., Steiner, H.-Y., and Hunt, M.D. (1996). Systemic acquired resistance. The plant cell *8*, 1809.

128. Lee, W.-S., Fu, S.-F., Li, Z., Murphy, A.M., Dobson, E.A., Garland, L., Chaluvadi, S.R., Lewsey, M.G., Nelson, R.S., and Carr, J.P. (2016). Salicylic acid treatment and expression of an RNA-dependent RNA polymerase 1 transgene inhibit lethal symptoms and meristem invasion during tobacco mosaic virus infection in Nicotiana benthamiana. BMC plant biology *16*, 1–14.

129. Schneider, C.A., Rasband, W.S., and Eliceiri, K.W. (2012). NIH Image to ImageJ: 25 years of image analysis. Nature methods *9*, 671–675.

130. Rivas-San Vicente, M., Larios-Zarate, G., and Plasencia, J. (2013). Disruption of sphingolipid biosynthesis in Nicotiana benthamiana activates salicylic acid-dependent responses and compromises resistance to Alternaria alternata f. sp. lycopersici. Planta *237*, 121–136. 10.1007/s00425-012-1758-z.

131. Lannoo, N., Vandenborre, G., Miersch, O., Smagghe, G., Wasternack, C., Peumans, W.J., and Van Damme, E.J. (2007). The jasmonate-induced expression of the Nicotiana tabacum leaf lectin. Plant and cell physiology *48*, 1207–1218.

132. Pérez-Sancho, J., Tilsner, J., Samuels, A.L., Botella, M.A., Bayer, E.M., and Rosado, A. (2016). Stitching organelles: organization and function of specialized membrane contact sites in plants. Trends in Cell Biology *26*, 705–717.

133. Grison, M.S., Brocard, L., Fouillen, L., Nicolas, W., Wewer, V., Dörmann, P., Nacir, H., Benitez-Alfonso, Y., Claverol, S., and Germain, V. (2015). Specific membrane lipid composition is important for plasmodesmata function in Arabidopsis. The Plant Cell *27*, 1228–1250.

134. Kraner, M.E., Link, K., Melzer, M., Ekici, A.B., Uebe, S., Tarazona, P., Feussner, I., Hofmann, J., and Sonnewald, U. (2017). Choline transporter-like1 (CHER 1) is crucial for plasmodesmata maturation in Arabidopsis thaliana. The plant journal *89*, 394–406.

135. Iswanto, A.B.B., Shon, J.C., Liu, K.H., Vu, M.H., Kumar, R., and Kim, J.-Y. (2020). Sphingolipids modulate secretion of glycosylphosphatidylinositol-anchored plasmodesmata proteins and callose deposition. Plant physiology *184*, 407–420.

136. Haupt, S., Cowan, G.H., Ziegler, A., Roberts, A.G., Oparka, K.J., and Torrance, L. (2005). Two plant–viral movement proteins traffic in the endocytic recycling pathway. The Plant Cell *17*, 164–181.

137. Levy, A., Zheng, J.Y., and Lazarowitz, S.G. (2015). Synaptotagmin SYTA forms ER-plasma membrane junctions that are recruited to plasmodesmata for plant virus movement. Current Biology *25*, 2018–2025.

138. Du, Y., Tejos, R., Beck, M., Himschoot, E., Li, H., Robatzek, S., Vanneste, S., and Friml, J. (2013). Salicylic acid interferes with clathrin-mediated endocytic protein trafficking. Proceedings of the National Academy of Sciences *110*, 7946–7951.

139. Wang, C., Hu, T., Yan, X., Meng, T., Wang, Y., Wang, Q., Zhang, X., Gu, Y., Sánchez-Rodríguez, C., and Gadeyne, A. (2016). Differential regulation of clathrin and its adaptor proteins during membrane recruitment for endocytosis. Plant Physiology *171*, 215–229.

140. Ishikawa, K., Tamura, K., Fukao, Y., and Shimada, T. (2020). Structural and functional relationships between plasmodesmata and plant endoplasmic reticulum–plasma membrane contact sites consisting of three synaptotagmins. New Phytologist *226*, 798–808. 10.1111/nph.16391.

141. Lewis, J.D., and Lazarowitz, S.G. (2010). Arabidopsis synaptotagmin SYTA regulates endocytosis and virus movement protein cell-to-cell transport. Proceedings of the National Academy of Sciences *107*, 2491–2496.

142. Uchiyama, A., Shimada-Beltran, H., Levy, A., Zheng, J.Y., Javia, P.A., and Lazarowitz, S.G. (2014). The Arabidopsis synaptotagmin SYTA regulates the cell-to-cell movement of diverse plant viruses. Frontiers in Plant Science *5*.

143. Visualising endocytosis in plants: past, present, and future - DRAGWIDGE - 2020 - Journal of Microscopy - Wiley Online Library https://onlinelibrary.wiley.com/doi/abs/10.1111/jmi.12926.

144. Pérez-Sancho, J., Vanneste, S., Lee, E., McFarlane, H.E., Esteban del Valle, A., Valpuesta, V., Friml, J., Botella, M.A., and Rosado, A. (2015). The Arabidopsis Synaptotagmin1 Is Enriched in Endoplasmic Reticulum-Plasma Membrane Contact Sites and Confers Cellular Resistance to Mechanical Stresses. Plant Physiology *168*, 132–143. 10.1104/pp.15.00260.

145. Gene identification with sequenced T-DNA tags generated by transformation of Arabidopsis cell suspension - Mathur - 1998 - The Plant Journal - Wiley Online Library https://onlinelibrary.wiley.com/doi/abs/10.1046/j.1365-313X.1998.00059.x.

146. Abràmoff, M.D., Magalhães, P.J., and Ram, S.J. (2004). Image processing with ImageJ. Biophotonics international *11*, 36–42.

147. Walter, Gerard G. (2010). Deaf and hard-of-hearing students in transition: Demographics with an emphasis on STEM education. National Technical Institute for the Deaf.

# APPENDIX 1

## Approaches for investigating plasmodesmata and effective communication

A version of this chapter was originally published by Amie F. Sankoh and T. M. Burch-Smith.

Sankoh, Amie F., and Tessa M. Burch-Smith. "**Approaches for investigating plasmodesmata and effective communication.**" *Current opinion in plant biology* 64 (2021): 102143.

***Abstract***

Plasmodesmata are integral plant cell wall components that provide routes for intercellular communication, signaling and resource sharing. They are therefore essential for plant growth and survival. Much effort has been put forth to understand how PD are generated and their structure is refined for function, and to determine how they regulate intercellular trafficking. This review provides an overview of some of the approaches that have been used to study PD structure and function, highlighting those that may be more widely adopted to address questions of PD cell biology and function. Additionally, we address communication in the research lab, focusing on challenges faced by our deaf/hard-of-hearing colleagues and how we can improve communication with them.

## The importance of communication for a diverse scientific workforce

In our lab, our interest in communication extends beyond that mediated by PD. One of the authors of this review is a Deaf scientist and our lab frequently engages other early career deaf and hard- of hearing individuals in our research. Similar to how diversity enriches an eco-system with species capable of using different resources and thriving in different microenvironments, science also benefits from the full range of perspectives present in our population. Deaf and hard-of- hearing (d/hh) individuals are part of the diverse views that can strengthen our science community. Careers in STEM

provide a route for improved economic outcomes for the d/hh, as d/hh individuals in STEM careers with bachelor's degrees earn twice more than those without degrees[147].

People learn in lots of diverse ways; Deaf people preferably learn everything visually. Often their visual attention is divided between a teacher, an interpreter, and a visual such as a slide or video. One of the biggest challenges encountered when training Deaf scientists is communication, and careful, effective communication is a major benefit for everyone. American Sign Language (ASL) is the preferred medium for communication for many d/hh persons, however, there is an absence of signs for many terms used in science. One striking example is the term 'culture'. The ASL sign for culture incorporates the sociological and historical aspects of the noun, while in the lab 'culture' is used to refer to growth under lab conditions. Another frequent challenge we have encountered is a vague hesitance to accommodate the use of ASL and ASL interpreters at scientific forums; a frequent assumption being that there are technological solutions that are equally effective and cheaper. Our experience is that closed captioning and even transcription by a human often fails to correctly caption scientific terms and contexts, resulting in nonsensical outputs like "the oxen levels in plants"! Happily, though most colleagues are willing to be flexible and make necessary accommodations as appropriate once they are made aware of the challenges facing d/hh scientists. In the same way we strive to develop and deploy effective means for understanding PD and intercellular trafficking in plants, we are endeavoring to develop effective approaches for communication with our d/hh colleagues in research since communication between scientists is as important as between plant cells. We are

hopeful that d/hh will one day be fully integrated into the research community as we become more cognizant of their needs.

# APPENDIX 2

## Chloroplast-to-nucleus retrograde signaling controls intercellular trafficking via plasmodesmata formation

A version of this chapter was originally published by Ganusova, Elena E., Brandon C. Reagan, Jessica C. Fernandez, Mohammad F. Azim, **Amie F. Sankoh**, Kyle M. Freeman, Tyra N. McCray, Kelsey Patterson, Chinkee Kim, and Tessa M. Burch-Smith.

Ganusova, Elena E., et al. "**Chloroplast-to-nucleus retrograde signalling controls intercellular trafficking via plasmodesmata formation**." *Philosophical Transactions of the Royal Society B* 375.1801 (2020): 20190408.

## Abstract

The signalling pathways that regulate intercellular trafficking via plasmodesmata (PD) remain largely unknown. Analyses of mutants with defects in intercellular trafficking led to the hypothesis that chloroplasts are important for controlling PD, probably by retrograde signalling to the nucleus to regulate expression of genes that influence PD formation and function, an idea encapsulated in the organelle-nucleus-PD signalling (ONPS) hypothesis. ONPS is supported by findings that point to chloroplast redox state as also modulating PD. Here, we have attempted to further elucidate details of ONPS. Through reverse genetics, expression of select nucleus-encoded genes with known or predicted roles in chloroplast gene expression was knocked down, and the effects on intercellular trafficking were then assessed. Silencing most genes resulted in chlorosis, and the expression of several photosynthesis and tetrapyrrole biosynthesis associated nuclear genes was repressed in all silenced plants. PD-mediated intercellular trafficking was changed in the silenced plants, consistent with predictions of the ONPS hypothesis. One striking observation, best exemplified by silencing the PNPase homologues, was that the degree of chlorosis of silenced leaves was not correlated with the capacity for intercellular trafficking. Finally, we measured the

distribution of PD in silenced leaves and found that inter-cellular trafficking was positively correlated with the numbers of PD. Together, these results not only provide further support for ONPS but also point to a genetic mechanism for PD formation, clarifying a longstanding question about PD and intercellular trafficking. This article is part of the theme issue ‘Retrograde signaling from endosymbiotic organelles.

## Introduction

Cell-to-cell communication in plants occurs via microscopic but complex pores known as plasmodesmata (PD). PD are membrane-lined cytoplasmic passages that allow movement of metabolites and signaling molecules between neighboring plant cells. They are, therefore, essential for plant growth, development and defense [1]. They are also conduits for the trafficking of carbon fixed by photosynthesis (in the form of sugars) to the vasculature in source tissues and from the vasculature into sink tissues, thereby facilitating energy distribution throughout the plant [2,3]. The relatively small number of reported PD mutants underscores the importance of PD to plant growth and development. Plants have evolved a number of mechanisms to control PD function including the regulated deposition and removal of callose in the cell wall surrounding PD [4–7]. PD function also changes in response to plant hormones upon abiotic and biotic signals from the environment and to developmental programmes [8,9]. Besides callose metabolism and hormones, there is increasing evidence supporting the postulate that chloroplasts exert control over the development and function of PD.

Nuclear genes encode approximately 95% of chloroplast proteins, with the remainder encoded by the chloroplast genome. Disrupting chloroplast function leads to

changes in expression of specific nuclear genes. This chloroplast-to-nucleus signaling is referred to as chloroplast retrograde signaling (CRS), [10]. Several CRS pathways and the molecules that initiate them have been identified, and the mechanistic details are under intensive investigation[11–15]. Gene expression analyses have identified a core suite of 39 genes that respond to all chloroplast-generated signals [16]. This suite includes genes that affect cell wall synthesis and/or modification, sugar transport, stress responses, and reactive oxygen species (ROS) responses. This indicates that chloroplast functional status can regulate the expression of nuclear genes including, but not limited to, photosynthesis-associated nuclear genes [17]. Several CRS pathways have been identified, and among the best characterized are those involving the *genomes uncoupled (gun)* mutants [15,18]. The *gun*2,3,4,5 and 6 mutations affect proteins that participate in the tetrapyrrole biosynthetic pathway that eventually produces chlorophyll and haem [18]. GUN4 and GUN5 are part of the Mg chelatase that couples Mg to tetrapyrroles on the chlorophyll branch of the pathway [19–22]. GUN2, GUN3 and GUN6 belong to the pathway that couples protoporphyrin IX to iron, eventually producing haem and phytochromobilin [18].

Studies with the chloroplast-resident RNA helicase ISE2have served as an entry point to further probing the chloroplast-PD relationship. ISE2 is a chloroplast DEAH-type RNA helicase critical for chloroplast RNA processing and translation, and it is conserved among green photosynthetic organisms [23,24]. Plants with reducedISE2expression have decreased photosynthetic capacity and defects in chloroplast development [25]. In addition, *Arabidopsis ise2* mutant embryos and *Nicotiana benthamiana* leaves in which

ISE2was silenced by virus induced gene silencing (VIGS) had defects in intercellular trafficking and PD formation [26,27]. Deficiency in *ISE2* expression also led to changes in the expression of target genes of CRS pathways as well as changes in the expression of several genes implicated in PD function, e.g., callose metabolism genes like *ATBG-PPAP*, and numerous genes with roles in cell wall biosynthesis or modification [25]. Based on these gene expression analyses, a relationship between chloroplasts and PD was proposed and articulated in the organelle-nucleus-PD signaling (ONPS) hypothesis [25,28]. One predicted consequence of ONPS is that it would be a mechanism by which chloroplasts could regulate carbon partitioning.

The signals that connect chloroplasts with PD function and biogenesis remain to be elucidated and this is the question investigated in this study. One challenge with examining this question is the embryonic or seedling lethality of mutants with defects in chloroplast and/or PD function [29,30]. Therefore, we adopted *N. benthamiana* and VIGS as a model system for assessing theacuteeffectsofchloroplastdysfunctiononPD-mediatedintercellular trafficking. Expression of several genes with known roles in regulating chloroplast gene expression was knocked down and intercellular trafficking was then measured in the silenced leaves. CRS was then assessed in plants with altered intercellular trafficking. Finally, we measured the effects of CRS resulting from the silencing of the target genes on PD formation. Here, we present data suggesting that intercellular trafficking is correlated with numbers of plasmodesmal pores. We interpret these results to mean that CRS exerts influence on intercellular trafficking by controlling the formation of PD.

## *Material and methods*

### *(a) Plant material and growth conditions*

*Nicotiana benthamiana* plants were grown in light carts with 16 h light (approx. 120 µmol $m^{-2}s^{-1}$) and 8 h dark. Silencing was done on 3-week-old plants (around the time 2–4 true leaves were present). After infiltration with silencing constructs, plants were grown on the light cart for an additional two weeks until silencing of *PHYTOENE DESATURASE (PDS)*, the positive control, could be observed and other analyses were per-formed. Photographs of plants were taken with a Nikon D60 camera (Nikon, Inc.).

### *(b) RNA extraction and complementary DNA synthesis*

Wild-type or silenced *N. benthamiana* tissue was collected and snap frozen in liquid nitrogen. RNA from three independent samples was isolated using the Trizol method (Thermo Fisher Scientific, Waltham, MA) according to manufacturer's instructions. RNA was DNAse treated using the DNA-free DNA removal kit (Invitrogen, Carlsbad, CA). Complementary DNA (cDNA) was synthesized using oligo-dT primers with M-MLV reverse transcriptase (Promega, Madison, WI) according to the manufacturer's instructions. cDNA was used for gene cloning or quantitative-polymerase chain reaction (qPCR).

### *(c) Gene cloning and generation of recombinant virus induced gene silencing vectors*

*Nicotiana benthamiana* gene sequences were obtained from the Sol Genomics Network Database (https://solgenomics.net) or the University of Sydney's *N.*

*benthamiana* genome page (http://benthgenome.qut.edu.au/). Gene fragments were cloned by PCR and inserted into the multiple cloning site of pYL156 (pTRV-RNA2) vector [31] by restriction digestion–ligation to generate silencing constructs. The primers for cloning VIGS fragments are listed in the electronic supplementary material, table S1. The resulting plasmids were transformed into chemically competent *Agrobacterium tumefaciens* strain GV3101. Infiltrations for VIGS were done according to published protocols [32].

***(d) Carotenoid and chlorophyll determination***

Total carotenoids x + c (xanthophylls and carotenes), chlorophyll a and b were extracted with 100% acetone. The extracts were centrifuged at room temperature for 5 min at 500g and supernatants were used to measure the absorption at 661.6 nm, 644.8 nm and 470 nm. The level of total carotenoids x + c, chlorophyll a and b were determined following the equation in [33].

***(e) Measuring intercellular trafficking by movement assay***

Movement assays to measure intercellular trafficking were performed as described previously [34]. Briefly, silenced leaves were infiltrated with *Agrobacterium* carrying a binary construct for expression of green fluorescent protein (GFP) (p35S: GFP) at optical density $(OD)_{600}$ = 0.0001, and then imaged approximately 48 h later. z-stacks of foci of GFP were collected on a Leica SP8 confocal microscope with a White Light Laser (Leica Microsystems, Buffalo Groove, IL) with a 10× lens and z-stacks were reconstructed and analyzed in ImageJ [35,36]. For analysis of movement, the number of

layers of cells in the epidermis surrounding the original cell expressing GFP was scored, and the highest number was recorded. Movement assays were performed for at least three biological replicates and each replicate included at least 10 foci. Statistical significance was measured with the Mann–Whitney U test ($p < 0.05$) compared to non-silenced wild-type + tobacco rattle virus (WT+TRV) samples.

### *(f) Optimization of primers and measuring transcript abundance by quantitative-polymerase chain reaction*

All qPCR primers were designed using the Primer BLAST tool (https://www.ncbi.nlm.nih.gov/tools/primer-blast/). Mfold ([37], web server http://www.bioinfo.rpi.edu/applications/mfold/) was used to avoid secondary structures in the amplicons. To optimize the qPCR primers, the full-length target genes were amplified from cDNA of wild-type *N. benthamiana* (electronic supplementary material, table S2) and then cloned into the linearized pMiniT 2.0 vector using a NEB PCR Cloning kit (NEB, Ipswich, MA) followed by transformation of competent *Escherichia coli*. Plasmids were isolated using miniprep kit (QIAGEN, Germantown, MD) followed by sequencing for confirmation of successful cloning. CFX Manager software (Bio-Rad, v. 1.6) was used to generate a standard curve to calculate amplification efficiency from five dilution points of isolated plasmid for three technical replicates. Primer pairs with efficiency between 90 and 110% were selected for further use.

To measure the expression of photosynthesis associated nuclear genes and other genes in silenced plants, cDNA from silenced leaves was diluted 1: 5 with nuclease-free water. qPCR was performed using the LightCycler 480 SYBR Green I

Master Mix and a LightCycler 480 Real-Time PCR system (Roche, Indianapolis, IN, USA) with the following thermal cycling programme: 95°C for 10 min followed by 40 cycles of 95°C for 10 s, 59°C for 10 s and 72°C for 20 s. The raw data generated were analyzed by calculating cycle threshold values and normalized to the expression of *GAPDH* and *EF1α* as reference genes and also with wild-type.

***(g) Measuring plasmodesmata density***

(i) PDLP1 expression for measuring pitfield distribution

*Arabidopsis* PDLP1 fused to GFP (p35S:PDLP1-GFP) was transiently expressed in leaves of silenced and non-silenced control *N. benthamiana* plants via *Agrobacterium* infiltration at $OD_{600}$ = 0.001. Images were collected 72 h post infiltration with a Leica SP8 confocal microscope with a White Light Laser (Leica Microsystems, Buffalo Groove, IL, USA) using a 25× water emersion objective with 4.00× optical zoom. All images were collected with the same laser power and gain settings, and 15 µm z-stacks were collected of epidermal cells expressing PDLP1-GFP at a step-size of 1 µm. A total of 60 stacks were collected across three biological replicates for the control and each of the silenced plants.

***(ii) Image analysis for measuring pitfield distribution***

All image analysis was performed using ImageJ. Maximum intensity projections were generated for each the z-stacks collected. Cell wall lengths were measured by tracing the cell wall in the field of view. For quantification of the total number of GFP punctae in the image, images were converted to 8-bit images and inverted. The

brightness and contrast were adjusted in order to ensure that all pitfields were clearly defined. Binary images were generated by adjusting the threshold of intensity. The Particle Analyzer function in ImageJ was used to count the total number of punctae in the image. For measuring pitfield area and fluorescence intensity, a copy of the inverted 8-bit maximum projection was generated to use as a reference image for measurements. A binary image was generated from the original maximum projection by setting the threshold using the auto-threshold function. The particle analyser was used to measure the area and the integrated density (IntDen, i.e. the average intensity of all the pixels x the area) of each GFP punctum in the unedited reference image for the regions defined in the binary image.

***(iii) Quantifying the plasmodesmata density score***

To assess the total number of PD within each field of view, the following calculation was performed:

$$\text{PD density score} = \text{pitfield density} \times \text{average integrated density}$$

This measure generates a single value that accounts for differences in number of PDLP1-GFP punctae, their size, and their fluorescence intensity. Statistical significance was measured using the Mann–Whitney U-test ($p < 0.0001$) compared to non-silenced WT+TRV controls.

## Results

### *(a) Silencing genes for chloroplast gene expression produces varying degrees of chlorosis*

Reduced expression of the genes encoding the RNA helicase ISE2 or the plastid ribosomal protein uL15c led to increased intercellular trafficking via PD [27,38]. ISE2 also interacted with numerous proteins involved in chloroplast gene expression [38]. In order to test whether chloroplast gene expression was broadly involved in ONPS and regulating PD, we silenced six genes encoding proteins found to interact with ISE2 or be important for expression of the plastid genome and then monitored intercellular trafficking via PD in silenced tissues. For this, we used VIGS with vectors derived from the TRV in *N. benthamiana* [31,39]. The silenced genes were those encoding RNA helicases RH22 [40], RH39 [41] or RH3 [42], a gene encoding a pentratricopeptide repeat (PPR) protein reported to be important for translation in maize plastids and found to interact with ISE2 (here called IPI1) [38,43], the RNA surveillance factor RNase J [44], and the RNA maturation and degradation factor PNPase [45]. In all experiments, wild-type plants infected with TRV but with no silencing were used as the negative control, and VIGS of PDS was used as a positive control for silencing. The inclusion of *ISE2* in the silencing experiments also served as an internal control because the behaviour of *ISE2*-silenced plants has been well characterized.

Silencing of the target genes was confirmed by quantitative real time-PCR and gene expression in all cases was reduced by at least 87% (electronic supplementary material, figure S1). Knockdown of *RH22* expression produced plants that were almost

indistinguishable from the non-silenced WT+TRV control plants in both appearance and photosynthetic pigment content (figure 23*a–b,k–m*). Silencing *RH39* caused mild chlorosis in newly emerged leaves (figure 23*c*,*k–m*) while silencing a single or both *PNPase* homologues led to more severe yellowing, similar to that observed with silencing ISE2 (figure 23*d–f,k–m*). Plants with reduced expression of *RNaseJ, IPI1* or *RH3* yielded severe chlorotic phenotypes and reduction in photosynthetic pigment contents that were similar to those observed in plants where *PDS* was silenced (figure 23*g–m*). Despite chlorosis, the silenced plants continued to grow, and they eventually matured and set seed.

### *(b) Intercellular trafficking changes in plants with defective chloroplast RNA processing*

Intercellular trafficking via PD was measured in silenced leaves. For this, we used movement of a GFP probe from a single cell into adjacent, contiguous layers of epidermal cells to report on PD function [**27**,**34**,**46**]. In this assay, GFP travels variable distances, generating foci of GFP of different sizes (figure 24*a*). Because of the inherent variation in the sizes of foci in any sample, movement data are presented in two ways. Figure 24*b* presents the complete distribution of foci sizes observed for a sample, while figure 24*c* presents a quantification of the average (median) size of foci for a given sample. In *RH22*-silenced leaves, there was no difference in the average size of foci compared to those observed in the non-silenced WT+TRV control leaves (figure 24*c*). In leaves where *RH39*, *ISE2* or *PNPaseA* were silenced and chlorosis was more severe, there was an increase in the size of GFP foci and hence, intercellular trafficking

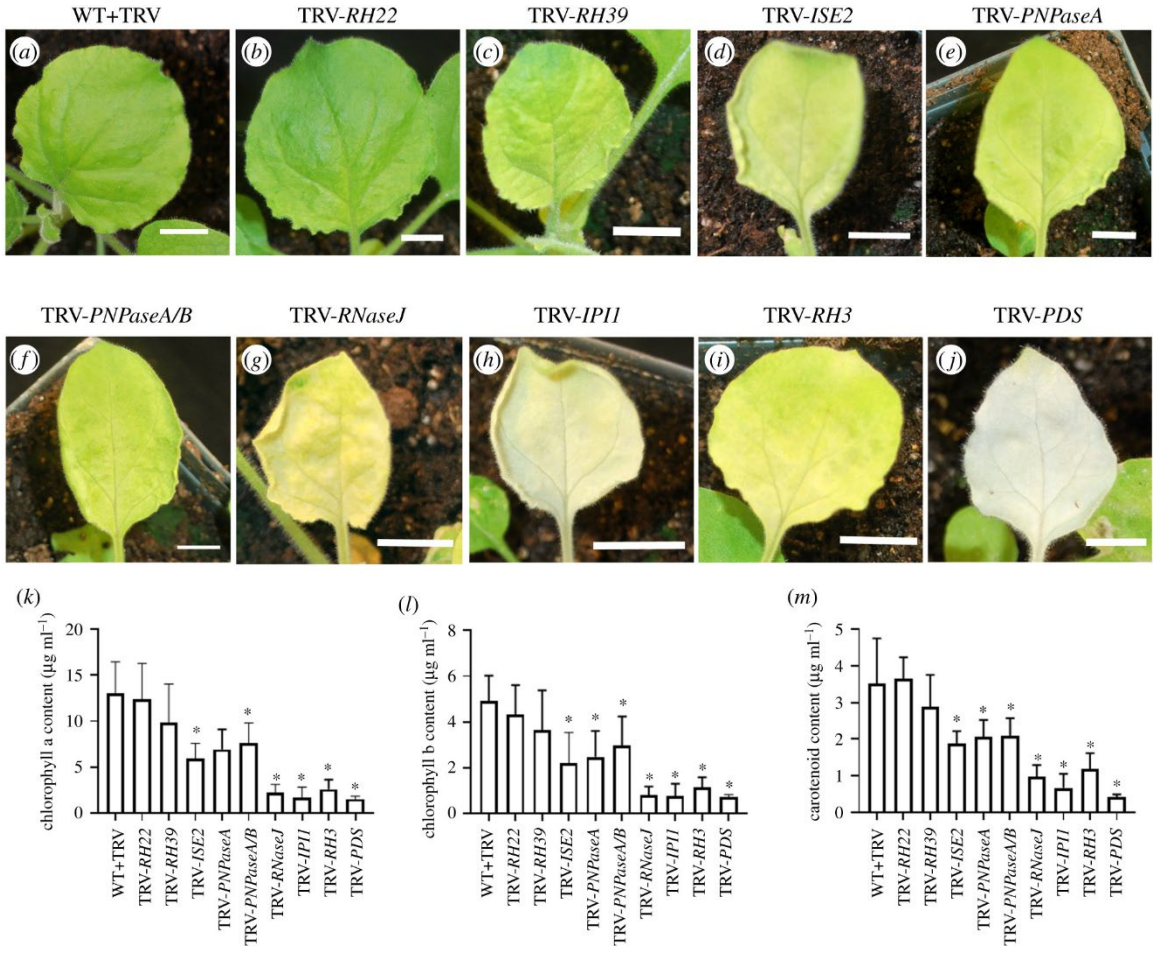


**Figure 23: Phenotypes of silenced plants and their photosynthetic pigment content.**

(*a–j*) Representative leaves from silenced plants. Silenced gene is shown above figure. WT *N. benthamiana* infected with TRV virus only (*a*). (*b–k*) Plants with silenced *RH22* (*b*), *RH39* (*c*), *ISE2* (*d*), *PNPaseA* (*e*), *PNPaseA/B* (*f*), *RNaseJ* (*g*), *IPI1* (*h*), *RH3* (*i*), and *PDS* (*j*). Silencing of *PDS* results in severely chlorotic tissue. Chlorophyll *a* and *b* content of silenced plants (*k*,*l*), and total carotenoid content of silenced plants (*m*). Asterisk denotes statistical significance, Student's *t*-test $p < 0.05$.

(figure 24*b,c*). Strikingly, when *RNAseJ, IPI1 or RH3* was silenced and leaves exhibited severe chlorosis (figure 23), there were large decreases in the size of GFP foci reflected in the increase in the proportion of foci that were restricted to one cell layer, indicating reduced intercellular trafficking (figure 24). Leaves in which both *PNPase* genes were silenced (TRV-*PNPaseA/B*) also showed a large decrease in GFP foci sizes, in striking contrast to the results from silencing only *PNPaseA*. It should be noted that there were no differences in the chlorosis or the photosynthetic pigment content between the *PNPaseA* or *PNPaseA/B*-silenced plants (figure 23). These data support previous observations that chloroplast function modulates intercellular trafficking. However, they also reveal a more complex relationship in which the degree of chloroplast (dys)function does not exclusively determine changes to intercellular trafficking.

### *(c) Chloroplast retrograde signalling is triggered in plants with defective chloroplast gene expression*

ONPS predicts that CRS is a likely mechanism for regulating PD function [**25**]. To explicitly test this hypothesis, the expression of marker genes known to respond to CRS was measured in silenced plants with altered PD-mediated intercellular trafficking. GOLDEN2-LIKE1 (GLK1) is a transcription factor that is important for chloroplast development [**47**] and *GLK1* expression is suppressed when CRS is activated [**48**]. We, therefore, first measured *GLK1* transcript levels in silenced plants. In six of the eight silenced lines with defective intercellular trafficking, *GLK1* transcript levels were reduced (figure 25). Next, *Lhcb* genes encoding the antennae proteins of the photosystem-associated light-harvesting complexes and *RBCS1A* encoding one of the isoforms of the rubisco small subunit were selected as likely conserved targets of retrograde

**Figure 24: Measurement of PD-mediated intercellular trafficking in silenced plants.**

PD-mediated trafficking was measured by counting the layers of epidermal cells to which GFP spread. At least 10 foci were scored for each of three biological replicates. (*a*) Representative images depicting GFP trafficking between contiguous layers of epidermal cells. The presence of GFP in cell nuclei was used to determine the presence of GFP in a cell. The cell labelled ‘0' showed expression of GFP in the primary transformed cell but no GFP was seen in surrounding epidermal layers. In the image labelled ‘1', GFP expression was observed in the primary transformed cell and in the nuclei of cells immediately adjacent to the transformed cell only. For subsequent images, the number below the image corresponds to the number of layers away from the primary transformed cell that showed GFP accumulation in the nucleus. Scale bar = 100 μm. (*b*) Qualitative representation of GFP trafficking data showing the distribution of foci sizes observed for each silenced plant. (*c*) Layers were assigned values (0 layers = 0, 1 layer = 1, 2 layers = 2, 3 layers = 3, greater than 3 layers = 4) and the median value is shown. Statistical significance was determined by the Mann–Whitney *U*-test. *$p < 0.05$.

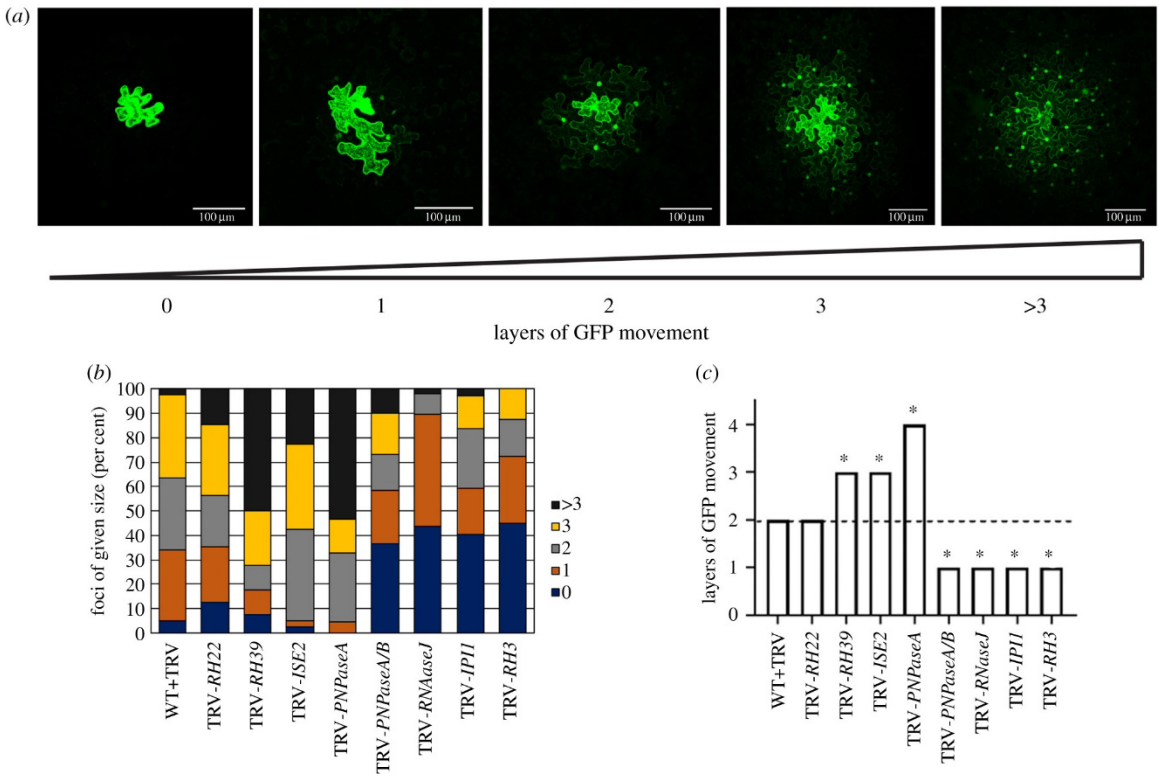
(a)
100 µm
0
1
2
3
>3
layers of GFP movement
(b)
foci of given size (per cent)
>3
3
2
1
0
WT+TRV
TRV-RH22
TRV-RH39
TRV-ISE2
TRV-PNPaseA
TRV-PNPaseA/B
TRV-RNAaseJ
TRV-IPI1
TRV-RH3
(c)
layers of GFP movement
WT+TRV
TRV-RH22
TRV-RH39
TRV-ISE2
TRV-PNPaseA
TRV-PNPaseA/B
TRV-RNaseJ
TRV-IPI1
TRV-RH3

**Figure 25: Silencing of genes involved in chloroplast gene expression results in altered expression of CRS target genes.**

Relative normalized expression of *GLK1*, *LHCB1.2*, *LHCB2.1*, *RBCS1A* and *XTH5* of *N. benthamiana* in non-silenced TRV-infected controls (WT+TRV) versus (*a*) TRV-*RH22*, (*b*) TRV-*RH39*, (*c*) TRV-*ISE2*, (*d*) TRV-*PNPaseA*, (*e*) TRV-*PNPaseA/B*, (*f*) TRV-*RNaseJ*, (*g*) TRV-*IPI1*, and (*h*) TRV-*RH3* silenced plants. Expression was normalized against non-silenced TRV-infected controls and relative expression was calculated using *GAPDH* and *EF1α* as reference genes. Data represent mean (± s.e.) from three technical replicates of a representative biological replicate. Statistical analysis was performed by Student's *t*-test. *$p < 0.05$. (*i*) Heatmap showing expression levels of CRS marker genes (*GLK1*, *LHCB1.2*, *LHCB2.1*, *RBCS1A* and *XTH5*) in silenced plants. The rows represent CRS marker genes and the columns represent silenced genes. Scale is shown on right.

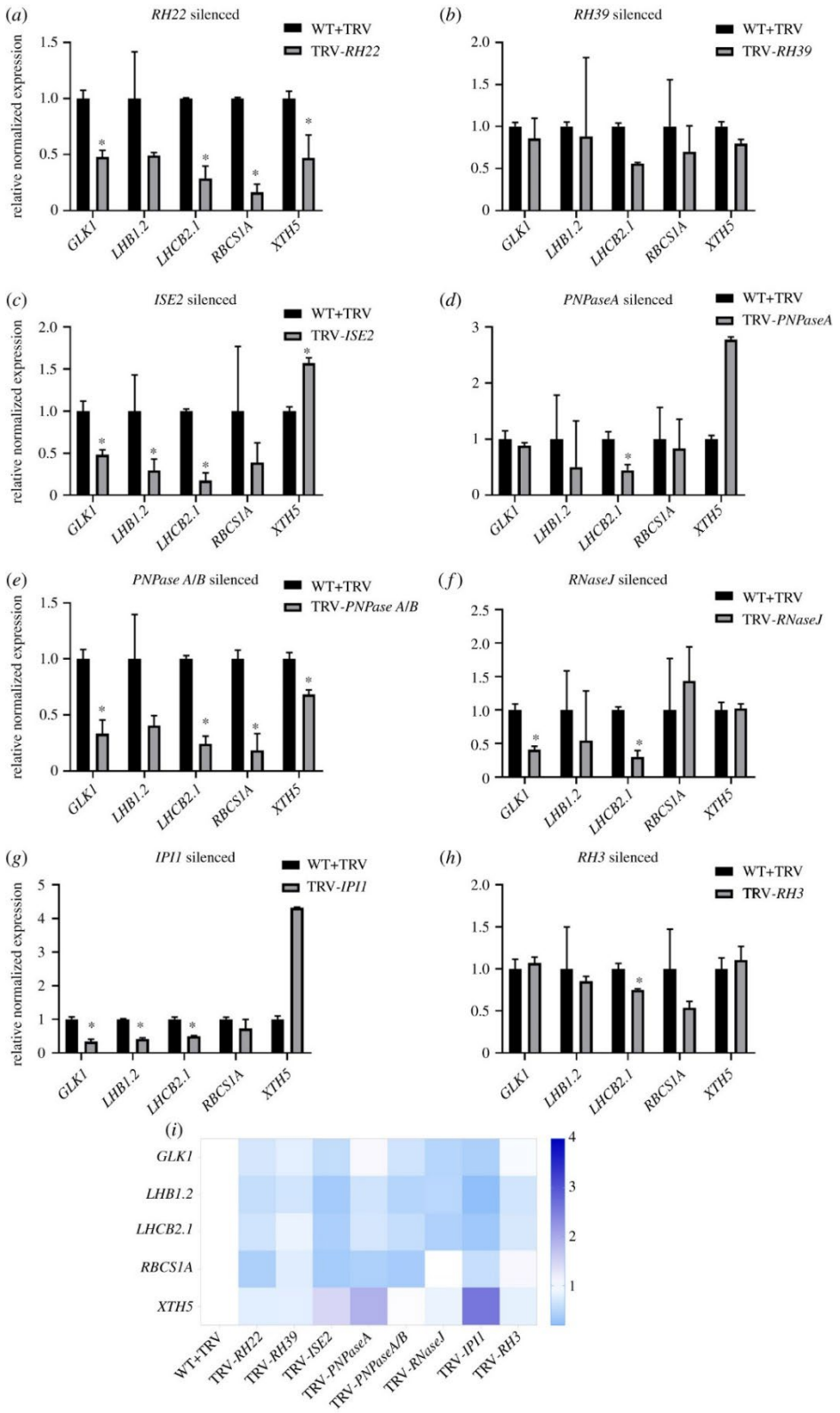
(a)
RH22 silenced
WT+TRV
TRV-RH22
relative normalized expression
GLK1
LHB1.2
LHCB2.1
RBCS1A
XTH5
(b)
RH39 silenced
WT+TRV
TRV-RH39
(c)
ISE2 silenced
WT+TRV
TRV-ISE2
(d)
PNPaseA silenced
WT+TRV
TRV-PNPaseA
(e)
PNPase A/B silenced
WT+TRV
TRV-PNPase A/B
(f)
RNaseJ silenced
WT+TRV
TRV-RNaseJ
(g)
IPI1 silenced
WT+TRV
TRV-IPI1
(h)
RH3 silenced
WT+TRV
TRV-RH3
(i)
WT+TRV
TRV-RH22
TRV-RH39
TRV-ISE2
TRV-PNPaseA
TRV-PNPaseA/B
TRV-RNaseJ
TRV-IPI1
TRV-RH3

signaling in *N. benthamiana*. In most of the silenced lines, expression of *Lhcb1.1* and *Lhcb2.1* was suppressed, consistent with those tissues undergoing CRS. However, *RBCS1A* suppression of its expression was less common, with only *RH22*- or *PNPaseA/B*-silenced lines showing statistically significant reductions in expression (figure 25). This suggests that *RBCS1A* may not be responsive to CRS in *N. benthamiana*. Nonetheless, together these data demonstrate CRS occurring in silenced plants with altered PD-mediated intercellular trafficking.

To further examine possible pathways for CRS that could be involved in ONPS, we also measured transcript levels of *XYLOGLUCAN ENDOTRANSGLUCOSYLASE-HYDROLASE5* (*XTH5)*, a gene whose expression is regulated by the HY5 transcription factor [**49**]. The XTH family is a large group of enzymes involved in cell wall remodeling [**50**]. HY5 is an important regulator of chloroplast development, and it is emerging as an important hub for integrating chloroplast retrograde signals to control plant development [**51**]. In most silenced plants transcript levels of *XTH5* were significantly different from those in the corresponding TRV-infected non-silenced controls (figure 3). This suggests that CRS modulated by HY5 may be involved in ONPS. However, no clear correlation between *XTH5* expression and changes in PD-trafficking capacity were observed. While *NbXTH5* expression was statistically significantly decreased in *RH22*- and *RH39*-silenced plants that had increased intercellular trafficking, its expression was statistically significantly increased in *ISE2*- or *PNPaseA*–silenced plants which also had enhanced intercellular trafficking (figure 3).

### *(d) Tetrapyrrole biosynthesis genes have altered expression in silenced plants with changes in intercellular trafficking*

Tetrapyrrole biosynthesis and use is universal among photosynthesizing organisms, and tetrapyrrole metabolism is important for CRS [**52**]. We, therefore, examined the involvement of genes involved in tetrapyrrole biosynthesis with a focus on the *GENOMES UNCOUPLED* (*GUN*) genes, known components of retrograde signalling, and *HEMA1*, required for the first, rate-limiting step in tetrapyrrole biosynthesis in ONPS. While *HEMA1* expression was altered in all of the silenced lines, no clear correlation with altered intercellular trafficking was observed. Similarly, expression of *GUN2–5* was altered in all silenced plants compared to non-silenced controls (figure 26). *GUN2* transcript levels were mostly unchanged in silenced plants except for a reduction in *RH22*-silenced plants and a small increase in *RH39*-silenced plants. In comparison, *GUN3* transcript levels were significantly increased in all silenced lines except TRV-*RH22. GUN2 (HO1)* and *GUN3 (HY2*) both act in the haem branch of the tetrapyrrole pathway, suggesting that production of haemoproteins could be upregulated in those silenced lines with increased *GUN3* expression. *GUN4* encodes the regulatory subunit of the Mg-chelatase complex and *GUN5* (*CHLH*) encodes the catalytic subunit of the complex [**20**]. Silencing of genes related to chloroplast gene expression led to repressed expression of *GUN4.* By contrast, *GUN5* transcripts accumulated in all silenced lines except for TRV-*IPI1*. These results indicate that haem and tetrapyrrole metabolism is disrupted in silenced plants, consistent with the chlorosis of silenced leaves. Moreover, they demonstrate that tetrapyrrole biosynthesis genes

**Figure 26: Silencing of genes involved in chloroplast gene expression results in changes in expression of genes of the tetrapyrrole biosynthesis pathway**.
qPCR analysis of expression of *HEMA1, GUN2, 3, 4* and *5* in non-silenced TRV-infected controls (WT+TRV) and (*a*) TRV-*RH22*, (*b*) TRV-*RH39*, (*c*) TRV-*ISE2*, (*d*) TRV-*PNPaseA*, (*e*) TRV-*PNPaseA/B*, (*f*) TRV-*RNaseJ*, (*g*) TRV-*IPI1*, and (*h*) TRV-*RH3* silenced plants. *GAPDH* and *EF1α* were used as reference genes for calculating the relative expression and normalized with TRV infected wild-type (WT+TRV). The data are presented as the mean (±s.e.) from three technical replicates of a representative biological replicate. Statistical analysis was performed by Student's *t*-test. *$p < 0.05$. (*i*) Heatmap showing expression levels of *HEMA1* and the *GUN* genes in silenced plants. Scale is on right.

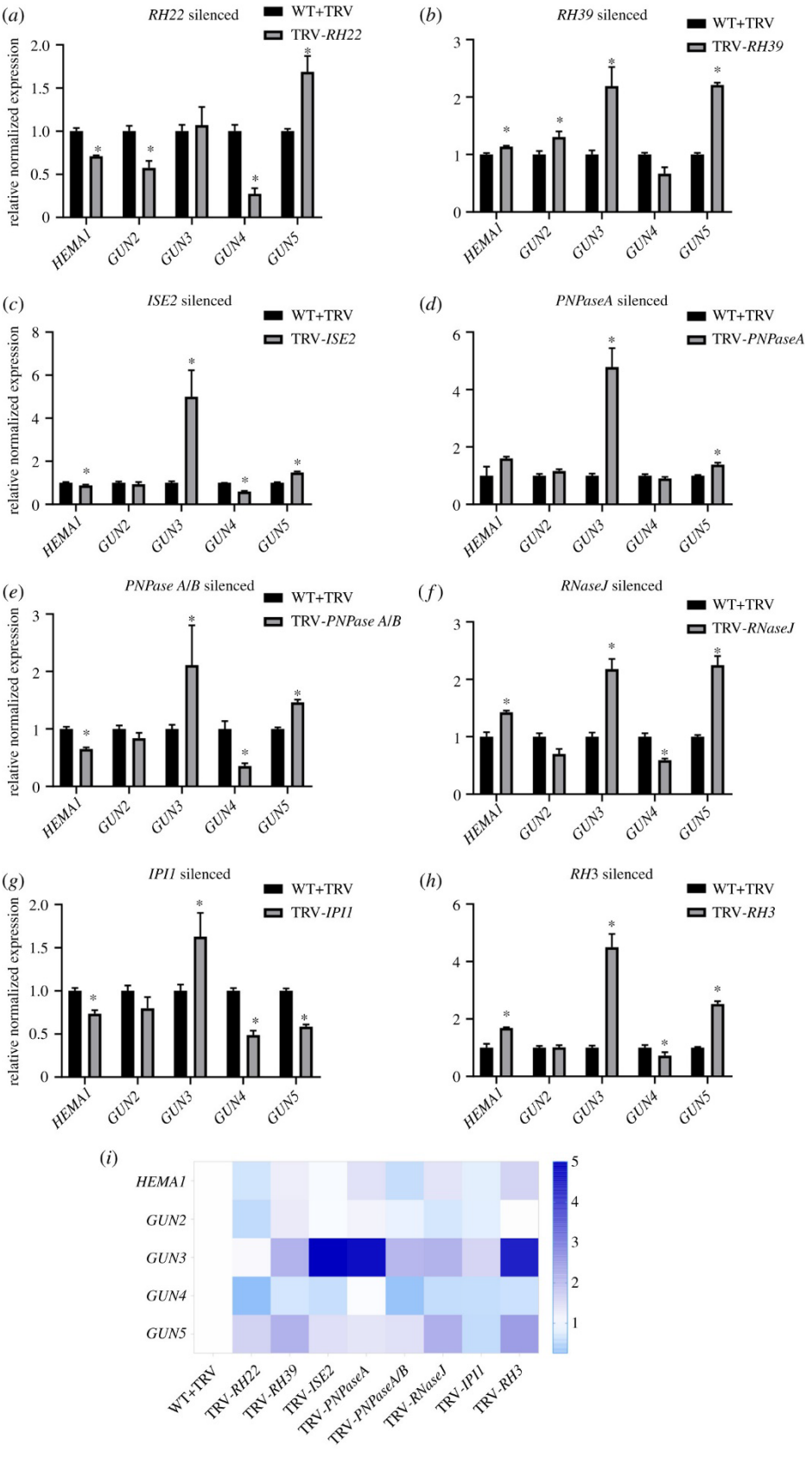
(a)
RH22 silenced
WT+TRV
TRV-RH22
relative normalized expression
HEMA1
GUN2
GUN3
GUN4
GUN5
(b)
RH39 silenced
WT+TRV
TRV-RH39
(c)
ISE2 silenced
WT+TRV
TRV-ISE2
(d)
PNPaseA silenced
WT+TRV
TRV-PNPaseA
(e)
PNPase A/B silenced
WT+TRV
TRV-PNPase A/B
(f)
RNaseJ silenced
WT+TRV
TRV-RNaseJ
(g)
IPI1 silenced
WT+TRV
TRV-IPI1
(h)
RH3 silenced
WT+TRV
TRV-RH3
(i)
HEMA1
GUN2
GUN3
GUN4
GUN5
WT+TRV
TRV-RH22
TRV-RH39
TRV-ISE2
TRV-PNPaseA
TRV-PNPaseA/B
TRV-RNaseJ
TRV-IPI1
TRV-RH3

respond strongly to defects in chloroplast gene expression and to chloroplast-derived signals.

### *(e) Plasmodesmata density is altered in plants with defective chloroplast gene expression*

The silencing of genes important for chloroplast gene expression resulted in defects in intercellular trafficking (figure 24). In *ISE2*-silenced plants, defects in intercellular trafficking were associated with changes in PD [**27**]. We, therefore, tested whether changes in PD were also involved in the changes to intercellular trafficking observed in the silenced plants. For this, *Arabidopsis* PLASMODESMATA-LOCATED PROTEIN1 (PDLP1-GFP), a general marker for PD [**53**], was expressed in leaves equivalent to those used in the trafficking assays. Using confocal fluorescence microscopy, we monitored the appearance of GFP punctae in cell walls. PD are nanopores with an average diameter of 30 nm, so for our analysis we assumed that the fluorescent foci we observed were owing to clusters of PD in the cell wall, called pitfields [**54**]. Direct observation by microscopy revealed striking changes in the patterns of pitfields compared to those in non-silenced TRV-infected controls. In some silenced plants there were more, larger punctae that had greater fluorescence intensity (measured under the same imaging settings) than in control plants, exemplified by TRV-*PNPaseA* (figure 26*a,b*). In other plants, as shown for TRV-*IPI1*, the GFP punctae were much less abundant and had weaker fluorescence intensity compared to the control plants (figure 26*c*). Images of cells were collected as *z*-stacks and then the maximum intensity projections were used to measure the number, size and fluorescence intensity

of GFP punctae in a field of view (figure 26*d*). Based on these parameters, a ‘PD density score' was developed to quantitatively describe these observations (see Material and methods). In *RH22-*, *RH39-*, *ISE2-* and *PNPaseA*-silenced plants, the average PD density was higher than that of non-silenced control plants and in all cases, this difference was statistically significant (figure 26*e*). Note that, except for *RH22,* silencing these genes led to increased intercellular trafficking of GFP (figure 24). By contrast, in epidermal cells in leaves where *RNaseJ*, *IPI1* or *RH3* were silenced, there were drastic, statistically significant decreases in PD density (figure 26*e*). Silencing of those genes had led to decreased intercellular trafficking (figure 24). Relative to the non-silenced control, silencing both *PNPase* homologues with the TRV-*PNPaseA/B* construct did not affect the PD density (figure 26*e*), although it led to decreased intercellular trafficking (figure 24). Comparing intercellular trafficking to PD density revealed a positive correlation between PD density and intercellular trafficking (figure 26*f*). However, the data for TRV-*RH22* and TRV-*PNPaseA/B* do not fit the curve suggesting that other factors beyond PD density may contribute to the changes observed in intercellular trafficking.

## Discussion

In this study, we took a reverse genetics approach to investigating the relationship between chloroplasts and PD in coordinating intercellular trafficking, called ONPS. Expression of genes encoding factors needed for chloroplast gene expression was knocked down by VIGS, resulting in varying degrees of chlorosis in the silenced plants. Movement assays in epidermal cells of silenced leaves revealed that in seven of the

eight samples examined, perturbing chloroplast gene expression disrupted intercellular trafficking (figure 24). The use of reverse genetics allowed us to sidestep one of the main challenges that encumbers investigations of PD. Mutants with defects in PD are scarce, probably owing to their embryonic and seedling lethality [**30**,**55**]. Similarly, *Arabidopsisrh22*, *rh3*, *rh39*, *pnpase*, *ipi1* and *rnase j* mutants all display embryonic or seedling lethality [**40**–**42**,**56**–**58**]. It would, therefore, be difficult to examine the roles of these genes in other aspects of plant development. The use of VIGS in *N. benthamiana* plants provides a relatively straightforward system to reduce gene expression and measure effects on PD function. Another advantage of *N. benthamiana* and VIGS is that it allows the acute effects of perturbation of gene expression to be assessed. Plants are wild-type until initiation of VIGS, and have presumably induced relatively few responses to cope with the loss of gene function as they would in a true genetic mutant. Thus, *N. benthamiana* and VIGS represent a powerful new system for probing CRS and ONPS.

Using quantitative measurement of transcript levels of known markers for CRS (*Lhcb* and *RBCS1A* genes), we showed that CRS was altered in the silenced plants compared to non-silenced controls (figure 25). Changes in chloroplast gene expression are well known to modify CRS and alter expression of nuclear genes [**14**,**59**]. ISE2 is involved in multiple aspects of chloroplast RNA processing including group II intron splicing, rRNA processing and C-to-U editing [**23**]. RH3, RH22 and RH39, are required for rRNA processing in chloroplasts with RH3 having additional roles in splicing group II introns [**40**–**42**]. The maize homologue of IPI1 is PPR103, and it is required for

processing rpl16 mRNAs and ribosome accumulation in maize [**43**]. RNaseJ is necessary to prevent the overaccumulation of chloroplast antisense RNAs, thereby ensuring correct expression of the chloroplast genome [**44**,**60**]. Chloroplast PNPase is needed for multiple steps of RNA processing including correct 3′end maturation of rRNA and mRNA, RNA degradation, intron processing and non-coding RNAs [**45**,**60**]. In plants where any of these genes is silenced, it is expected that chloroplast gene expression would be altered, leading to the production of chloroplast molecules that would act as a retrograde signal to influence expression of the nuclear genome. We hypothesize that in our system, silencing each gene would produce a distinct perturbation of chloroplast gene expression and function, leading to unique signals or signal signatures that in turn has a specific effect on expression of genes important for PD formation or function. This hypothesis is borne out by the unique patterns of nuclear gene expression observed in the silenced plants (figures 3 and 4).

In the silenced plants, changes in expression of genes in the tetrapyrrole synthesis pathway were observed, although only the reduced expression of *GUN4* was common to all silenced plants (figure 26). These changes in tetrapyrrole-related gene expression are consistent with the chlorosis of the silenced plants. Further, they are also similar to changes in gene expression analysis revealed by tiling microarray in *ise2* embryos. The microarray studies showed that numerous genes associated with tetrapyrrole metabolism had altered expression in the mutant embryos including *GUN2, GUN5* and *GUN6* [**25**]. Disruption of the *GUN* tetrapyrrole-associated genes led to the accumulation of intermediates that are known mediators of CRS [**61**]. While

tetrapyrroles are candidate signals for ONPS, other retrograde signals cannot be ruled out. Chloroplast-generated ROS and redox state have been shown to regulate PD-mediated intercellular trafficking [**62**,**63**], and they are also known to act as retrograde signals [**12**]. Investigating other CRS pathways involved in ONPS in this system will be a goal of future investigations.

Exogenous application of oxidizing or reducing agents to plant samples was shown to influence PD-mediated intercellular trafficking [**64**]. Interestingly, low concentrations of hydrogen peroxide increased PD-mediated trafficking in *Arabidopsis* roots, while at higher concentrations trafficking was inhibited. Thus, it seems that mild stress induces one PD response while more, or a different stress, can induce a distinct PD response. The results from the silencing of the *PNPase* homologues support the notion that there is complex regulation of PD responses to signals. The *PNPase* genes are highly similar, encoding proteins with 97% identity (electronic supplemental material, figure S3). When only *PNPaseA* was silenced, the plants displayed chlorosis and there was greatly increased PD-mediated intercellular trafficking (figure 24). When both genes were silenced, the plants displayed the same degree of chlorosis—as when only *PNPaseA* was silenced—but there was a striking change in PD function. Silencing both homologues of *PNPase* drastically decreased intercellular trafficking (figure 24). While the results from the other silenced plants suggest that degree of chlorosis is predictive for PD, the results from *PNPase* clearly argue against this. Indeed, when *ISE1,* a gene encoding a mitochondrial DEAD-box RNA helicase, was silenced in parallel to *ISE2*, the *ISE1*-

silenced plants had milder chlorosis than *ISE2*-silenced plants but had a larger increase in intercellular trafficking between epidermal cells than did *ISE2*-silenced plants [**27**].

Interestingly, *PNPaseA*-silenced leaves contained increased PD density while *PNPaseA/B*-silenced leaves showed no difference in PD density relative to the non-silenced controls (figure 27). The increased PD density and intercellular trafficking observed in *PNPaseA*-silenced plants agree with the general trend observed for the other silenced lines (figure 27*e*) and support a simple model in which the increased cell-to-cell diffusion of free GFP is facilitated by having more PD pores. The results from *PNPaseA/B* confound this simple model and suggest that it is not only the availability of PD pores that accounts for intercellular trafficking. Similarly, *RH22*-silenced leaves had no change in intercellular trafficking relative to the controls but showed a marked increase in PD density (figure 27*e*). Previous analysis of *ISE2*-silenced plants and *ise2* mutant embryos revealed increased occurrence of twinned and branched PD along with increased intercellular trafficking, suggesting that the formation of secondary (complex) PD facilitates increased cell-to-cell trafficking [**27**]. Often overlooked in discussions of PD is their variety and apparent subfunctionalization. Primary PD form during cytokinesis when strands of the endoplasmic reticulum (ER) are trapped in the nascent cell wall while secondary PD form *de novo* across existing cell walls in the absence of cytokinesis [**9**]. In mature tissues, PD are more elaborate with branching channels that may contain large central cavities compared to the simpler linear pores that are often observed in developing tissues. This change in structure may be associated with changes in their trafficking capacities.

**Figure 27: Quantification of PD density in silenced plants. PD in pitfields were labelled with the general PD marker PDLP1-GFP.**

Representative maximum projections of fields of view showing PDLP1-GFP-labelled pitfields in (*a*) WT+TRV, (*b*) TRV-*PNPaseA* (increased number of pitfields), and (*c*) TRV-*IPI1* (decreased numbers of pitfields) plants. (*d*) Individual images (confocal planes 3–14 of a confocal stack) from *z*-stacks used to generate maximum projections (MP) showing the distribution of pitfields in the *z*-axis. Images correspond to the region outlined in white in (*a*). Scale bar = 10 μm. (e) PD density scores were calculated for each image from three biological replicates (rep. 1 (blue squares), rep. 2 (yellow circles) and rep. 3 (red diamonds). See Material and methods for more details. Statistical significance was determined by Mann–Whitney *U*-test. *$p < 0.0001$. (*f*) Linear regression curve showing the positive correlation of PD density score with layers of GFP movement. The average PD density score and the median layers of movement across the three biological replicates were used to generate the graph.

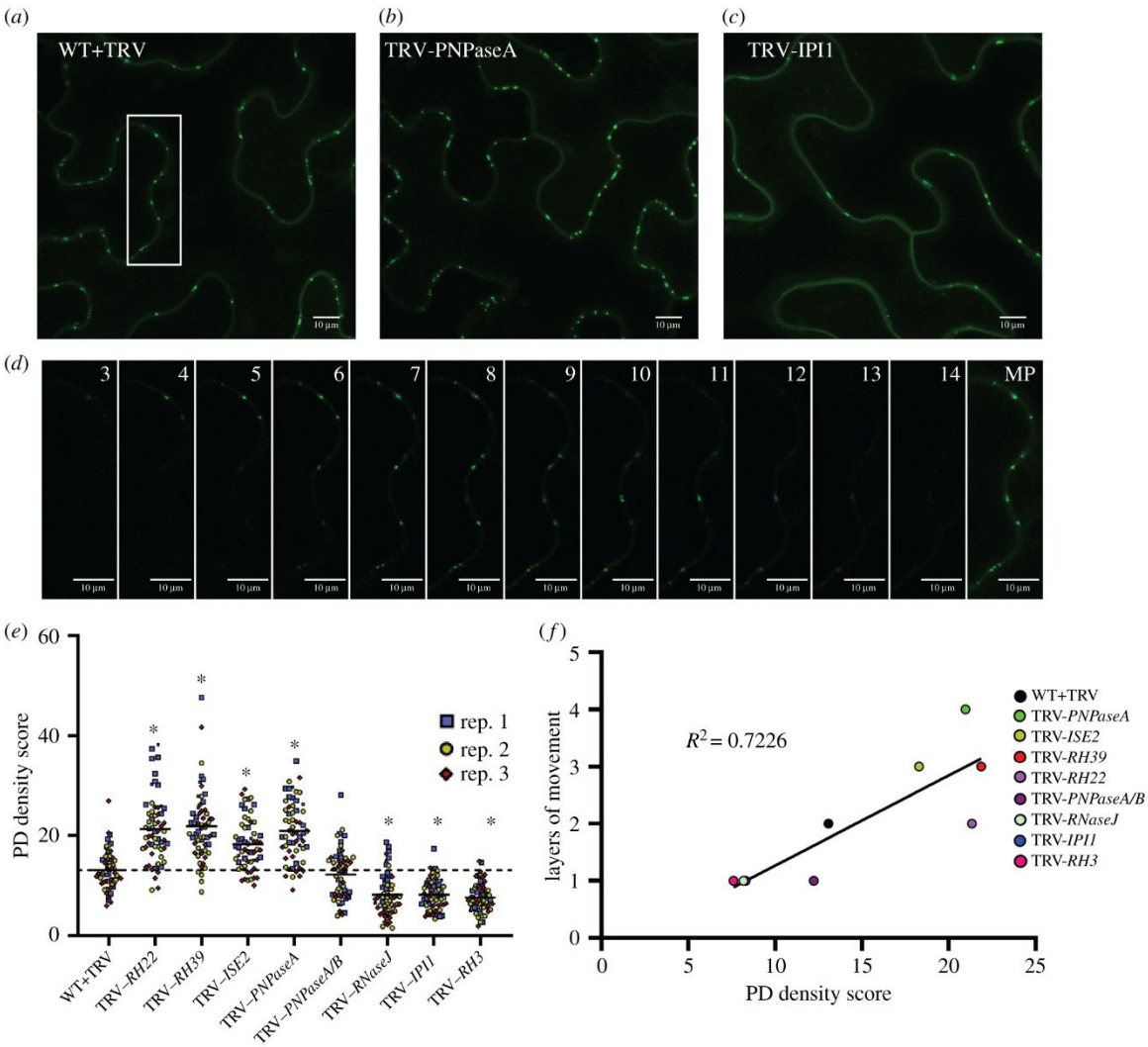
(a)
WT+TRV
(b)
TRV-PNPaseA
(c)
TRV-IPI1
(d)
3
4
5
6
7
8
9
10
11
12
13
14
MP
(e)
PD density score
rep. 1
rep. 2
rep. 3
WT+TRV
TRV–RH22
TRV–RH39
TRV–ISE2
TRV–PNPaseA
TRV–PNPaseA/B
TRV–RNaseJ
TRV–IPI1
TRV–RH3
(f)
layers of movement
PD density score
$R^2 = 0.7226$
WT+TRV
TRV-PNPaseA
TRV-ISE2
TRV-RH39
TRV-RH22
TRV-PNPaseA/B
TRV-RNaseJ
TRV-IPI1
TRV-RH3

Simple PD in sink leaves were reported to allow trafficking of larger molecules than do the branched PD of source leaves [**3**]. The PD marker used in this study, PDLP1-GFP, localizes to all PD and does not distinguish between simplex and more complex PD in the manner of other markers, e.g. MP17-GFP derived from the potato leafroll virus [**53**,**65**]. Thus, the possibility that silencing different chloroplast-related genes resulted in the formation of different classes of PD (primary versus secondary, and simple versus branched) with distinct trafficking properties cannot be ruled out. Taken together, our results can be integrated into a model where during leaf development CRS regulates expression of PD associated nuclear genes (PDANGs) to control the formation of secondary PD that would complement the existing primary PD generated during cell division, allowing the flux of carbon into or out of cells to match the developmental state of chloroplasts (figure 28*a*). When chloroplast development and CRS are disrupted, the regulation of PDANGs expression is disturbed and, depending on the strength and identity of the signalling molecules regulating gene expression, the number of secondary PD formed exceeds or falls short of normal levels, resulting in altered intercellular trafficking (figure 28*b*). Further examination of PD ultrastructure in our system to delineate the contributions of simple or complex and PD of primary or secondary origins to intercellular trafficking is therefore warranted. Such studies would address longstanding questions regarding the function of different classes of PD. However, studies on ONPS are constrained by our limited understanding of the genetic underpinnings of PD formation and function. Further elucidation of ONPS will depend on

the identification of PDANGs whose expression in response to CRS can be validated and used as reliable markers for chloroplast-nuclear communication for PD regulation.

## Conclusion

Our findings support the role of chloroplasts in regulating intercellular trafficking via PD. The tetrapyrrole biosynthetic pathway has been identified in this study as one potential source of CRS that mediate changes in PD-mediated intercellular trafficking. However, other CRS may also be involved in communicating the physiological state of the chloroplasts to the nucleus to then modulate expression of genes important for PD function. A positive correlation between PD density and intercellular trafficking was measured, suggesting that the presence of more pores can allow increased diffusion of molecules from one cell to another. However, the results also suggest that other factors in addition to simple numbers of PD are important for determining intercellular flux and these will be the subjects of future investigation. The system used in these studies, consisting of VIGS in *N. benthamiana*, is amenable to the study of chloroplast- and/or PD-related genes whose loss results in lethality, and this system should prove useful for further studies of ONPS and PD formation and function.

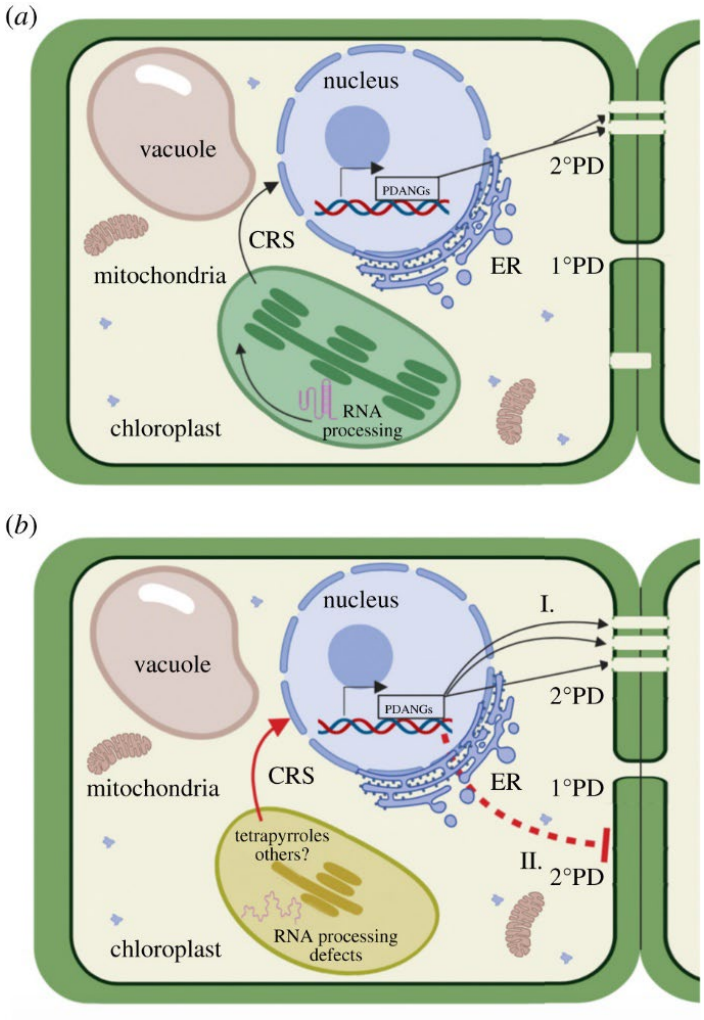


**Figure 28: Model for the control of formation of secondary PD by CRS. Primary PD (1° PD) are formed during cell division while secondary PD (2° PD) arise in the absence of cell division.**

Under normal control conditions or in WT plants with normal RNA processing (*a*), CRS (black arrow) regulates the expression of PDANGs that are involved in the formation of secondary PD. Disruption of chloroplast RNA processing and gene expression, as in the silenced plants used in this study, leads to defects in chloroplast development and function, causing altered CRS (red arrow) which results in changes in the expression of PDANGs (*b*). These changes result in increased (I) or decreased (II) secondary PD formation.

# Appendix References


1. Lucas WJ, Lee JY. 2004Plasmodesmata as a supracellular control network in plants. *Nat. Rev. Mol. Cell Biol.* **5**, 712-726. (**doi:10.1038/nrm1470**)
2. Patrick JW. 2013Does Don Fisher's high-pressure manifold model account for phloem transport and resource partitioning?*Front. Plant Sci.* **4**, 184. (**doi:10.3389/fpls.2013.00184**)
3. Oparka KJet al.1999Simple, but not branched, plasmodesmata allow the nonspecific trafficking of proteins in developing tobacco leaves. *Cell* **97**, 743-754. (**doi:10.1016/S0092-8674(00)80786-2**)
4. Wu SW, Kumar R, Iswanto ABB, Kim JY. 2018Callose balancing at plasmodesmata. *J. Exp. Bot.* **69**, 5325-5339. (**doi:10.1093/jxb/ery317**)
5. Amsbury S, Kirk P, Benitez-Alfonso Y. 2017Emerging models on the regulation of intercellular transport by plasmodesmata-associated callose. *J. Exp. Bot.* **69**, 105-115. (**doi:10.1093/jxb/erx337**)
6. De Storme N, Geelen D. 2014Callose homeostasis at plasmodesmata: molecular regulators and developmental relevance. *Front. Plant Sci.* **5**, 138. (**doi:10.3389/fpls.2014.00138**)
7. Zavaliev R, Ueki S, Citovsky V, Epel BL. 2011Biology of callose (beta-1,3-glucan) turnover at plasmodesmata. *Protoplasma* **248**, 117-130. (**doi:10.1007/s00709-010-0247-0**)
8. Sager RE, Lee JY. 2018Plasmodesmata at a glance. *J. Cell Sci.* **131**, jcs209346. (**doi:10.1242/jcs.209346**)
9. Burch-Smith TM, Stonebloom S, Xu M, Zambryski PC. 2011Plasmodesmata during development: re-examination of the importance of primary, secondary, and branched plasmodesmata structure versus function. *Protoplasma* **248**, 61-74. (**doi:10.1007/s00709-010-0252-3**)
10. Pogson BJ, Woo NS, Forster B, Small ID. 2008Plastid signalling to the nucleus and beyond. *Trends Plant Sci.* **13**, 602-609. (**doi:10.1016/j.tplants.2008.08.008**)

11. Chan KX, Phua SY, Crisp P, McQuinn R, Pogson BJ. 2016Learning the languages of the chloroplast: retrograde signaling and beyond. *Annu. Rev. Plant Biol.* **67**, 25-53. (**doi:10.1146/annurev-arplant-043015-111854**)
12. Bobik K, Burch-Smith TM. 2015Chloroplast signaling within, between and beyond cells. *Front. Plant Sci.* **6**, 781. (**doi:10.3389/fpls.2015.00781**)
13. Gollan PJ, Tikkanen M, Aro EM. 2015Photosynthetic light reactions: integral to chloroplast retrograde signalling. *Curr. Opin Plant Biol.* **27**, 180-191. (**doi:10.1016/j.pbi.2015.07.006**)
14. Kleine T, Leister D. 2016Retrograde signaling: organelles go networking. *Biochim. Biophys. Acta* **1857**, 1313-1325. (**doi:10.1016/j.bbabio.2016.03.017**)
15. Brunkard JO, Burch-Smith TM. 2018Ties that bind: the integration of plastid signalling pathways in plant cell metabolism. *Essays Biochem.* **62**, 95-107. (**doi:10.1042/EBC20170011**)
16. Glasser Cet al.2014Meta-analysis of retrograde signaling in *Arabidopsis thaliana* reveals a core module of genes embedded in complex cellular signaling networks. *Mol. Plant* **7**, 1167-1190. (**doi:10.1093/mp/ssu042**)
17. Surpin M, Larkin RM, Chory J. 2002Signal transduction between the chloroplast and the nucleus. *Plant Cell* **14**, S327-S338. (**doi:10.1105/tpc.010446**
18. Larkin RM. 2016Tetrapyrrole signaling in plants. *Front. Plant Sci.* **7**, 1586. (**doi:10.3389/fpls.2016.01586**)
19. Larkin RM, Alonso JM, Ecker JR, Chory J. 2003GUN4, a regulator of chlorophyll synthesis and intracellular signaling. *Science* **299**, 902-906. (**doi:10.1126/science.1079978**)
20. Adhikari ND, Froehlich JE, Strand DD, Buck SM, Kramer DM, Larkin RM. 2011GUN4-porphyrin complexes bind the ChlH/GUN5 subunit of Mg-Chelatase and promote chlorophyll biosynthesis in *Arabidopsis*. *Plant Cell* **23**, 1449-1467. (**doi:10.1105/tpc.110.082503**)
21. Voigt C, Oster U, Bornke F, Jahns P, Dietz KJ, Leister D, Kleine T. 2010In-depth analysis of the distinctive effects of norflurazon implies that tetrapyrrole

biosynthesis, organellar gene expression and ABA cooperate in the GUN-type of plastid signalling. *Physiol. Plant.* **138**, 503-519. (**doi:10.1111/j.1399-3054.2009.01343.x**)

22. Kobayashi K, Masuda T. 2016Transcriptional regulation of tetrapyrrole biosynthesis in *Arabidopsis thaliana*. *Front. Plant Sci.* **7**, 1811. (**doi:10.3389/fpls.2016.01811**)
23. Bobik K, McCray TN, Ernest B, Fernandez JC, Howell KA, Lane T, Staton M, Burch-Smith TM. 2017The chloroplast RNA helicase ISE2 is required for multiple chloroplast RNA processing steps in *Arabidopsis thaliana*. *Plant J.* **91**, 114-131. (**doi:10.1111/tpj.13550**)
24. Carlotto N, Wirth S, Furman N, Ferreyra Solari N, Ariel F, Crespi M, Kobayashi K. 2016The chloroplastic DEVH-box RNA helicase INCREASED SIZE EXCLUSION LIMIT 2 involved in plasmodesmata regulation is required for group II intron splicing. *Plant Cell Environ.* **39**, 165-173. (**doi:10.1111/pce.12603**)
25. Burch-Smith TM, Brunkard JO, Choi YG, Zambryski PC. 2011Organelle-nucleus cross-talk regulates plant intercellular communication via plasmodesmata. *Proc. Natl Acad. Sci. USA* **108**, E1451-E1460. (**doi:10.1073/pnas.1117226108**)
26. Kobayashi K, Otegui MS, Krishnakumar S, Mindrinos M, Zambryski P. 2007INCREASED SIZE EXCLUSION LIMIT 2 encodes a putative DEVH box RNA helicase involved in plasmodesmata function during *Arabidopsis* embryogenesis. *Plant Cell* **19**, 1885-1897. (**doi:10.1105/tpc.106.045666**)
27. Burch-Smith TM, Zambryski PC. 2010Loss of INCREASED SIZE EXCLUSION LIMIT (ISE)1 or ISE2 increases the formation of secondary plasmodesmata. *Curr. Biol.* **20**, 989-993. (**doi:10.1016/j.cub.2010.03.064**)
28. Burch-Smith TM, Zambryski PC. 2012Plasmodesmata paradigm shift: regulation from without versus within. *Annu. Rev. Plant Biol.* **63**, 239-260. (**doi:10.1146/annurev-arplant-042811-105453**)
29. Bryant N, Lloyd J, Sweeney C, Myouga F, Meinke D. 2011Identification of nuclear genes encoding chloroplast-localized proteins required for embryo

development in *Arabidopsis*. *Plant Physiol.* **155**, 1678-1689. (**doi:10.1104/pp.110.168120**)

30. Kim I, Hempel FD, Sha K, Pfluger J, Zambryski PC. 2002Identification of a developmental transition in plasmodesmatal function during embryogenesis in *Arabidopsis thaliana*. *Development* **129**, 1261-1272.
31. Liu Y, Schiff M, Marathe R, Dinesh-Kumar SP. 2002Tobacco Rar1, EDS1 and NPR1/NIM1 like genes are required for N-mediated resistance to tobacco mosaic virus. *Plant J.* **30**, 415-429. (**doi:10.1046/j.1365-313X.2002.01297.x**)
32. Liu Y, Burch-Smith T, Schiff M, Feng S, Dinesh-Kumar SP. 2004Molecular chaperone Hsp90 associates with resistance protein N and its signaling proteins SGT1 and Rar1 to modulate an innate immune response in plants. *J. Biol. Chem.* **279**, 2101-2108. (**doi:10.1074/jbc.M310029200**)
33. Lichtenthaler HK. 1987Chlorophylls and carotenoids: pigments of photosynthetic membranes. *Methods Enzymol.* **148**, 350-382. (**doi:10.1016/0076-6879(87)48036-1**)
34. Brunkard JO, Burch-Smith TM, Runkel AM, Zambryski P. 2015Investigating plasmodesmata genetics with virus-induced gene silencing and an agrobacterium-mediated GFP movement assay. *Methods Mol. Biol.* **1217**, 185-198. (**doi:10.1007/978-1-4939-1523-1_13**)
35. Schindelin Jet al.2012Fiji: an open-source platform for biological-image analysis. *Nat. Methods* **9**, 676-682. (**doi:10.1038/nmeth.2019**)
36. Schneider CA, Rasband WS, Eliceiri KW. 2012NIH Image to ImageJ: 25 years of image analysis. *Nat. Methods* **9**, 671-675. (**doi:10.1038/nmeth.2089**)
37. Zuker M. 2003Mfold web server for nucleic acid folding and hybridization prediction. *Nucleic Acids Res.* **31**, 3406-3415. (**doi:10.1093/nar/gkg595**)
38. Bobik K, Fernandez JC, Hardin SR, Ernest B, Ganusova EE, Staton ME, Burch-Smith TM. 2019The essential chloroplast ribosomal protein uL15c interacts with the chloroplast RNA helicase ISE2 and affects intercellular trafficking through plasmodesmata. *New Phytol.* **221**, 850-865. (**doi:10.1111/nph.15427**)

39. Burch-Smith TM, Anderson JC, Martin GB, Dinesh-Kumar SP. 2004Applications and advantages of virus-induced gene silencing for gene function studies in plants. *Plant J.* **39**, 734-746. (**doi:10.1111/j.1365-313X.2004.02158.x**)
40. Chi W, He B, Mao J, Li Q, Ma J, Ji D, Zou M, Zhang L. 2012The function of RH22, a DEAD RNA helicase, in the biogenesis of the 50S ribosomal subunits of *Arabidopsis* chloroplasts. *Plant Physiol.* **158**, 693-707. (**doi:10.1104/pp.111.186775**)
41. Nishimura K, Ashida H, Ogawa T, Yokota A. 2010A DEAD box protein is required for formation of a hidden break in *Arabidopsis* chloroplast 23S rRNA. *Plant J.* **63**, 766-777. (**doi:10.1111/j.1365-313X.2010.04276.x**)
42. Asakura Y, Galarneau E, Watkins KP, Barkan A, van Wijk KJ. 2012Chloroplast RH3 DEAD box RNA helicases in maize and *Arabidopsis* function in splicing of specific group II introns and affect chloroplast ribosome biogenesis. *Plant Physiol.* **159**, 961-974. (**doi:10.1104/pp.112.197525**)
43. Hammani K, Takenaka M, Miranda R, Barkan A. 2016A PPR protein in the PLS subfamily stabilizes the 5'-end of processed rpl16 mRNAs in maize chloroplasts. *Nucleic Acids Res.* **44**, 4278-4288. (**doi:10.1093/nar/gkw270**)
44. Sharwood RE, Halpert M, Luro S, Schuster G, Stern DB. 2011Chloroplast RNase J compensates for inefficient transcription termination by removal of antisense RNA. *RNA* **17**, 2165-2176. (**doi:10.1261/rna.028043.111**)
45. Germain A, Herlich S, Larom S, Kim SH, Schuster G, Stern DB. 2011Mutational analysis of *Arabidopsis* chloroplast polynucleotide phosphorylase reveals roles for both RNase PH core domains in polyadenylation, RNA 3'-end maturation and intron degradation. *Plant J.* **67**, 381-394. (**doi:10.1111/j.1365-313X.2011.04601.x**)
46. Ganusova EE, Rice JH, Carlew TS, Patel A, Perrodin-Njoku E, Hewezi T, Burch-Smith TM. 2017Altered expression of a chloroplast protein affects the outcome of virus and nematode infection. *Mol. Plant Microbe Interact.* **30**, 478-488. (**doi:10.1094/MPMI-02-17-0031-R**)

47. Fitter DW, Martin DJ, Copley MJ, Scotland RW, Langdale JA. 2002GLK gene pairs regulate chloroplast development in diverse plant species. *Plant J.* **31**, 713-727. (**doi:10.1046/j.1365-313X.2002.01390.x**)
48. Kakizaki T, Matsumura H, Nakayama K, Che FS, Terauchi R, Inaba T. 2009Coordination of plastid protein import and nuclear gene expression by plastid-to-nucleus retrograde signaling. *Plant Physiol.* **151**, 1339-1353. (**doi:10.1104/pp.109.145987**)
49. Xu Xet al.2016Convergence of light and chloroplast signals for de-etiolation through ABI4-HY5 and COP1. *Nat. Plants* **2**, 16066. (**doi:10.1038/nplants.2016.66**)
50. Cosgrove DJ. 2016Catalysts of plant cell wall loosening. *F1000Res* **5**. (**doi:10.12688/f1000research.7180.1**)
51. Ortiz-Alcaide M, Llamas E, Gomez-Cadenas A, Nagatani A, Martinez-Garcia JF, Rodriguez-Concepcion M. 2019Chloroplasts modulate elongation responses to canopy shade by retrograde pathways involving HY5 and abscisic acid. *Plant Cell* **31**, 384-398. (**doi:10.1105/tpc.18.00617**)
52. Brzezowski P, Richter AS, Grimm B. 2015Regulation and function of tetrapyrrole biosynthesis in plants and algae. *Biochim. Biophys. Acta* **1847**, 968-985. (**doi:10.1016/j.bbabio.2015.05.007**)
53. Fitzgibbon J, Beck M, Zhou J, Faulkner C, Robatzek S, Oparka K. 2013A developmental framework for complex plasmodesmata formation revealed by large-scale imaging of the *Arabidopsis* leaf epidermis. *Plant Cell* **25**, 57-70. (**doi:10.1105/tpc.112.105890**)
54. Faulkner C, Akman OE, Bell K, Jeffree C, Oparka K. 2008Peeking into pit fields: a multiple twinning model of secondary plasmodesmata formation in tobacco. *Plant Cell* **20**, 1504-1518. (**doi:10.1105/tpc.107.056903**)
55. Benitez-Alfonso Y, Cilia M, San Roman A, Thomas C, Maule A, Hearn S, Jackson D. 2009Control of *Arabidopsis* meristem development by thioredoxin-dependent regulation of intercellular transport. *Proc. Natl Acad. Sci. USA* **106**, 3615-3620.

56. Walter M, Kilian J, Kudla J. 2002PNPase activity determines the efficiency of mRNA 3'-end processing, the degradation of tRNA and the extent of polyadenylation in chloroplasts. *EMBO J.* **21**, 6905-6914. (**doi:10.1093/emboj/cdf686**)
57. Cushing DA, Forsthoefel NR, Gestaut DR, Vernon DM. 2005*Arabidopsis* emb175 and other ppr knockout mutants reveal essential roles for pentatricopeptide repeat (PPR) proteins in plant embryogenesis. *Planta* **221**, 424-436. (**doi:10.1007/s00425-004-1452-x**)
58. Chen H, Zou W, Zhao J. 2015Ribonuclease J is required for chloroplast and embryo development in *Arabidopsis*. *J. Exp. Bot.* **66**, 2079-2091. (**doi:10.1093/jxb/erv010**)
59. Gray JC, Sullivan JA, Wang JH, Jerome CA, MacLean D. 2003Coordination of plastid and nuclear gene expression. *Phil. Trans. R. Soc. Lond. B* **358**, 135-144; discussion 144–135. (**doi:10.1098/rstb.2002.1180**).
60. Hotto AM, Schmitz RJ, Fei Z, Ecker JR, Stern DB. 2011Unexpected diversity of chloroplast noncoding RNAs as revealed by deep sequencing of the *Arabidopsis* transcriptome. *G3 (Bethesda)* **1**, 559-570. (**doi:10.1534/g3.111.000752**)
61. Mochizuki N, Brusslan JA, Larkin R, Nagatani A, Chory J. 2001*Arabidopsis* genomes uncoupled 5 (GUN5) mutant reveals the involvement of Mg-chelatase H subunit in plastid-to-nucleus signal transduction. *Proc. Natl Acad. Sci. USA* **98**, 2053-2058. (**doi:10.1073/pnas.98.4.2053**)
62. Benitez-Alfonso Y, Jackson D. 2009Redox homeostasis regulates plasmodesmal communication in *Arabidopsis* meristems. *Plant Signal Behav.* **4**, 655-659. (**doi:10.1073/pnas.0808717106**)
63. Stonebloom S, Brunkard JO, Cheung AC, Jiang K, Feldman L, Zambryski P. 2012Redox states of plastids and mitochondria differentially regulate intercellular transport via plasmodesmata. *Plant Physiol.* **158**, 190-199. (**doi:10.1104/pp.111.186130**)

64. Rutschow HL, Baskin TI, Kramer EM. 2011Regulation of solute flux through plasmodesmata in the root meristem. *Plant Physiol.* **155**, 1817-1826. (**doi:10.1104/pp.110.168187**)
65. Hofius D, Herbers K, Melzer M, Omid A, Tacke E, Wolf S, Sonnewald U. 2001Evidence for expression level-dependent modulation of carbohydrate status and viral resistance by the potato leafroll virus movement protein in transgenic tobacco plants. *Plant J.* **28**, 529-543. (**doi:10.1046/j.1365-313X.2001.01179.x**)

# VITA

Amie Sankoh was born in Sierra Leone, West Africa. When she was three years old, she suffered a high fever from malaria, and she was lucky to survive but was left profoundly deaf in both ears. Despite this setback, her parents tried their hardest to support her educational needs and those of her siblings. Growing up, the barriers caused by her deafness made it nearly impossible for her to learn in the same way as her hearing siblings. At 12 years old, Sankoh was sent to the United States to access better resources and the possibility of medical treatment. While the latter was not realistic for her condition, she was fortunate to have her world opened by learning American Sign Language (ASL). ASL allowed her to access information like never before and connect with the Deaf community. She worked tirelessly to catch up to her hearing peers throughout high school and college. It was then that she fell in love with science, specifically chemistry.

Before becoming a Ph.D. candidate, Sankoh earned an Associate of Applied Science degree in laboratory science technology and a Bachelor of Science in biochemistry at the Rochester Institute of Technology (RIT). Along with her strong academic record, she has several summers of relevant research experience and has received several scholarships and other recognitions. Sankoh has completed two scientific publications, a national-level oral presentation, and multiple poster presentations.

At the doctoral program in the Biochemistry & Cellular and Molecular Biology (BCMB) department at the University of Tennessee, Knoxville (UT), Amie Sankoh is

interested in studying intercellular communication critical for cell growth and functions. Sankoh was awarded the Program for Excellence & Equity in Research (PEER) fellowship, an NSF-GRFP, and NIH F31 fellowship. Her current project investigates hormones' effects on plasmodesmata (PD)-mediated trafficking in *Nicotiana Benthamiana*.

Her unique background has given her great focus on frequent and successful outreach, drawing from her own experiences as an underrepresented minority and Deaf woman scientist. She is a dedicated learner and is actively involved in outreach efforts with Schools for the Deaf to increase accessibility for Deaf students and professionals. One cannot overemphasize the importance of diverse Deaf scientists in the modern world.